Ore Geology Reviews 101 (2018) 349–383

Contents lists available at ScienceDirect

Ore Geology Reviews

journal homepage: www.elsevier.com/locate/oregeorev

Invited Review Article

Ore-forming processes within granitic pegmatites

David London

School of Geology & Geophysics, University of Oklahoma, Norman, OK 73019, USA

ARTICLE INFO

Keywords:
Pegmatite
Granite
Fractional crystallization
Liquidus undercooling
Constitutional zone refining
Industrial minerals
Rare metals
Gemstones

ABSTRACT

Pegmatites are texturally complex igneous rocks marked by some combination of coarse but variable crystal size, mineralogical zonation, prominent anisotropy of crystal orientations from the margins inward, and skeletal, radial, and graphic intergrowth habits of crystals. The vast majority of pegmatites are granitic in composition, and this article pertains to these rocks. Pegmatites occur as segregations near the roofward contact of their source pluton, as dike swarms emanating from their plutons into the surrounding igneous and metamorphic rocks, and as planar to lenticular intrusive bodies whose sources are not exposed. Granitic pegmatites are important economic sources of industrial minerals (feldspars, quartz, spodumene, petalite) for glass, ceramic, and electronic applications, of a wide variety of lithiophile rare elements (Li, Cs, Be, Nb, Ta, Sn, etc.) that are incompatible in the predominant rock-forming minerals of granites, and of colored gemstones and valuable mineral specimens (of beryl, tourmaline, topaz, etc.).

All of the salient features of pegmatites – their mineral habits, distinctive rock fabrics, and spatial zonation of mineral assemblages, including monomineralic bodies – arise from appreciable liquidus undercooling (by ~200° ± 50 °C) of viscous granitic liquids prior to the onset of crystallization. The ore-forming processes within granitic pegmatites are entirely igneous as a result of extended fractional crystallization of large granitic plutons, and in response to crystallization at a highly supersaturated state of the melt in pegmatite-forming bodies.

Constitutional zone refining, wherein a flux-enriched boundary layer of liquid develops adjacent to the crystallization front and eventually becomes the last liquid in the pegmatite body, appears to be the most likely mechanism to account for increasing crystal dimensions (and consequently decreasing numbers of crystals) and late-stage bodies of rare-metal ores that are the hallmarks of the class of rare-element pegmatites. The most prevalent manifestation of mineralogical zonation, in which plagioclase (initially An_{10-20}) dominates the outer zones, K-feldspar follows in intermediate zones, and quartz is concentrated in the last-formed core units, can be rationalized by the relative magnitudes of the Gibbs Free Energies of crystallization of feldspars versus quartz and of plagioclase versus K-feldspar solid solutions. Importantly, the sequential crystallization of feldspars and quartz at a highly undercooled state of melt is predicted on thermodynamic grounds even for melts of eutectic composition. Highly contrasting diffusivities of alkalis versus high field-strength elements (HFSE) in pegmatite-forming liquids lead to long-range and short-range effects of element migration or concentration: low diffusivities of HFSE promote boundary-layer pile-up and local, episodic saturation of minerals at the crystallization front. Long-range diffusivities of alkalis give rise to the spatial segregation of plagioclase and K-feldspar along opposing margins of dikes, and of isolated but gigantic crystals of rare minerals such as pollucite.

Exploration for pegmatites as sources of economic commodities relies entirely on surface discoveries. However, the regional zonation of pegmatite bodies, and the chemistry of metasomatic alteration in the host rocks to rare-element pegmatites, give some indications of the probability of finding deposits of ceramic materials, rare-metal ores, and even gemstones.

1. The nature of granitic pegmatites

Pegmatites are textural variants of the more common plutonic igneous rocks, including the compositions of granite, gabbro, syenite, and rarely others. Whereas the common plutonic magmas tend to form large bodies of texturally and mineralogically uniform rock, their pegmatites are precisely the opposite: small in volume and texturally and mineralogically diverse in their internal fabrics.

Granitic pegmatites are found on every continent, within old cratons and in younger, marginal mountain belts. Rocks that geologists normally recognize as pegmatites do not occur in the oceanic basins nor at mid-oceanic ridges; rare granophyres in the final rhyolitic stages of

E-mail address: dlondon@ou.edu.

https://doi.org/10.1016/j.oregeorev.2018.04.020
Received 10 January 2018; Received in revised form 10 April 2018; Accepted 19 April 2018
Available online 18 May 2018

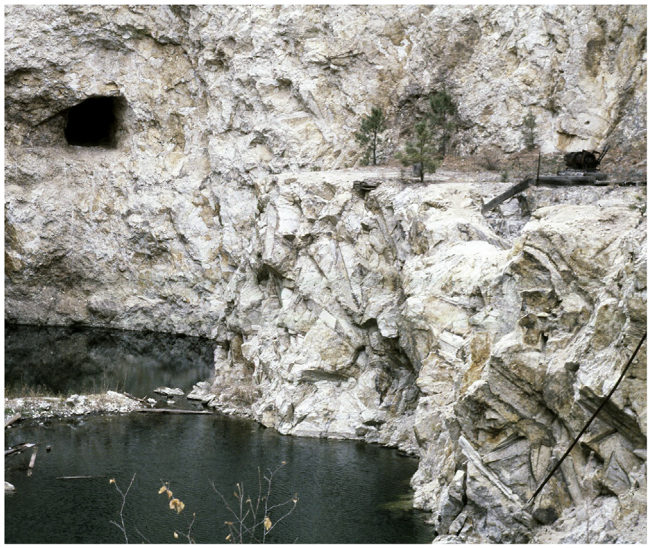

Fig. 1. A view of the Etta mine, Black Hills district, near Custer, South Dakota, illustrates the gigantic size of spodumene crystals there. Remnants of spodumene crystals and their molds in quartz are evident in the right half of the photo. An adit and pine trees are ~2.5 m tall.

some basaltic volcanoes (Marsh et al., 1991) could be construed as pegmatitic based on the similarity of their texture and origin to graphic granite (e.g., Barker, 1970; London, 2008).

This article presents a broad review of what pegmatites are, where they originate, how they are classified, and how they evolve to the point of forming important ore deposits of industrial minerals, rare metals, and gem and mineral specimens. An understanding of ore-forming processes in pegmatites requires an appreciation of the pegmatite-forming process itself. The paradigm for pegmatites has undergone radical change in recent years. This paper presents an overview of that new paradigm, which is detailed in London (2008), as the basis for explaining the processes that govern the occurrence of economic deposits.

1.1. A definition of pegmatite

Pegmatite (pĕg' mə tīt') is an essentially igneous rock (London, 2008), mostly of granitic composition, that is distinguished from other igneous rocks by (1) the extremely coarse and systematically variable size of its crystals, typically increasing by a $\sim 10^2$ from margins to center (Fig. 1), or (2) by an abundance of crystals with skeletal, graphic, or other strongly directional growth habits (Fig. 2), or (3) by a prominent spatial zonation of mineral assemblages, including monomineralic zones (Fig. 3). Any one of these textural attributes might be sufficient to define a pegmatite body (Fig. 4), but they tend to be occur together (Fig. 5).

By defining pegmatites as igneous (London, 2008), their compositions are restricted to those that might be derived by partial melting of crustal and mantle sources. Such partial melts produce the common igneous rocks themselves, which consist mostly of three principal mineral components in or close to their eutectic proportions at elevated pressures. Thus, by definition, an igneous origin would exclude rocks that consist of one mineral, or even an assemblage of minerals, whose known or likely solidus temperatures exceed plausible pressure-temperature conditions for the generation of partial melts of the ordinary magma types. Examples include silexite, construed as an igneous rock composed of at least 90% quartz (Miller, 1919), and topazite, a quartz-topaz rock that is interpreted as igneous in origin (Eadington and Nashar, 1978). Such rocks might originate by hydrothermal processes, or they may be cumulate bodies that are not representative of the melt composition from which they formed (e.g., Kortemeier and Burt, 1988; Dolejš and Baker, 2007), but they do not represent igneous liquid compositions.

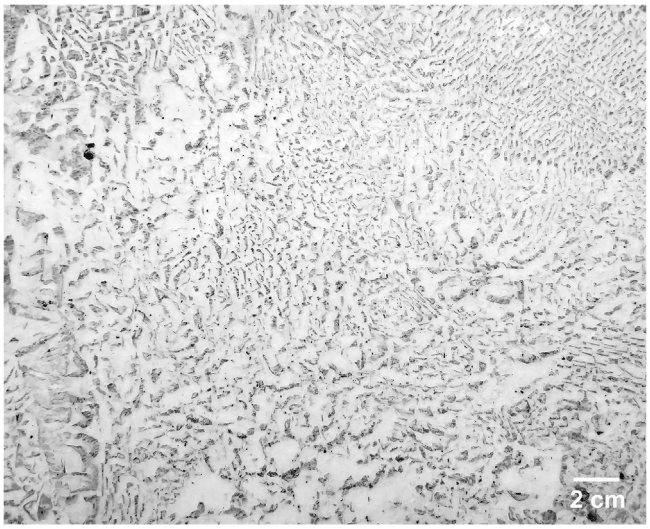

Fig. 2. Graphic granite, the uniquely pegmatitic intergrowth of quartz (gray) in K-feldspar (white), Hale quarry, Portland, Connecticut.

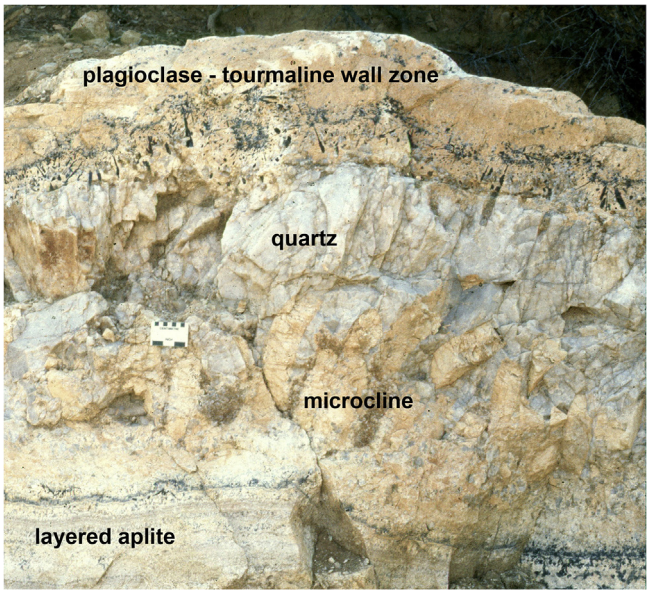

Fig. 3. Pegmatite outcrop at the San Diego mine, Mesa Grande district, San Diego County, California. The lower contact of the dike is not exposed. Giant K-feldspar crystals with unidirectional solidification texture (UST) grew upward from the layered aplite. The hanging wall border and wall zones are dominated by plagioclase plus quartz with accessory tourmaline showing UST. The center of the dike is pure massive quartz. Top of scale marker is in centimeters.

Pegmatites and hydrothermal veins share several textural attributes. These include unidirectional solidification texture (referred to as UST, the elongate growth of crystals inward from a contact with host rock), radial and skeletal habits of crystals, mineral segregations in spatially distinct zones that are parallel to the contacts, and increasing crystal dimensions from the margin to the center (Fig. 5). It is partly for this reason that an aqueous solution – the medium from which veins form – has been invoked for the genesis of pegmatites from some of the earliest stages of study up to modern times (e.g., Hunt, 1871; Merritt, 1924, Ramberg, 1952, Gresens, 1969, Roedder, 1981). In pegmatites, skeletal crystals (i.e., incomplete crystals dominated by edges and corners) form intergrowths with other mineral phases. One phase is considered the host that drives the texture, the other is an interstitial phase that

Fig. 4. An example of a pegmatite that is not distinguished by the enormous size of its crystals. Despite its small size, this dike near Moodus, Connecticut, possesses pegmatitic textures that include (1) a sharp increase in crystal size of tourmaline (black) from fine-grained margin to prismatic crystals within, (2) inward unidirectional orientation of tourmaline and feldspar (white) crystals, (3) uncommonly large feldspar crystals that span the entire width of the dike, (4) skeletal intergrowth of feldspar and quartz, and spatial segregation of feldspar and quartz.

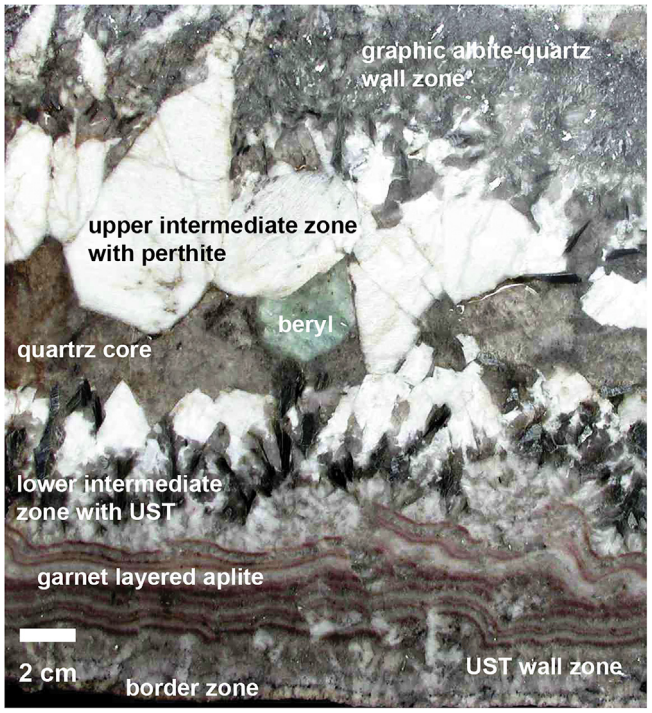

Fig. 5. A complete section of a pegmatite dike, 29 cm thick, from near Palomar Mountain, San Diego County, California (USA).

precipitates between the segments of skeletal crystals. The most common of these intergrowths in pegmatites is graphic granite, in which K-feldspar hosts skeletal quartz (Fig. 2). Graphic granite is unique to pegmatites, and it is their defining texture: the term ***pegmatite***, from Greek πεγνυμι, alludes to this intergrowth (London, 2008).

Pegmatitic textures occur in gabbros, syenites, some komatiites (e.g., spinifex texture), and even in carbonatites. Ores of platinum and chromite are associated with pegmatitic portions of gabbros (e.g., Roberts et al., 2007), and deposits of zirconium, lanthanide rare earths, and niobium are found in pegmatitic zones of syenites (e.g., Salvi and Williams-Jones, 2005). London (2008), however, put forward an explanation for why granitic pegmatites are so common, whereas pegmatites of other igneous compositions are not. That is, the high viscosity of granitic liquids impedes the ionic diffusion that is necessary to initiate crystallization. For this reason, granitic liquids tend to persist to temperatures well below their liquidus before crystallization commences. When crystallization does commence, the melt is at a high degree of supersaturation with respect to the crystalline components, and the result is pegmatitic texture. By virtue of their lower silica compositions, liquids of gabbroic and syenitic compositions possess lower viscosities from which crystals nucleate more readily. These melt compositions crystallize closer to their liquidus temperature, and uniform, isotropic rock fabrics are the result. This article pertains only to pegmatites of granitic composition because these are by far more abundant and voluminous than any others. The processes that lead to pegmatitic textures are the same regardless of the composition of the melt. For the sake of brevity, the term pegmatite as used hereafter will refer to those of granitic composition.

2. General characteristics of pegmatites

2.1. Occurrence

Pegmatites form segregations within the top tens of meters of the roof zones of their source plutons, and they are common as dike swarms that emanate from the roof. In the cupolas of some granites, the pegmatitic segregations are sharply bounded by typical granitic fabric. In others, the transition from granitic to pegmatitic textures is gradual over a span of decameters; in this latter case, so-called “pegmatitic granite” (e.g., Goad and Černý, 1981) consists of skeletal K-feldspar megacrysts, some with graphic quartz intergrowths, in a coarse plagioclase-quartz groundmass (Fig. 6). As a system of dikes, pegmatites by

Fig. 6. Porphyritic pegmatitic granite, Popham Beach, Maine. White rectangles are skeletal K-feldspar crystals with plagioclase-quartz granite within.

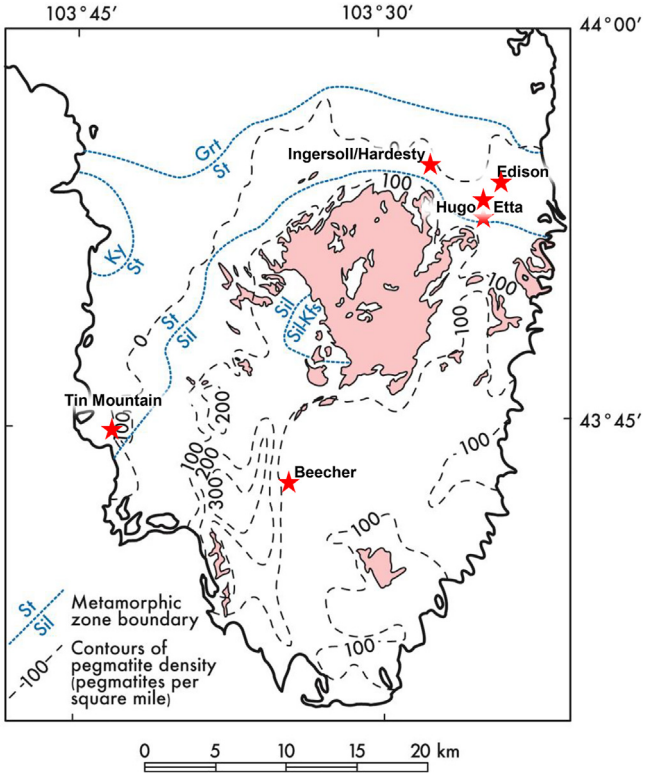

Fig. 7. Pegmatite density contour map (pegmatite bodies per square mile) in the Black Hills district, South Dakota, redrafted from Redden et al. (1982). Metamorphic zones and isograd reactions are shown in blue. Granite bodies are presented in pink. Six of the largest Li-rich pegmatites in the district are plotted as red stars. Reprinted from London (2016b).

the hundreds to thousands may surround their source pluton (Fig. 7). Regional structures can control their distribution (e.g., Rossovskiy and Konovalenko, 1979), but where regional influences appear to be minimal, the majority of dikes close the pluton are more or less conformable with the contacts of their source granite, following the same structural conduits as the granite (London, 1985; Černý, 1991b). Cross-cutting relations of pegmatite and aplite bodies within this marginal zone indicate that the derivation of pegmatite-forming melts is somewhat protracted, not entirely simultaneous as a single pulse of melt (e.g., Duke et al., 1988). The numbers of individual dikes decreases rapidly beyond about a kilometer from source (Fig. 7), and their distribution follows more local zones of weakness or dilation in their host rocks. Cross-cutting dike relationships are rare, though some dikes merge and divide.

Dikes emplaced into competent host rocks, such as other igneous rocks, gneisses, and amphibolites, tend to form planar bodies that persist laterally for distances of a kilometer or more of outcrop. In contrast, dikes that intrude less competent hosts, such as micaceous schists, are more commonly ellipsoidal and isolated bodies "like beads on a string" (p. 18 of Jahns, 1952). These different aspect ratios arise from contrasts in ductility of the host rocks at the depths of dike emplacement (Černý, 1991b), in the range of 6 to 9 km and corresponding to pressures of 200 to 300 MPa (Brisbin, 1986). Lateral continuity of dikes, or the lack of it, carries implications for resource assessment.

A little-known but important feature of pegmatites is that they do not contain phenocrysts entrained from the source. All indications are that pegmatites are emplaced as entirely silicate liquid, which entails exceptionally efficient separation of crystals and melt upon extraction from the source granites at a high degree of crystallization. This is not an unrealistic process, as vitric obsidians represent late-stage liquids that are extracted from highly crystallized granite mush (Bachmann and Bergantz, 2004).

The escape of granitic liquids as dikes from their source pluton was modeled by Rubin (1995). The principal variables of that model include the temperatures of the granitic liquid and of the host rocks surrounding the pluton at the time of the escape of the dike-forming liquids, the viscosity of the granitic liquid, density contrasts between liquid and host rock, and the driving pressure of the granitic liquid, which was construed as mostly the result of its buoyancy. The magma driving pressure is the least well known of these variables; for example, recharge by hot, buoyant magma at the base of a crystal mush can cause upward compaction of crystals and substantially increase the fluid pressure of magma within that crystal pile (e.g., Pistone et al., 2017). Rubin's (1995) general conclusion was that granitic dikes (i.e., pegmatite-forming liquids) are unlikely to migrate beyond the thermal aureole created by their pluton.

At continental crustal depths on the order of 6 to 9 km, host rock temperatures at their geothermal gradient, ~20 °C/km (e.g., Burke and Kidd, 1978; Catlos et al., 2001) are low, and their cooling effect on magma migration results in a sharp increase in the viscosity of the granitic melts. The viscosity of granitic liquid that is saturated in H_2O at its minimum or eutectic temperature of 685 °C at 200 MPa H_2O is approximately 10^5 Pa s (from Baker, 1996). This is the viscosity of road tar at 25 °C. The instantaneous juxtaposition of such a granitic melt against host rocks at ~145°–205 °C induces sharp cooling to ~400–425 °C along the dike contacts. At 425 °C, the viscosity of the same hydrous granitic liquid composition increases to ~10^8 Pa s (op. cit.), which is approximately the viscosity of asphaltic pitch. Though technically a liquid, asphaltic pitch is sufficiently rigid and brittle that it shatters with the blow of a hammer (see http://smp.uq.edu.au/content/pitch-drop-experiment, last accessed June 2017).

It is for this reason that Rubin (1995) concludes that much of the heat content of a large magma body must permeate the surrounding host rocks, raising their temperatures well above the geothermal gradient, to make the escape of dikes possible. Using Rubin's model, Baker (1998) calculated that a source magma body of 1000 km^3 (10 × 10 × 10 km) could liberate enough heat to facilitate the transport of pegmatite-forming melt up to 10 km from the source. Rubin's (1995) mechanical model of dike emplacement is consistent with the longstanding hypothesis that pegmatite-forming liquids are derived late in the crystal-chemical evolution of a large parental granite body (e.g., Jahns and Burnham, 1969). Extended fractional crystallization of a large mass of granitic magma liberates the heat necessary for dikes to propagate outward, and it also generates melts that are enriched in incompatible components, including fluxes and rare elements, for which pegmatites are renown.

Rubin's (1995) model also leads to a conclusion that pegmatite-forming dikes propagate rapidly from source. It is clear from the preceding assessment that the slow migration of melt near its thermal minimum through rocks that are hundreds of degrees cooler will stall the movement of the melts, unless the driving pressure of the melt is sufficient to open conduits for magma quickly.

2.2. The granite-pegmatite association

Because pegmatite-forming dikes can and do migrate up to kilometers from their source, it is commonplace to observe pegmatites that lack any apparent parental granite. The converse is also true: large exposures of granite plutons may lack pegmatites because these would have been eroded above the level of exposure. There are many occurrences world-wide, however, where a continuum from granite to pegmatite dikes can be observed (e.g., Černý, 1991b; London, 2008). Where the source granites of pegmatites are known, these are normally small, chemically and texturally evolved plutons associated with the waning stages of much more voluminous granitic magmatism (e.g., Goad and Černý, 1981). Sweetapple and Collins (2002) have documented such a connection between the Ta-rich Archean pegmatites of

the Pilbara field, Western Australia. The pegmatites can be linked to small and chemically evolved granites (2890 to 2830 Ma: Sweetapple and Collins, 2002) that intrude much larger granite masses and intercalated greenstones toward the end of the granite magmatism in the craton (3600–2800 Ma: Sweetapple and Collins, 2002).

The fundamental relationship in which granites spawn pegmatites is not in doubt. This common knowledge among geoscientists was largely the impetus for the study of pegmatites in the 20th century that culminated with model of Jahns and Burnham (1969). However, the origins of rare-element pegmatites have been divorced from the granite-pegmatite paradigm by various workers over time. Stewart (1978) suggested that Li-rich pegmatites might form by very low degrees of partial melting of metamorphic rocks on the grounds that fractional crystallization of granitic melts to rare-element-rich compositions at low temperatures ought to be a reversible (i.e., an equilibrium) process. Roedder (1981) observed that common pegmatites are igneous, but that rare-element pegmatites might be hydrothermal deposits because of their non-granitic mineral assemblages. Shearer et al. (1992) proposed that Li-rich pegmatites of the Black Hills district, South Dakota, might be unrelated to the Harney Peak granite and its thousands of common pegmatites because Rayleigh fractionation trace-element models starting with the composition of the granites did not yield elemental abundances that matched the Li-rich pegmatites. Others advocate a direct anatectic origin because of the similarity of the pegmatite compositions to those of enclosing schists (e.g., Shaw et al., 2016; Simmons et al., 2016). These hypotheses are evaluated in a later section, but they hinge upon a knowledge of the pressures and temperatures attending crystallization, the compositions of pegmatites and of pegmatite-forming liquids (which may not be the same as the pegmatites they produce), and on the solubility-saturation relations of rare-element minerals in granitic melts.

3. Bulk compositions of pegmatites

The bulk compositions of pegmatites are poorly known because of the difficulty posed by representative sampling of such coarse-grained and heterogeneous bodies. Nonetheless, a grid, trench, and coring program conducted in Colorado (USA) during WWII generated modal analyses of 1803 pegmatites (Norton, 1966), the vast majority of which would be common granitic pegmatites that do not contain significant quantities of exotic minerals. The data spread out over the haplogranite system (Ab-Or-Qtz, see Fig. 1–6 of London, 2008), but with prominent modes that straddle the composition of the haplogranite minimum ($Ab_{38}Or_{29}Qz_{33}$) at approximately 200 MPa H_2O. These early studies confirmed that the compositions of pegmatites are those of granites in a strict sense, in which quartz, plagioclase, and alkali feldspar in subequal proportions constitute greater than 80% of the rock (Streckheisen, 1976). Very little modal analysis of whole pegmatite bodies has been published since (London et al., 2012b; Simmons et al., 2016). One important study entailed the Tanco pegmatite, Manitoba, which is the most fractionated and distal body of the Bernic Lake group, and has been the archetype of a giant rare-element pegmatite that has produced economic quantities of Ta, Li, and Cs for over half a century (Černý, 2005). Stilling et al. (2006) calculated a bulk composition for the Tanco pegmatite based on a 3D reconstruction of each of the mapped zones, coupled with modal analyses as documented in 1355 cored drill holes across and within the pegmatite to characterize the modal mineralogy of each zone. Quartz, sodic plagioclase, and alkali feldspar sum to 82% of the bulk composition, which makes Tanco granitic as well (Table 1).

The vast majority of pegmatites are common granites in which tourmaline (B), beryl (Be), apatite (P), and micas or fluorite (F) are present at minor (< 5%) to accessory (< 1%) levels (London, 2008). Pegmatites in which lithium aluminosilicates and phosphates, beryl, oxides of Sn, Nb, Ta, and REE, and pollucite are conspicuously abundant constitute only a minute fraction of pegmatites in a group or district. For example, of ~24,000 pegmatites mapped in the Black Hills district (Fig. 7), South Dakota, only 14 mines or prospects were recognized as lithium-bearing (Page et al., 1953). When major worldwide districts of granitic pegmatites were considered, Černý (1991b) estimated that < 2% of all pegmatites qualify for the rare-element classification. The compositions of pegmatite-forming liquids are addressed in a later section, but it is correct to say that pegmatites, even the most evolved ones, have compositions that plot in the field of granite (Streckheisen, 1976).

Table 1
Compositions of pegmatites and the Macusani obsidian.

	Spruce Pine[1]	Swamp[2]	Harding[1]	Tanco[3]	Macusani[4]
Oxide weight percent					
SiO_2	73.87	74.26	75.24	76.04	72.32
TiO_2	0.03	0.02	0.50	0.01	< 0.02
Al_2O_3	15.26	14.73	14.42	13.62	15.63
Fe_2O_3	0.03		0.14	0.01	
FeO	0.30	1.19	0.35	0.15	0.52
MnO	0.15	0.31	0.18	0.18	< 0.06
MgO	0.05	0.10	0.01	0.01	< 0.02
CaO	1.03	0.08	0.20	0.15	0.23
Na_2O	4.87	3.62	4.23	3.81	4.10
K_2O	4.12	5.00	2.74	3.08	3.53
P_2O_5	0.01	0.04	0.13	0.86	0.58
B_2O_3		0.69		0.21	0.62
F	0.00		0.64	0.14	1.30
ppm					
Li	46		3010	3523	3340
Be		2		169	39
Rb	503	221	1941	5680	1160
Cs	0	8	472	3036	580
Nb		8		56	51
Ta				300	24
Sn		5		71	200
Nb/Ta				0.1	1.1
K*[5]	0.36	0.48	0.29	0.35	0.36
ASI[6]	1.06	1.26	1.15	1.06	1.41

[1] Vaughn (1963).
[2] London et al. (2012b).
[3] Stilling et al. (2006), modified by Morgan and London (1987, 1989).
[4] London et al. (1988).
[5] mol K/(K + Na).
[6] mol Al/(Li + Na + K + Rb + Cs + 2Ca).

4. Regional zonation of pegmatite groups

Across a pegmatite group (a large population of pegmatites of common origin), the chemical fractionation and complexity of mineralogical zonation increase with distance from the source. A dense dike swarm adjacent to parental granites consists of common pegmatites (London, 2008), in which textures may be complex, but compositions are essentially those of the haplogranite minimum with minor quantities of micas and accessory amounts of garnet, apatite, or tourmaline. Outward, the pegmatite group expresses increasing chemical fractionation (Černý et al., 1985), which manifests itself in the sequential appearance of normally exotic minerals (Fig. 8). Their generalized zonation applies only to one of two chemical families, as discussed below, but the trend of increasing chemical fractionation with distance from source is regarded as characteristic of most pegmatite groups regardless of their chemical affiliation (e.g., Roda Robles et al., 2012; Hulsbosch et al., 2014). Vlasov (1961) introduced much the same concept of increasing chemical complexity with distance from source, but his presentation conveys the fact that each successive pegmatite body outward from the source inherits all or most of the mineralogical and textural zones of the more proximal pegmatites, with the addition of mineralogically and texturally complex internal zones. For the purposes of mineral exploration, the granitic zones that fully comprise the common, proximal pegmatites (lacking rare-element mineralization) are present

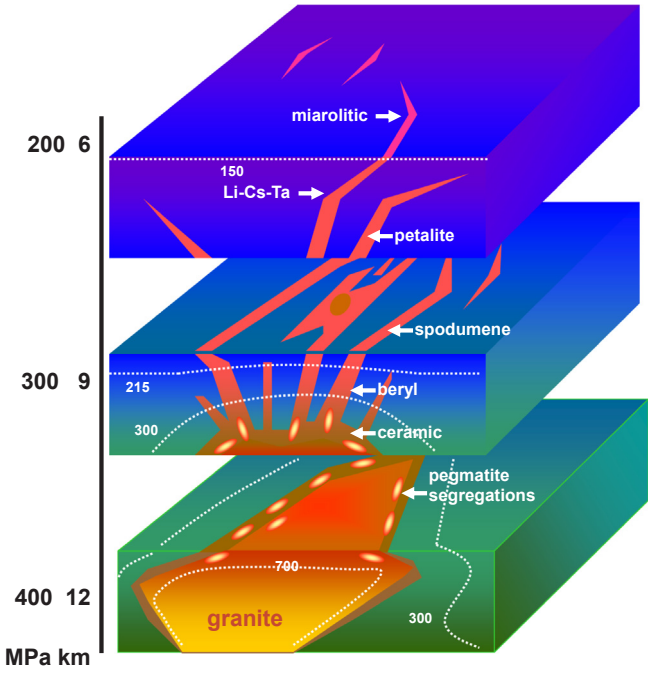

Fig. 8. Regional zonation within a pegmatite group of the LCT family. Pegmatite segregations ("facial pegmatites": Černý, 1991b) form along the upper margin of the pluton. These coalesce upward into the common "ceramic" pegmatites – the principal sources of feldspar and quartz for glass, ceramics, and electronics. Beyond the thermal aureole of the pluton, beryl appears as the first distinctive rare mineral of the rare-element pegmatites. Upward and outward, pegmatites fractionate with the appearance of spodumene-only (high P) or petalite-spodumene (lower P) inner assemblages, and the most evolved, and sometimes miarolitic pegmatites are located at the distal margin of the pegmatite group (see Fig. 7). Dotted white lines are isothermal surfaces. From London (2014a).

along the outer parts of even the most fractionated and distal bodies. Thus, along their margins, barren and rare element-mineralized pegmatites look much alike.

Trueman and Černý (1982) took the sequence of rare minerals that appear with distance from source as diagnostic markers of chemical fractionation in pegmatite-forming melts. Later, Černý (1991a) associated the chemical fractionation through a pegmatite group with the compositional attributes of the source granite. Moreover, he attributed the zonation through a pegmatite group to a similarly stratified and zoned melt within the source magma chamber. Černý (1991a) related the two systems – zoned silicic magma chambers and zoned pegmatite groups – to the process of thermal (Soret) diffusion, as it was originally envisioned by Hildreth (1981) for the Bishop Tuff of the Long Valley Caldera, California. Subsequently, Michael (1983) attributed the chemical zonation of the Bishop Tuff to an increasing extent of crystallization upward, and hence an increasing extent of fractionation in the dwindling interstitial residual liquid.

More recently, the upper portions of large-volume silicic magma chambers have been portrayed as nearly crystal-free liquids based upon the study of pumices (e.g., Hildreth and Wilson, 2007). Chemical models (e.g., Bea et al., 1994) and numerical simulations (e.g., Bachmann and Bergantz, 2004; Lee and Morton, 2015) mostly point to compaction of a crystal mush through crystal settling as a means to extract residual melt upward to the roof of a granitic magma chamber. To this extent, there is similarity between the models for large silicic magma chambers and for the origination of pegmatites along the roof zone of a granite body (Duke et al., 1988, 1992; Černý, 1991b). There is no thick carapace of early-formed granite that separates "facial pegmatites" (Černý, 1991b) from the host rocks for the entire pluton, and the pegmatite dike system, if present, emanates directly from the pegmatitic margin of the pluton. This is problematic for silicic magma chambers as currently understood and for pegmatite-granite relations in particular: if pegmatites are derived only after extended crystallization of larger silicic magma bodies, then the roofward portions of those magmas should be thickly and extensively crystallized (Fig. 9).

Černý (1991b) stressed the similarity of chemical zonation between a pegmatitic granite and its aureole of pegmatite bodies with that of the chemical zonation of erupted tuffs. By this analogy, the first melt expelled from the granite as a dike-forming system would be a small volume of the most differentiated liquid, because the fraction of crystallization is greatest near the roof of the body (Fig. 9a). In this scenario, the pegmatite-forming dikes become less fractionated and more

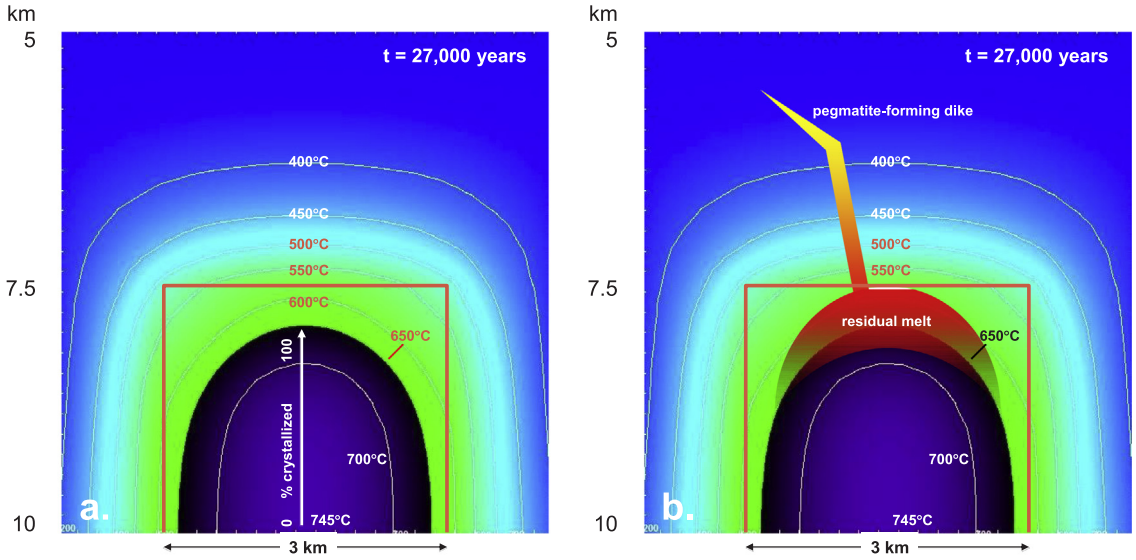

Fig. 9. (a) The distribution of isotherms in and around a granitic pluton of dimensions 2.5(H) × 3.0(W) km (boundaries denoted by red lines) emplaced at a depth of 7.5 km at 27,000 years after emplacement as calculated from the HEAT3D program of Wohletz (http://www.lanl.gov/orgs/ees/geodynamics/Wohletz/KWare/Index.htm, last accessed April 2018). The initial temperature at the top of the pluton, based on a geothermal gradient of 20 °C/km, was 175 °C. (b) As an illustration, this frame depicts the accumulation of late-stage melt and its expulsion as a pegmatite-forming dike from the roof of the pluton. Within 2 km of the granite margin, the pegmatite-forming dike spans a temperature gradient of 250 °C (600° → 350 °C) in the host rocks.

voluminous toward their source pluton as melt deeper in source drains out of the less crystalline and less fractionated portions of the granitic magma chamber. These chemical variations are manifested in ash-flow tuffs, but the chemical stratification is inverted upon eruption (Hildreth and Wilson, 2007).

5. Chemical affinities of granites and their pegmatites

5.1. Pegmatite families

Černý (1991a) proposed that the trace-element signatures of pegmatites fall into two distinct categories, which he referred to as pegmatite families. His two proposed families were LCT (Li-Cs-Ta) and NYF (Nb-Y-F), with the understanding that the signature of the family appears only in the most fractionated members of a group in the form of exotic minerals such as spodumene, tantalite, pyrochlore, pollucite, etc. Some trace elements were omitted from the three-element diagnostic because they are enriched in both families, but Černý (1991a) included them in the more descriptive characterization of the pegmatite families. The common granitic pegmatites, which are the vast majority of them and which are sources of ceramic and industrial minerals, are not included in the classification by family at all, though the chemical attributes of the family may be evident in the rock-forming mineralogy and its trace-element signature.

Černý's (1991a) chemical affiliation by family was not meant to apply to any particular pegmatite body, nor to be used as a guide to exploration for rare-element ores. It was proposed to establish a lineage between a pegmatite group and its parental granite, and it is only truly useful when the highly fractionated bodies of a pegmatite group are known. As intended, however, the classification works well, as much as can be expected of a two-tier model for a potentially endless variation of trace-element patterns in granites.

5.2. The LCT family

In Černý's (1991a) classification, the LCT pegmatites are affiliated with S-type granites (Chappell and White, 2001) that originate from marine sedimentary material, which is predominantly black shale. Following from that marine shale source, the characteristic of the LCT pegmatites includes enrichment in the three signature elements, but also in Be, Rb, Ga, Nb, Sn, B, P, and F. The lowest-melting fraction of metasedimentary micaceous rock is dominated by the reaction muscovite/paragonite + sodic plagioclase + quartz + H_2O = liquid, which produces a markedly potassic liquid composition with an ASI[1] of 1.3 in H_2O-saturated melt at 200 MPa (e.g., Icenhower and London, 1996; London et al., 2012a). High quantities of rare alkalis are incorporated in the clays (e.g., Wahlberg and Fishman, 1962) that become white and dark micas in the metamorphic products. Boron derived from seawater is adsorbed and include in the detrital sheet silicates and in serpentine formed during the hydrothermal alteration of adjacent oceanic crust (e.g., James and Palmer, 2000; Pabst et al., 2011). Much of that boron is incorporated in tourmaline that is stable to high metamorphic grade (e.g., Dutrow and Henry, 2011), but some is retained in micas. The high P content of the granites (Chappell, 1999) stems from biogenic apatite in marine sediments (Coveney, 2000); that high-phosphorus signature is manifested in pegmatites as amblygonite-montebrasite, lithiophilite-triphylite, arrojadite, triplite, and others in addition to apatite. Fluorine is also enriched in shales with an average of 1050 ppm F in a few analyses, nearly an order of magnitude greater than their chlorine content (Coveney, 2000).

Enrichments in Sn and Ta that are associated with the S-type granites and their pegmatites also can be traced to a marine source. Exhalative tin metal and Sn-Pb mixtures have been reported from sediments above fast-spreading oceanic ridges (e.g., Dekov et al., 1996). Detrital cassiterite is enriched in placers associated with near-shore platform deposits (e.g., Yin, 2000), and these may be incorporated with other deep-sea and mélange deposits during the tectonism that leads to the formation of S-type granites. A similar process of enrichment by authigenic or detrital processes might apply to Ta as well. The geochemical twins of Zr/Hf and Nb/Ta are highly fractionated from seawater onto the surfaces of Fe-Mn oxide particles of marine origin (Schmidt et al., 2014). Thus, elevated concentrations of Hf and Ta and of their Hf/Zr and Ta/Nb ratios that are hallmarks of the LCT pegmatites (Černý et al., 1985) have a plausible source of pre-enrichment in marine sediment.

REE abundances in the LCT pegmatites are negligible, largely owing to their high-silica and peraluminous liquid compositions in which REE are highly insoluble (< 500 ppm total REE: Duc-Tin and Keppler, 2015). Chondrite-normalized profiles of feldspars from the peraluminous South Mountain granites, Nova Scotia, tend to show a smoothly decreasing REE abundance from La to Yb, but large and erratic fluctuations in abundance with atomic number of the REE in their pegmatites (e.g., Kontak and Martin, 1997). The same generalization holds for tourmaline from margin to core in the Bob Ingersoll pegmatite, associated with the peraluminous, S-type Harney Peak granite: decreasing total REE and erratic patterns (Jolliff et al., 1987). The "tetrad effect" (Masuda and Ikeuchi, 1979), in which the REE pattern is broken into four segments, either concave or convex up, applies to apatite and zircon in other pegmatites of the LCT family (e.g., Liu and Zhang, 2005; Tang and Zhang, 2015).

Initial $^{87}Sr/^{86}Sr$ data that might elucidate the source characteristics of pegmatites or the relations of pegmatites to their host rocks are sparse. Peraluminous, beryl- and tourmaline-bearing pegmatites of the Middletown district, Connecticut, gave initial $^{87}Sr/^{86}Sr$ values of 0.743 for mineral separates (Brookins, 1986) and 0.7300–0.790 for whole rock samples from the Hale quarry, Portland (Methot, 1973). Initial $^{87}Sr/^{86}Sr$ ratios for albite and perthite from the Harding pegmatite, New Mexico, are 0.9010 and 3.6492, respectively, and micas lie at the high end of this range (Brookins et al., 1979) Whole-rock $^{87}Sr/^{86}Sr$ values for the Tanco pegmatite, Manitoba are ~0.81 (Camacho et al., 2012). If nothing else, this smattering of data reflects extremely Rb-rich sources of these pegmatites, which would be consistent with their derivation from the same parental materials as are S-type granites.

The LCT family of pegmatites and their peraluminous parental granites arise from anatexis of mostly juvenile (not previously melted) accretionary sediments in response to crustal thickening that accompanies continental collisions. The granites and their pegmatites almost always lack deformation or foliation other than minor flow features. Hence, they tend to be generated and emplaced in the waning stages of tectonism, after crustal thickening and the accumulation of radiogenic heat are sufficient to induce anatexis (see Bea, 2012).

Though Černý and Ercit (2005) note that the LCT pegmatites are derived "less commonly from I-type granites", they cite the general characteristics of this association as "subaluminous fertile granites and derived pegmatites poor in Cs, B, P…" The I-type granites, therefore, do not produce pegmatitic bodies that belong with the LCT lineage. Černý et al. (2012) make the further point that I-type granites generally do not spawn pegmatites at all, unless they contain manifestly elevated amounts of B or of F. In that case, the sources of the granites are mixed: they contain a component derived ultimately from seawater in the form of marine sediment, water expelled from marine sediment (e.g., Bebout et al., 2007; Mallik et al., 2016), or hydrothermally altered oceanic crust (e.g. Palmer and Swihart, 1996). Insofar as the I-type granites arise as direct melts from the mantle, or by remelting of ponded basalt, they are not sources of B that culminates in tourmaline-rich pegmatites (Ottolini et al., 2004) as, for example, in the Sierra Nevada batholith, California (J. Lawford Anderson, personal communication, 2012).

[1] ASI is molar Al divided by the sum of charge-balancing mono- and divalent cations, and usually expressed as Al/(Na + K + 2Ca) for simple granitic compositions.

5.3. The NYF family

Černý's (1991a) designation of NYF follows from a preponderance of Nb-dominant oxides (columbite, pyrochlore, ilmenorutile, euxenite, and fersmanite), an enrichment in HREE and Y in silicates and oxides, and from high F content with the common occurrence of Y-rich fluorite or of topaz. In their major element chemistry, the NFY pegmatites are subaluminous or metaluminous to weakly peralkaline as a result of Na in aegirine, but always quartz-saturated. Biotite is the dominant mica in the NYF pegmatites, as opposed to muscovite in the LCT family. Minerals of Zr including zircon and others, and of Ti including oxides and silicates, are common accessories. The NYF pegmatites are also markedly U- and Th-rich.

Černý and Ercit (2005) associate the NYF pegmatites principally with the A-type granites (A for anorogenic), which are a component of the bimodal gabbro-granite magmatism found in rift zones. Their sources have been ascribed to fractionation of direct partial melts from the upper mantle, to the remelting of basalts that accumulate beneath the thinned lithosphere, and to the partial melting of lower-crustal gneisses (e.g., Eby, 1990; Christiansen and McCurry, 2008). The granites and their pegmatites show kinship to the more alkaline suites found in association with crustal extension over mantle plumes within continents (e.g., Pirajno, 2015; Dostal, 2016). Though the principal mineralogy of the more silicic members of both suites is not much different, the entire collection of igneous rocks are markedly unlike one another. Magmatism associated with mantle plume heat sources (hot spots) is pervasively alkaline to peralkaline, mostly silica-undersaturated, rich in Ca and in P, with LREE enrichment prevailing, and ending with igneous carbonatites. In the advanced rift setting where A-type granites prevail, the mafic and felsic melts are mostly metaluminous, near or above silica saturation at all stages, with the granites notably depleted in Ca and P and possessing HREE enrichment. In the NYF pegmatites, mineralization is unmistakably primary, meaning magmatic in origin. In the more alkaline granites and syenites associated with mantle hot-spots, hydrothermal reworking of the primary pegmatitic assemblages is the rule (e.g., Gysi and Williams-Jones, 2013).

In a review, Ercit (2005) acknowledged that the NYF pegmatites are little-studied as compared to the more common peraluminous pegmatites that follow the LCT fractionation trend. The NYF subdivisions, are, however, quite varied in their combinations of elemental enrichment (Černý and Ercit, 2005). The NYF pegmatites and their granites are variously described as enriched in Be, Sn, Ta, and B, elements that are exceedingly depleted in peridotite and basalt (e.g., Ercit, 2005; Ottolini et al., 2004).

Černý and Ercit (2005) also associated the NYF family with I-type granites, with an emphasis on their F-rich character as an abundance of topaz. These could include, for example, the Mole granite, Queensland, Australia: a well-documented I-type that culminates in topaz-quartz veins, sometimes with beryl (Audétat et al., 2000).

6. Pegmatite families through geologic time

McCauley and Bradley (2014) elucidated the secular trends in the abundances of pegmatites based on radiometric ages derived mostly from zircon, and they associated pegmatite occurrences with their LCT and NYF affiliation where possible. They observe that the abundances of all pegmatites and of the rare-element pegmatites as subsets thereof correspond to the major intervals of global continental assembly from the Archean to the Neogene. For the LCT pegmatites, major spikes in their occurrence fall at ~2913, 2687, 2501, 1853, 1379, 1174, 988, 525, 483, 391, 319, and 72 Ma. Among the NYF types, for which only 20 data points were found, ages cluster around 2638, 1800, 962, 529, 485, 371, 309, and 274 Ma. Occurrences of the LCT pegmatites show maxima near the end of the Archean and in the Paleozoic. Those of NYF affinity peak at ~1000 Ma in the Proterozoic, coincident with the Grenville orogeny in what was Laurentia.

For the LCT pegmatites, ore resources of Li coincide with the cumulative peaks in the Archean and the Paleozoic (McCauley and Bradley, 2014). Those in the Archean derive mostly from the Greenbushes, Tanco, and Bikita pegmatites. Paleozoic deposits are dominated by pegmatites at King's Mountain, North Carolina, in the Appalachians. Principal ores of Ta are concentrated in the Archean, in the above-mentioned pegmatites led by Tanco.

7. Internal structure of pegmatites

7.1. Unzoned pegmatites

Not all pegmatites exhibit internal zonation – segregations by texture, mineralogy, or crystal size. Common pegmatites that lack internally heterogeneous fabrics are defined solely by their coarse grain size (several cm or larger) in relation to typical plutonic rocks. Plagioclase and quartz are anhedral and of uniform size, while K-feldspar tends to be porphyritic and commonly exhibits skeletal or graphic granite intergrowths (Fig. 6). Rock fabric is isotropic, meaning that crystal distributions and orientations appear as random (Fig. 5–8a of London, 2008) or oriented with prominent branching K-feldspar megacrysts that grew off of screens of host rock (e.g., Fig. 5–8c of London, 2008). Such pegmatites lie within the cupolas and in close proximity to the margins of their small, leucocratic source granites. The unzoned common pegmatites are the principal ore sources of feldspar, quartz, and mica. They include the "ceramic" pegmatites of Glover et al. (2012), the "pegmatitic granites" of Goad and Černý (1981), and the "granite and pegmatoid" of Vlasov (1961).

7.1.1. Unzoned spodumene pegmatites

Nothing in the study of pegmatites has adequately accounted for the fine-grained, unzoned, and homogeneous fabrics of a few economically important occurrences of spodumene pegmatites. Like the common pegmatites, these are mostly homogeneous rocks, in which spodumene tends to be slightly porphyritic to crystals of about 10 cm. Unidirectional solidification, mineral layering, and an organized spatial zonation of textures or assemblages are mostly absent. Deposits at Kings Mountain, North Carolina, represent the archetype of these pegmatites (Swanson, 2012). Much of the texture of the spodumene-bearing pegmatites is aplite containing sporadic "pods" of the coarser-grained porphyritic spodumene pegmatite (Swanson, 2012). The host rocks to the spodumene-bearing pegmatites at King's Mountain are amphibolites, but Swanson (2012) relates the pegmatites back to larger masses of granite that possess the chemical and isotopic signatures of derivation from aluminous gneisses and schists, and hence an LCT chemical affinity. The degree of chemical fractionation of the pegmatites is not unusual, but the fine-grained size and uncommonly homogeneous rock fabric are. The vast majority of mineralogically similar spodumene-bearing pegmatites exhibit the sharply bounded zonation by mineral assemblage and texture as described below.

The recent discovery of the Jiajika granite-pegmatite deposit in Sichuan, China, makes it the largest Li ore body in Asia (Chou and Li, 2014). Its drilled resource estimate of ~0.89 MT of Li metal (Tao Huang et al., unpublished data, 2017) puts it in the same class as the Greenbushes pegmatite, Western Australia (Kesler et al., 2012). Jiajika, however, is an unzoned body of mostly very-fine to fine-grained spodumene (sub-millimeter to several cm) aplite and pegmatitic granite that consists of multiple pulses of dike intrusions together with veining (Tao Huang et al., unpublished data, 2017). As a super-giant unzoned Li pegmatitic deposit, it is also unusual for its young age, 216 ± 2 Ma, and its host rocks, which are staurolite-bearing aluminous schists (Tao Huang et al., unpublished data, 2017).

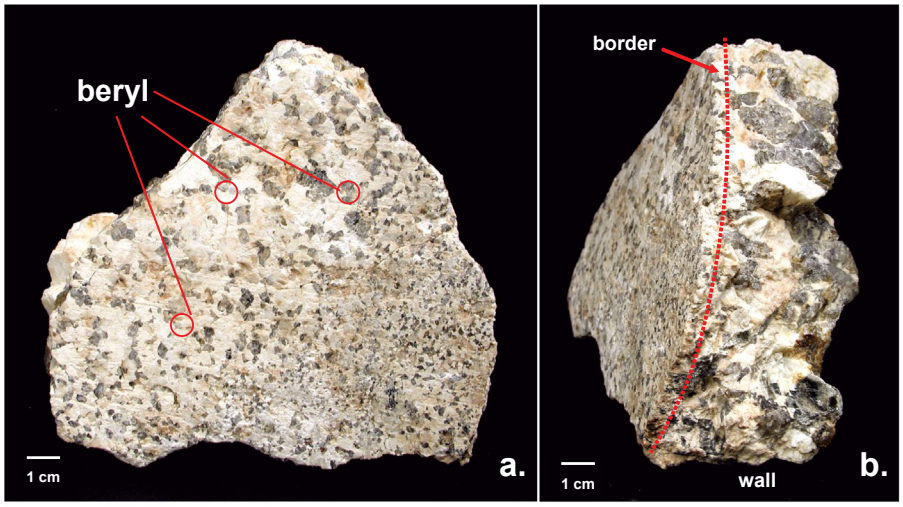

Fig. 10. Border and wall zone, Case #1 pegmatite, Portland, Connecticut. (a) A rare view of any pegmatite dike shows the variable density of crystal nucleation at the contact surface with the host rock. Red circles denote the locations of light-blue beryl crystals at the contact. (b) The thin border (~4 mm) transitions sharply into coarse-grained UST with skeletal gray quartz and creamy K-feldspar. The beryl crystals that nucleated on the surface do not project to the opposite surface on the wall zone (i.e., the pegmatite was undersaturated with respect to beryl only a few cm into the dike). Beryl shows up again in abundance in and along the quartz core of this body. From London (2008).

7.2. Zoned pegmatites

Pegmatites exhibit internal fabrics that are generally far more complex and diverse than are seen in other plutonic rocks. Three different aspects of fabric come into play: the habits of individual crystals, the orientation of the long axes of crystals, and the spatial segregation of minerals by zonal assemblages. Most of the terms that are in use today to describe the internal zonation were established by Cameron et al. (1949). These are reviewed by London (2008, 2014a), and readers are referred to any of these sources for details. With few additions, the essential components of a zoned pegmatite are:

7.2.1. Border zone

Border zones consist of a thin (1–3 cm) rind of fine-grained granitic rock at the contact with hosts (Fig. 10). Granophyric texture (microcrystalline intergrowths of quartz in feldspar) are common (Fig. 11). The mineralogy is dominantly plagioclase-quartz-muscovite, but the border zone is also one of the most mineralogically diverse units in pegmatites, commonly containing garnet, apatite, tourmaline, beryl, biotite, and columbite (Fig. 11). The anorthite component of plagioclase starts near An_{10-20} but falls rapidly inward.

7.2.2. Wall zone

Inward from the border, the wall zone is marked by an abrupt increase in crystal size (Fig. 10) and the development of UST, which is synonymous with comb texture and stockscheider. In UST, crystals are elongate perpendicular to the contacts of the body and they expand (flare) inward. Minerals that exhibit pronounced UST include K-feldspar, tourmaline, micas, and beryl. Skeletal and graphic intergrowths are prevalent. Cameron et al. (1949) noted that the mineralogy of the wall zones was essentially the same as that of the border, except with the addition of K-feldspar. The two zones, therefore, are distinguished

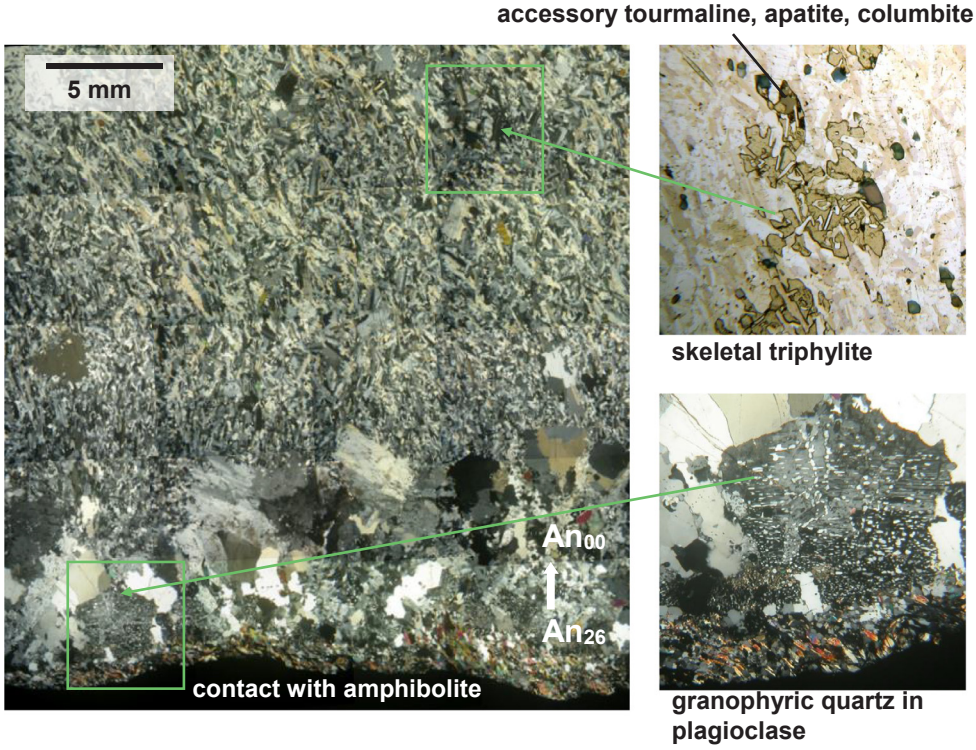

Fig. 11. Despite the size of the Tanco pegmatite (average ~40 m thick), Manitoba, its lower border zone possesses a granophyric intergrowth of quartz + plagioclase at the contact with amphibolite. The plagioclase composition in the granophyre is An_{26}, but the An content falls to zero within a few hundred micrometers. Inward, the texture is one of UST plagioclase with sieve-textured tourmaline and skeletal, inward branching crystals of triphylite, $Li(Fe,Mn)PO_4$. Ferrocolumbite and apatite are accessory minerals. From London (2015a).

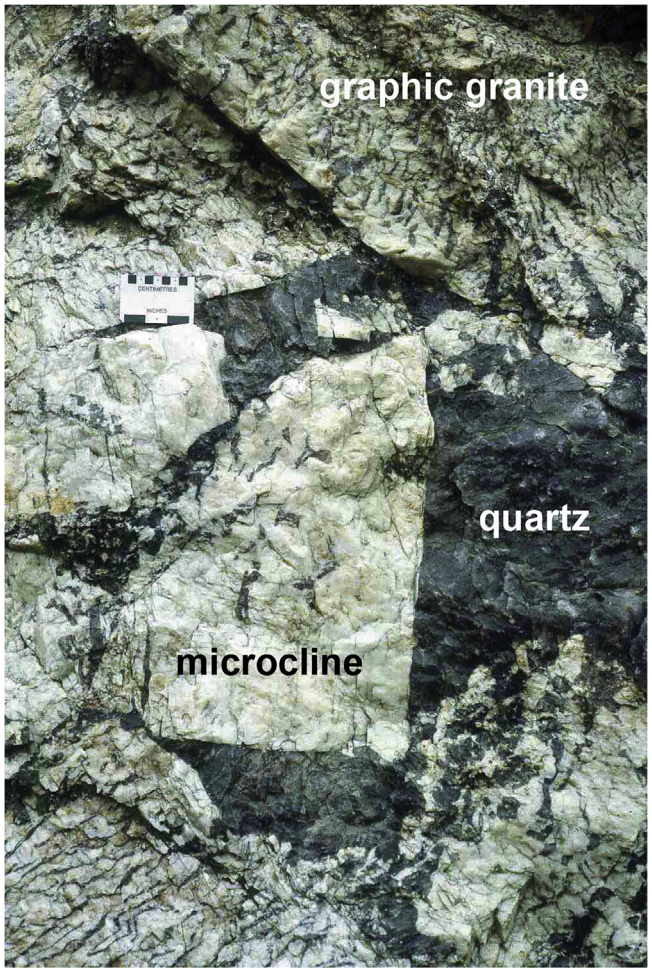

Fig. 12. The transition from graphic granite to monophase K-feldspar and quartz in the core zone of the Hale quarry, Portland, Connecticut.

principally on the basis of their textures. Üebel (1977) lumped the border and wall zones together into what he termed the pegmatite "shell" because of the prominence of anisotropic fabrics and fine grain size, including aplites and graphic granite intergrowths.

7.2.3. Intermediate zones

Inward from the wall zone, graphic granite intergrowths segregate into monophase K-feldspar and quartz of large crystal size (e.g., Fig. 12). Crystals are more equant, and those that are not rooted in the wall zone substrate become more random in their orientations (the term "jack-straw" has been used to describe random orientations of elongate crystals in the intermediate zones: Jahns, 1953). Cameron et al. (1949) and Norton (1983) identified a number of different intermediate zones, but most are variations on the modal abundance of K-feldspar, quartz, muscovite, and sodic plagioclase. Compared to the outer zones, the intermediate zones are richer in K-feldspar, and quartz increases in abundance. Lithium aluminosilicates and phosphates in quartz-rich assemblages constitute the innermost intermediate zones of most pegmatites of the LCT family.

The intermediate zones are abruptly coarser-grained than the border and wall zones. This sharp increase in crystal size is evident in Fig. 13, taken from Jahns (1953). Jahns (1953) derived this relationship of crystal size with position in the pegmatite from bodies of nearly the same thickness (~12 m). However, the sizes of crystals in the intermediate zones scale to the width of the pegmatite body: thicker bodies possess fewer (per unit volume) and larger crystals in their interior zones, which is not true of granites, but which is generally true of

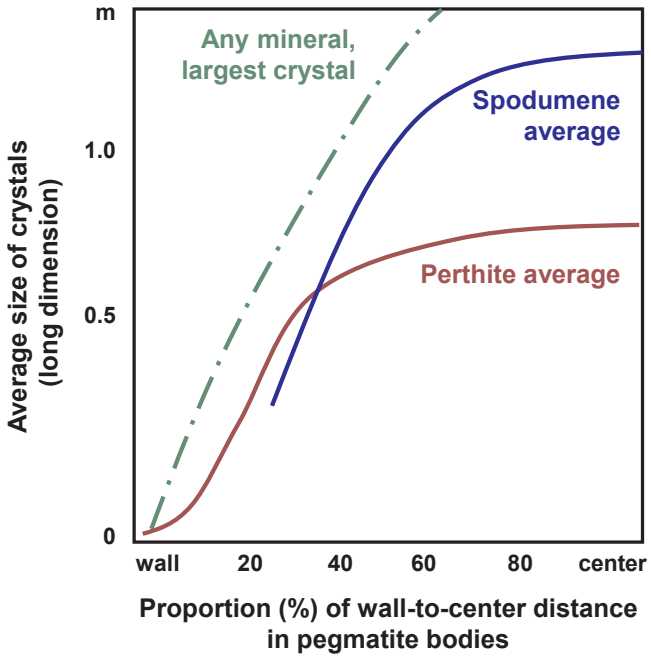

Fig. 13. Curves showing grain-size variations in large, zoned pegmatite bodies in the Hualapai, Bagdad, and White Picacho districts of western Arizona. From Fig. 11 of Jahns (1953).

hydrothermal veins.

7.2.4. Core

The core of most pegmatites is recognized as pure quartz. This position in the zoning sequence has conveyed the intended meaning that the quartz cores of pegmatites are the last units to form (Cameron et al., 1949). Jahns (1982) took exception later, stating that the quartz cores formed simultaneously with the more feldspathic marginal and intermediate zones. Jahns (1982) offered no evidence for this claim, but the constraints imposed by the crystallization of a eutectic composition at equilibrium on the solidus required it. Burnham and Nekvasil (1986) stated that the quartz cores must be largely hydrothermal in origin because in their understanding, a granitic melt of eutectic composition could not precipitate a monominerallic assemblage.

In Li-rich pegmatites, quartz bodies are not the last units. For example, Jahns and Ewing (1977) recognized a quartz-deficient mass of spodumene-albite-lepidolite with accessory apatite, beryl, and microlite as the principle core unit of the Harding pegmatite, New Mexico. Norton (1983) revised the classification of Cameron et al. (1949) to make the last-formed primary zone one rich in albite and lepidolite or spodumene, and with an abundance of rare-element minerals including beryl, phosphates, oxides, etc. In experiments with the Li-rich Macusani obsidian, London and Morgan (2017) succeeded in producing an albite-lepidolite assemblage that followed the crystallization of a pure quartz domain (Fig. 14).

7.2.5. Aplites, miarolitic cavities, and replacement bodies

Cameron et al. (1949) deemed each of these units to be insignificant based on their abundance in the pegmatite districts studied during the WWII mapping effort. Jahns (1953) largely concurred, but later (e.g., Jahns and Tuttle, 1963) placed much more significance on paired aplite-pegmatite bodies and the occurrence of miarolitic cavities based on his examination of pegmatites in San Diego County, California (e.g., Jahns, 1954, 1979).

In the U.S., Landes (1933) ascribed rare-mineral assemblages to an origin by replacement of pre-existing common granitic pegmatite via interactions with externally derived fluids. Subsequently, any units or

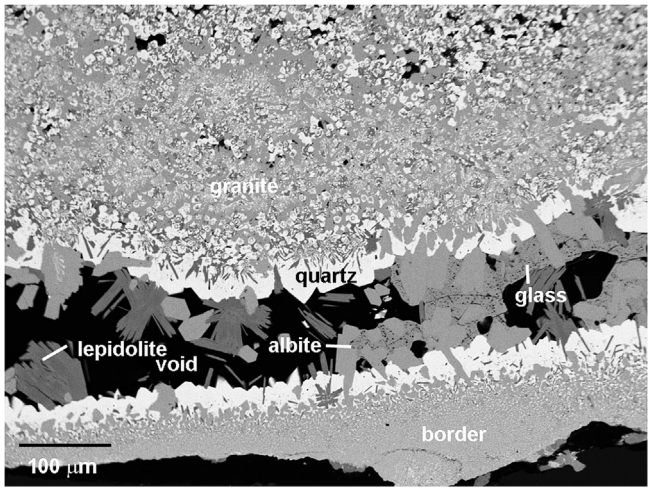

Fig. 14. A Si K α X-ray intensity map along the lower edge of MAC 229 (details in London and Morgan, 2017) shows variations in the abundance of quartz with crystallization toward a miarolitic cavity. Quartz is absent in that cavity, which contains only albite and lepidolite in addition to glass.

zones whose compositions deviated substantially from that of granite, and especially any monominerallic bodies, have been widely described as replacements of previous assemblages, especially by Soviet petrologists through the 20th century. In addressing Landes' (1933) concept, Cameron et al. (1949) acknowledged that some replacement of pre-existing pegmatite does occur in the more evolved pegmatites, but they viewed that as a normal consequence of peritectic reactions that should follow from the increasingly differentiated pegmatite-forming melt and earlier, less fractionated mineral assemblages. In the vast majority of cases, however, textural evidence for replacement, including resorption or pseudomorphism of prior crystals, is lacking. Healed fractures in quartz and perthitic exsolution in alkali feldspars are the most commonly observed subsolidus textures in pegmatites.

7.3. Patterns of zonation within pegmatites

7.3.1. Concentric zonation

Pegmatites of steep dip (when that dip reflects their attitude upon emplacement) have a tendency to exhibit bilateral symmetry from both margins toward center (Fig. 15). Zonation is symmetrical and concentric about the center line (in 2D, the line along which crystallization fronts merge from both sides), which occupies a more or less central location along the axial plane of the body (Cameron et al., 1949). As depicted by Cameron et al. (1949), Jahns and Burnham (1969), and many others, steeply dipping pegmatites acquire an increasing number of more chemically evolved internal zones in their upward direction. However, those same illustrations show the width of pegmatite bodies increasing upward, and there is a pronounced correlation between the width of a pegmatite body and the extent of its internal fractionation (see 7.4 Relations of Zonation to Dike Geometry below).

7.3.2. Layered zonation

In contrast, pegmatites with a shallow dip of emplacement tend to exhibit layered structure parallel to their contacts. Zonation by mineralogy and texture is not symmetric from side to side, and the dike center line lies above (or rarely below) the central axial plane of the body (Fig. 16). Norton (1983) proposed 24 possible zones in layered pegmatites, but the structure is much simpler. As is the case for concentric pegmatites, the first-formed units, border and wall zone, are markedly feldspathic. In what is thought of as the normal zoning sequence (Jahns and Burnham, 1969; Jahns, 1982), fine-grained sodic plagioclase predominates the footwall assemblage, while exceedingly coarse-grained potassic feldspar is enriched along the hanging wall. In San Diego County, California, where Jahns developed his model, approximately half of dikes examined by and figured in London (2008) show a reverse of this zonation, with K-feldspar prominent along the footwall portion, and plagioclase-rich assemblages along the hanging wall (e.g., Figs. 3, 16).

7.3.3. Layered aplites

Layered aplites, also known as "line-rock", are common units in layered pegmatites (Figs. 3, 16), where they normally occupy the footwall portion of a dike (but not always: London, 1985). Nearly pure albitic aplites occur in some layered pegmatites (e.g., Tanco: Černý, 2005), but most such bodies consist of rhythmic oscillations dominated by plagioclase plus quartz (light) versus K-feldspar plus mafic (dark) layers. Though analyses are scarce, the bulk compositions of layered aplites are more sodic than the granite minimum compositions but granitic in composition nonetheless (Jahns and Tuttle, 1963, Rockhold et al., 1987; Webber et al., 1997; Kleck and Foord, 1999; London et al., 2012b). Three chemical analyses through a layered aplite (same as in Fig. 16) from Ramona, California, show them to be close to the granite minimum (Table 2). Though Jahns (1982) represented the layered aplites as the first zone along the footwall side of the dike, that is incorrect in most occurrences: an intervening border and wall zone as described above separates the layered aplites from the lower contact of the pegmatite body. It is this asymmetric distribution of the line rock zone, usually lying on the footwall side between the lower wall zone and the overlying intermediate zone, that displaces the center line of the pegmatite body to a position approximately two-thirds of the way above (or below) the margins of these dikes.

Jahns (Jahns and Tuttle, 1963; Jahns, 1982) viewed the aplitic and pegmatitic portions of pegmatites as simultaneous and complementary parts of the same magma body. However, the aplites always serve as the substrate for the adjacent overlying pegmatite, which is an intermediate zone with UST that is paired with a similar zone along the hanging wall of the pegmatitic portion of paired aplite-pegmatite dikes (Figs. 3, 5, 16). Morgan and London (1999) and London et al. (2012b) used the compositions of garnets and plagioclase to determine that the footwall portions of the Main Dike at Ramona, California, were mostly crystallized through the zone of layered aplite before the rest of the overlying pegmatitic portion formed. The footwall units, including aplite, therefore, preceded all of the coarse-grained intermediate zones of the pegmatite (e.g., Černý, 2005; see Chapters 7 and 8 of London, 2008).

Aplitic line rock sometimes exhibits flat parallel layering, or complex contortions that may or may not be mechanical folds (Fig. 17). Some line rock units possess UST that is perpendicular to layering (e.g., Webber et al., 1997), which would not be the case if the layering arises from viscous flow. Contortions in layering can arise when layers grow around a phenocryst, such as K-feldspar or quartz (Fig. 18).

In the Jahns-Burnham model (1969), aplites are the result of supersaturation of melt when aqueous fluid extracts K from the melt and conveys it upward through the buoyancy of the aqueous bubbles. London (2008) detailed numerous problems with this hypothesis, including (1) experimental evidence that the aqueous fluid in equilibrium with haplogranitic melt is slightly more sodic than potassic (also see Burnham and Nekvasil, 1986), and (2) the inferred addition of K to the pegmatite-forming melt on the hanging wall would displace its composition a commensurate distance from the eutectic as along the sodic footwall, thereby bringing both domains of melt to a similar degree of supersaturation.

An additional problem is evident in the assumption that aqueous bubbles would rise rapidly through viscous melt (Burnham and Nekvasil, 1986). As explained in London (2008), the solution of Stokes's Law for the velocity at which a vapor bubble 1 mm in diameter (as proposed by Burnham and Nekvasil, 1986) would rise through the chilled melt along the footwall boundary of a pegmatite yields an ascent rate of $9*10^{-12}$ m/s, which is < 0.3 mm/year. With a viscosity of 10^5 Pa s for H_2O-saturated granitic melt at 700 °C upon emplacement, the

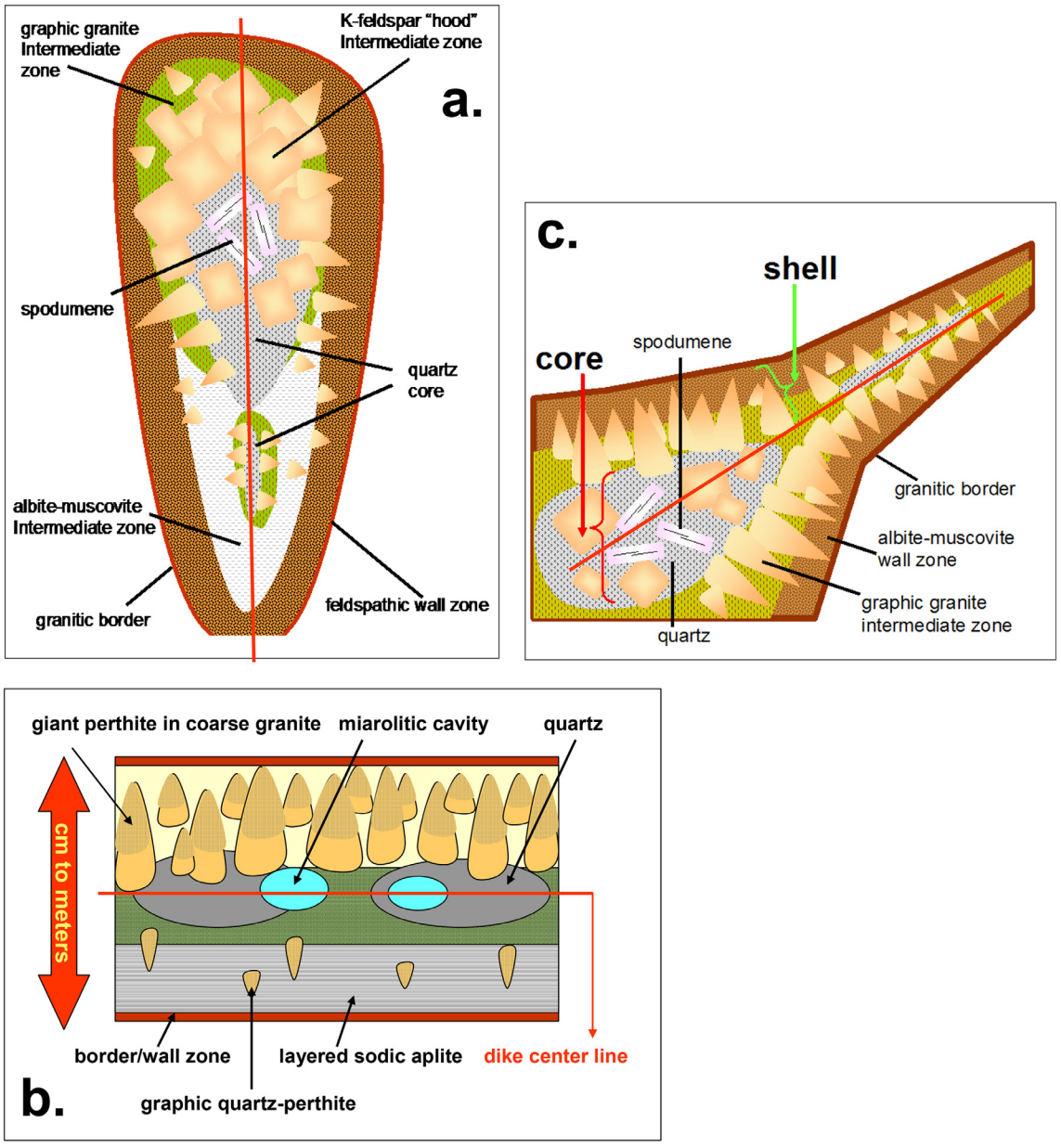

Fig. 15. Schematic representations of subvertical, subhorizontal, and tapering pegmatite dikes as represented by (a,b) Jahns and Burnham (1969) and (c) Üebel (1977). (a) Zonation is bilaterally symmetrical about the dike center line (heavy red line), but the more potassic and chemically fractionated zones are displaced toward the top, which was also depicted as the widest portion of the dike. (b) A subhorizontal layered dike possesses an sodic aplite footwall, giant K-feldspar hanging wall, central quartz core, and plagioclase-rich pegmatite with miarolitic cavities. As depicted by Jahns and Burnham (1969), the center line of the dike occupies the midpoint of the dike; in actuality, it is displaced upwards because this rendition does not include the potassic lower wall zones that are prevalent in these dikes. (c) As noted by Üebel (1977), dikes that taper upward are generally less fractionated than their lower, thicker portions.

ascent rate of a 1-mm bubble is only 2.8 cm/year. In neither case is bubble ascent viable for pegmatite-forming dikes if their rates of cooling to their glass transition (viscosity $\geq 10^{12}$ Pa s) are in the range of days to a few tens of years at most (see 8.2.4 Conductive cooling models below).

Kleck and Foord (1999) proposed that layered aplites arise from crystal settling. Using the same boundary conditions as above, London (2008) demonstrated that the settling rate of a 1 mm grain of albite, for example, was near zero on the time frame of cooling. Moreover, the layering in line rock parallels the contact, even when the contact turns vertical (Fig. 8-3 of London, 2008).

Most explanations of layered aplites invoke the episodic exsolution of an aqueous fluid (Jahns and Tuttle, 1963; Rockhold et al., 1987; Webber et al., 1997) or crystal settling (Kleck and Foord, 1999), though the mechanistic connection between the process and the texture has not been rationalized or validated. London (2014a) suggested that the formation of the fine-grained aplites was a normal consequence of sharp changes in the nucleation density of crystals as a function of liquidus undercooling. Given the diversity of compositions and observed fabrics, it is unlikely that a single process could account for all such rocks.

7.3.4. Miarolitic cavities

Miarolitic cavities are most commonly found along the center line in the subhorizontal layered pegmatites (Fig. 19). The prevalence of open- or clay-packed miaroles in subhorizontal pegmatites (Fig. 20) has historically been attributed to shallower levels of emplacement as compared to the non-miarolitic pegmatites (e.g., Černý, 1991a). That presumption is predicated on the increasing molar volume of aqueous fluid

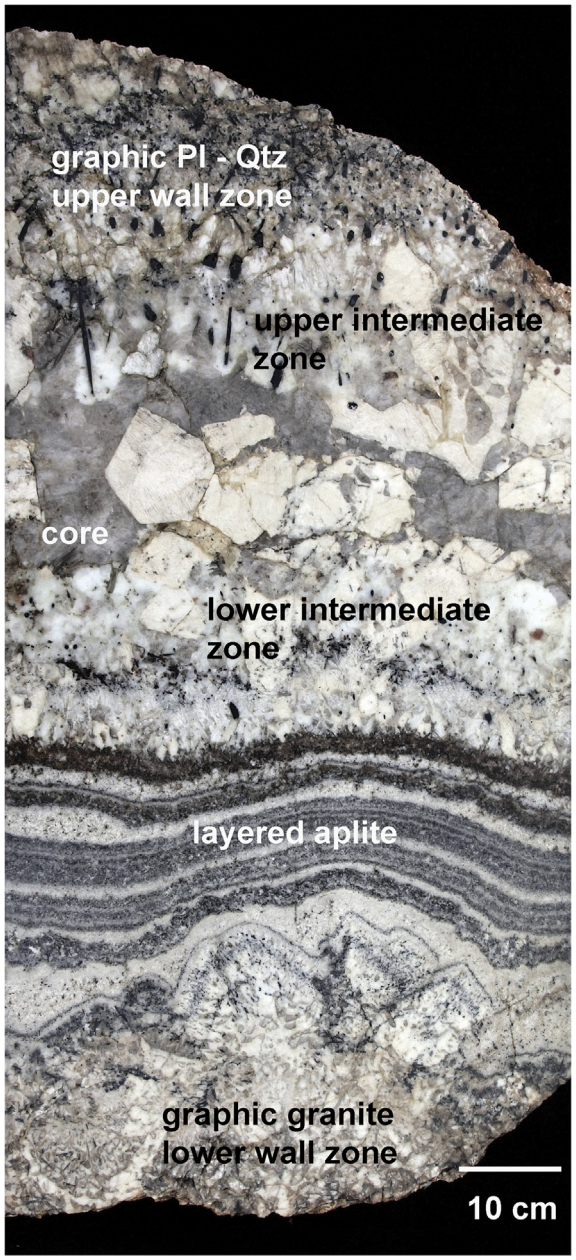

Fig. 16. A complete cross section of a small dike from the Little Three mine, Ramona, San Diego County, California. Also see Fig. 5.

Table 2
Normative compositions of aplite, Little Three mine, California. See Fig. 16 and Fig. 4 of London et al. (2012b).

	Qtz	Ab	An	Or	C
LT3-4f	37.20	37.33	3.35	15.68	2.50
LT3-4e	37.10	35.06	2.76	19.38	2.30
LT3-4d	37.02	33.54	2.91	20.49	2.34
AVG	37.11	35.31	3.01	18.52	2.38
SD	0.09	1.91	0.31	2.52	0.11

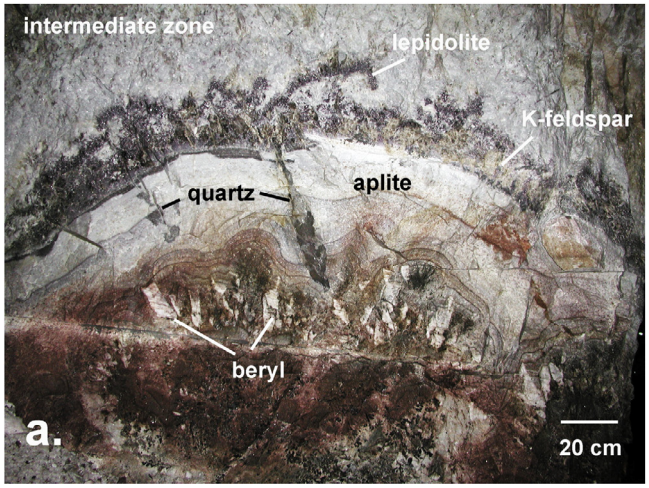

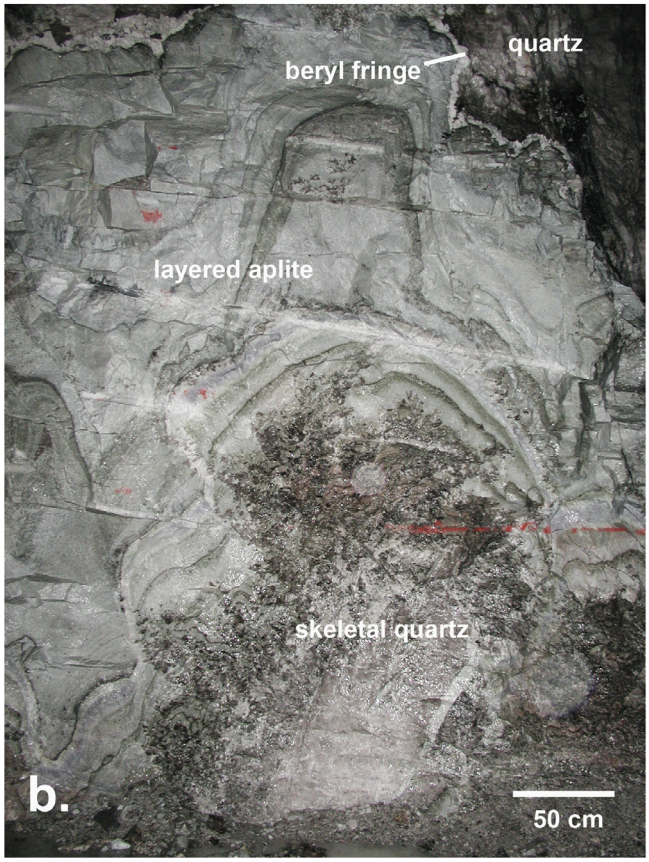

Fig. 17. Layered aplite at the Tanco mine, Bernic Lake, Manitoba. (a) A small exposure of a domed portion of the lower wall zone, which includes beryl (white) with prominent UST, is overlain by layered aplite through which a couple of skeletal quartz crystals have grown from below. Above the aplite, texturally complex aggregates of lepidolite and K-feldspar grew upward from the aplite surface into a plagioclase-rich domain that is the lower surface of what would be called the lower intermediate zone at Tanco. (b) An arborescent quartz crystal at the top of the lower wall zone is overlain by layered aplite. A monomineralic layer of white beryl separates the aplite from the quartz core.

with decreasing pressure at high temperature (Burnham et al., 1969): equivalent masses of aqueous fluid occupy more space at lower pressures. London (1986b) noted that many of the most important gem-producing miarolitic pegmatites (Brazil, Afghanistan, United States) contain the assemblage spodumene plus quartz.

This constrains those pegmatites to have crystallized at pressures in excess of 200 MPa (Fig. 21), which is not much different from that of the massive spodumene-rich pegmatites that lack miaroles (e.g., the Tanco pegmatite: London, 1986a; Brisbin, 1986). The origins of pegmatitic textures have long been ascribed to the exsolution of aqueous solution from granitic melt, in which the aqueous solution forms an interconnected network of bubbles (Jahns and Burnham, 1969), and in

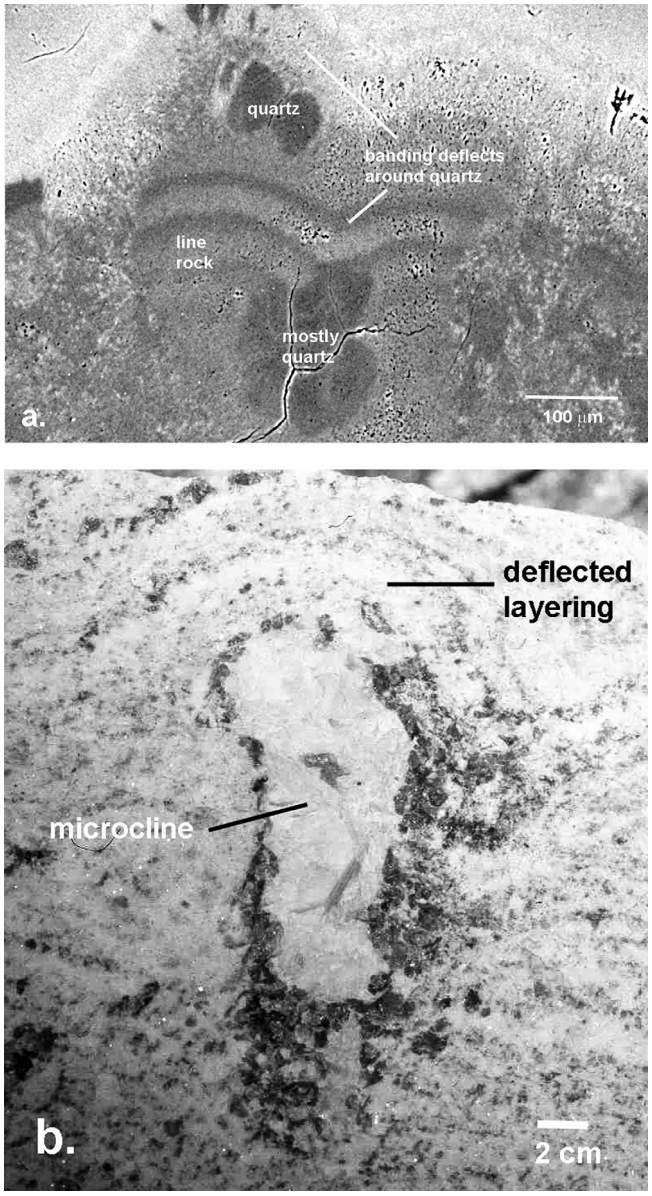

Fig. 18. (a) A backscattered electron image of an experiment (London, 1999), in which alternate layering in an aplitic texture deflects inward past a large quartz crystal, giving rise to convolutions in layering. (b) Deflection of layering around a K-feldspar at the Hale quarry, Portland, Connecticut, initiated curvature in the line rock front.

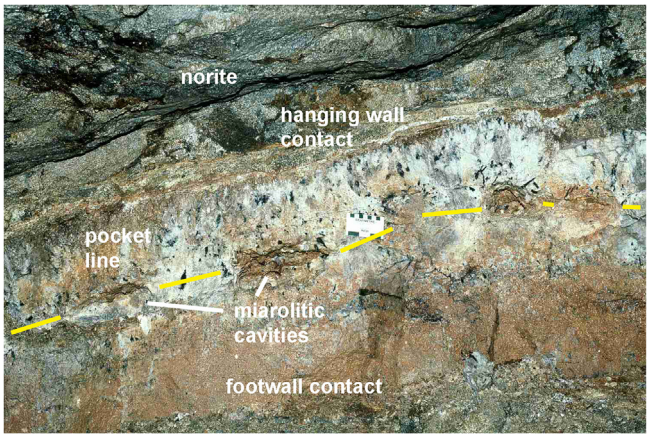

Fig. 19. A view of the San Diego pegmatite, Mesa Grande district, California. Small miarolitic cavities that were filled with polychrome tourmaline packed in dense clay lie along a well-defined center line (pocket line, yellow) of the pegmatite, where footwall and hanging wall portions of the dike met. Scale is centimeters at top.

Fig. 20. Dense kaolinite filled the Silver Dollar Pocket (October 2012) that produced abundant blue-green tourmaline at the Havey pegmatite, Oxford County, Maine (Jeff Morrison photo).

which bubbles of aqueous solution ascend through granitic liquid and the upper domains of pegmatite-forming melts to make miarolitic cavities (Jahns, 1982; Simmons et al., 2012). If this paradigm were correct, then all pegmatites should have an appreciable fraction of void space as miarolitic cavities (refer to Gem-Bearing Pegmatites below). As it is, miarolitic pegmatites constitute a minute fraction of all known bodies, and within them, miarolitic space generally occupies < 5% (e.g., London, 2013).

7.4. Relations of zonation to dike geometry

Some schematic renderings of the distribution of zones within a single pegmatite body also show a distribution of zones along the length of the body, such that the most fractionated units lie in the up-dip direction (Vlasov, 1961; Jahns and Burnham, 1969; Černý, 1991a; Černý and Lenton, 1995). Černý and Lenton (1995) rejected gravitational segregation, that is, the buoyant separation of a low-density aqueous solution from silicate melt, to account for extreme fractionation in the updip direction within pegmatites whose overall attitudes dip only 2°–7° and that are non-miarolitic.

It is a fact that pegmatites of a group become more fractionated with distance from source, and in the up-dip direction to the extent that this correlates with distance from source. Üebel (1977), however, illustrated a more local relationship between different portions of the same pegmatite dike. Thicker portions of a dike contain coarser crystals and exhibit a greater degree of chemical fractionation toward their centers than do thinner segments of the same dike, regardless of the direction of dip (e.g., see Figs. 8-2 and 8-3 of London, 2008). One interpretation is that wider dikes remain open longer to an influx of increasingly fractionated melt (Černý and Lenton, 1995); if this were true, then more fractionated melt might accumulate where dilation of the dike-forming fracture is greatest, or widest. However, open-system behavior is only rarely evident where multiple dikes merge, and it is otherwise absent in isolated lenticular bodies. Virtually every mapped rendering of a lenticular pegmatite body (e.g., scores of line-drawing maps in Cameron

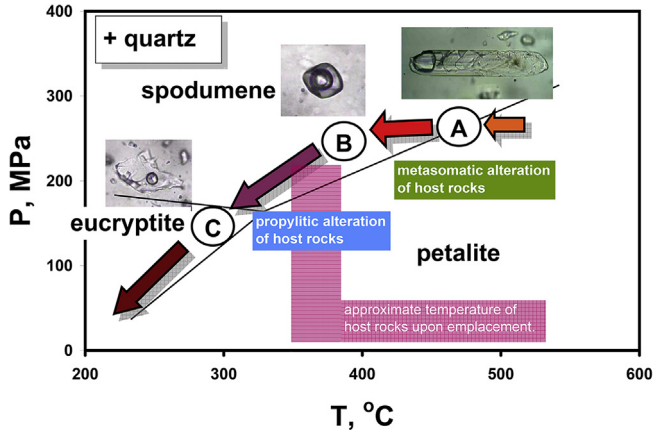

Fig. 21. The lithium aluminosilicate phase diagram, with a cooling history, and fluid inclusion data, and wallrock alteration as applied to the Tanco pegmatite, Manitoba, from London (1984, 1986a) and Morgan and London (1987). Crystal-rich inclusions (A) are present in petalite and spodumene; these melt to a quenchable homogeneous glass between 375°–450 °C. The earliest, highest-temperature inclusions in quartz consist of a single aqueous-carbonic fluid (B). By the time the pegmatite crossed from the field of spodumene into the field of eucryptite + quartz, the single aqueous-carbonic fluid had exsolved into essentially immiscible and coexisting aqueous (C) and carbonic fluid inclusions. An inflection in the cooling curve for the Tanco is taken to represent the temperature of the host amphibolite upon emplacement of the pegmatite, with isobaric cooling of the pegmatite to that temperature.

et al., 1949, 1954; Page et al., 1953; Norton, 1964; Stilling et al., 2006) shows the narrowed ends of the pegmatite to consist solely of the outer pegmatitic units, with the coarse and refined units confined to the thickest central portions.

The significance of Üebel's (1977) observation pertains to the processes by which pegmatites become zoned via crystallization. The most widely applied model, Rayleigh fractional crystallization, in which the surface of a mineral remains in chemical equilibrium with the bulk melt whose composition changes continuously with crystallization, results in the same degree of chemical refinement at a given percentage of crystallization independently of the volume of melt that is crystallizing. As illustrated schematically in Fig. 22a, two dikes, one twice the thickness of the other, will culminate with the same concentration of incompatible component, C_i, if Rayleigh fractionation is the only process involved in their chemical evolution. If zone refining operates (Fig. 22b), the final concentration of component *i* will be higher in both

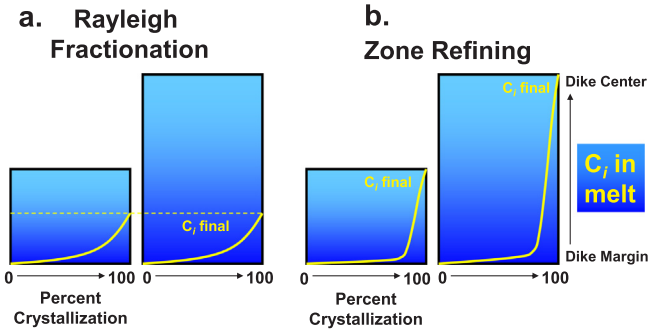

Fig. 22. Illustrations of fractionation in thin and thick dikes via (a) Rayleigh fractionation and (b) zone refining. Rayleigh fractionation results in the same final concentration of an incompatible element, C_i, in dikes whose thickness varies by a factor of two. Zone refining produces "L" shaped concentration profiles of C_i. The relationship illustrates that the extent of fractionation achieved by zone refining is greater than can be achieved by Rayleigh fractionation from an equal volume of melt, and that the extent of fractionation by zone refining is a function of the volume of melt crystallized, which increases with the thickness of dikes in this case.

Table 3
Published values for temperature and pressure of pegmatite crystallization.

Pegmatite	Temperature, °C[1]	Pressure, MPa	Source
La Posta, California	70–425	200–300	[18]
Mesa Grande, California	150–420		[18]
Tanco, Manitoba	~262		[3]
Muiane, Mozambique	277–610		[32]
Morefield, Virginia	~300	250	[8]
Tin Mountain, South Dakota	~340	270	[16]
Harney Peak, South Dakota	340	270	[10]
Tin Mountain, South Dakota	~350–400		[13]
Ramona, California	375–425		[7]
Mt Mica, Maine	391–505		[21]
Borborema, Brazil	400	350	[26]
Franqueira, Spain	~400	220–270	[9]
Tablada I, Argentina	420		[30]
Tanco, Manitoba	~450	260–290	[2]
Harding, New Mexico	~450	300–350	[5]
Sinceni, Swaziland	450–500	500–600	[27]
Varutrask, Sweden	450–600		[29]
Potrerillos, Argentina	475–600	300–370	[24]
Ramona, California	~475		[17]
Tanco, Manitoba	~475		[31]
Vlastějovice Lithium, Czech Republic	500–570	310–430	[25]
Cerro Moreno, Argentina	522		[30]
Mesa Grande, California	540–750		[28]
East Kemptville, Nova Scotia	~550–600		[11]
Leskhozovskaya, Russia	550–615	220–380	[15]
Kuradawe, Iraq	550–782		[19]
Gorikho and Zakhin-tsokhio, Mongolia	573	100	[6]
Brazil Lake, Nova Scotia	600	350–400	[14]
Rožná, Czech Republic	~610		[22]
Vlastějovice Barren, Czech Republic	600–640	420–580	[25]
Peggy's Cove, Nova Scotia	600–650	330–350	[12]
Mt Mica, Maine	630–650	300	[20]
Znětínek and Vladislav, Czech Republic	~670		[22]
Tanco, Manitoba	~720–780	270–290	[4]
Mina do Santino and Jacú, Brazil	870–900		[23]
Tanco, Manitoba		280	[1]

[1] Brisbin (1986), [2] London (1986), [3] Thomas et al. (1988), [4] Thomas and Spooner (1988) [5] Chakoumakos and Lumpkin (1990) [6] Schmidt and Leeder (1992) [7] Morgan VI and London (1999), [8] Smorkanicz and Dusas (1999), [9] Fuertes-Fuente et al. (2000), [10] Sirbescu and Nabelek (2001), [11] Kontak et al. (2001), [12] Kontak et al. (2002), [13] Boyd et al. (2003), [14] Kontak (2006), [15] Smirnov et al. (2009), [16] Sirbescu and Nabelek (2003), [17] London et al. (2012b), [18] Gammel and Nabelek (2016), [19] Mohammad et al. (2016), [20] Simmons et al. (2016), [21] London and Morgan (2017), [22] Breiter et al., 2014, [23] Palinkaš et al. (2014), [24] Lira et al. (2012), [25] Ackerman et al. (1999), [26] Beurlen et al. (2001), [27] Trumbull (1995), [28] Taylor et al. (1979), [29] Siegel et al. (2016), [30] Colombo et al. (2012), [31] Thomas and Spooner (1992), [32] Thomas and Davidson (2010).

[1] Pairs of temperatures with 0 or 5 in the last place (XX0 or XX5) reflect an unspecified uncertainty in the accuracy of the values. Pairs of temperatures with any another digit in the last place are meant to convey a range of temperatures as measured from different portions of a single pegmatite body.

dikes, and approximately twice the concentration in the thick dike as in the thin dike.

8. Pressure and temperature of crystallization

Granites contain relatively few minerals or assemblages that serve to constrain their depths and temperatures of crystallization. The depths of emplacement at which granites crystallize is practically unknown by any direct method. The Al content of hornblende (Thomas and Ernst, 1990) is a widely-used geobarometer for intermediate plutonic rocks, but its applications to chemically evolved granites and their pegmatites are nil. Indirect methods compare the composition of the granite to the experimental compositions of granitic liquids at various

Table 4
Selected elemental compositions of the Tanco pegmatite, and temperatures of mineral saturation.

Component	Tanco[1] bulk	Tanco[2] corrected	Saturation[3] at 700 °C		% of Saturation at 700 °C	Saturation[4] at Temperature
Oxide, wt%						
P_2O_5	0.86	0.86	7.19	12%	montebrasite	~535 °C[5]
Element, ppmw						
Be	169	169	339	50%	beryl	~635 °C
Li	3453	***3523***	7000	50%	petalite	
Cs	2641	***3036***	51,880	6%	pollucite	~384 °C
Cs[6]					pollucite	~401 °C
B	216	***655***	3384	19%	tourmaline	~506 °C
Nb	56	56	146	38%	Mn-columbite	~645 °C
Ta	300	300	915	33%	Mn-tantalite	~605 °C

[1] From Stilling et al. (2006).
[2] Corrected for losses to host rocks (***bold italics***), based on Morgan and London (1987).
[3] Elemental concentrations in melt at saturation in beryl (Evensen et al., 1999), petalite (Stewart, 1978), pollucite (London et al., 1998), tourmaline (Wolf and London, 1997) and Mn-columbite and Mn-tantalate (Linnen and Cuney, 2005).
[4] Calculated temperature of mineral saturation in the Tanco pegmatite from the corrected concentrations based on data from Evensen et al. (1999), London et al. (1998, 1999, 2001), Linnen and Cuney (2005). See Fig. 25.
[5] Based on the equilibrium among petalite-quartz-montebrasite-melt, from London et al. (1999).
[6] Based on the leucite component of pollucite, from London et al. (1998).

pressures and H_2O contents (e.g., Tuttle and Bowen, 1958; Holtz et al., 1992, 1999). However, the bulk composition of the granite may be unrelated to the final conditions of emplacement at which most crystallization commences (e.g., Morgan and London, 2012).

A compendium of published estimates of the pressure-temperature regimes for pegmatites fall in a rather narrow range of pressure, ~200 to 300 MPa, which is the more poorly constrained of these variables, and a wide range of temperature (Table 3). The estimates of temperature form a continuum but can be roughly divided into three groups. Those below 350 °C stem almost entirely from fluid inclusion studies. Values > 550 °C originate from fluid inclusion and stable isotope studies. Temperatures in between come mostly from various mineral geothermometers involving silicates and phosphates, and from some fluid inclusion studies. The estimated temperatures for the Tanco pegmatite listed in Table 4 are not included in this compendium.

8.1. Pressure-depth relations

For the LCT family of pegmatites that culminate in assemblages of spodumene (α-$LiAlSi_2O_6$) and/or petalite, the stability relations among these primary minerals and secondary eucryptite (α-$LiAlSiO_4$) are functions of pressure and temperature only because all of these minerals occur as nearly pure end-member compositions with quartz (London, 1984). Spodumene occupies a field analogous to kyanite, and petalite and eucryptite fall close to the fields of sillimanite and andalusite, respectively (Fig. 21). The stability fields of the lithium aluminosilicates derive from their densities, which increase toward spodumene, a dense pyroxene in which Li is in octahedral coordination, compared with tetrahedral coordination in petalite and eucryptite. The lower pressure limit of the spodumene stability field, ~200 MPa, corresponds to depths of ~6 km. London (1986a) used the stability relations among the three lithium aluminosilicates to elucidate a cooling curve for the Tanco pegmatite (Fig. 21), and in combination with fluid inclusion analysis put the pressure attending the crystallization of the body at 260–290 MPa (8–9 km). Using an entirely different method, Brisbin (1986) arrived at a pressure of 280 MPa (Table 4). Pegmatites in which spodumene is the only primary lithium aluminosilicate solidify at greater depths; for example, Chakoumakos and Lumpkin (1990) estimated an emplacement pressure of 300 MPa for the spodumene-rich Harding pegmatite, New Mexico. The lithium-rich pegmatites are the most distal of a zoned pegmatite group, which means that less fractionated pegmatites and their source granites lie at greater depths.

8.2. Temperatures of crystallization

8.2.1. Mineral thermometry

The most widely utilized means of assessing temperatures of crystallization in igneous and metamorphic rocks employ experimental calibrations of heterogeneous mineral equilibria (e.g., the lithium aluminosilicate system, Fig. 21), and of homogeneous exchange equilibria of elements and isotopes among coexisting minerals. The application of experimental results to natural rocks hinges upon two important premises: (1) the experimental results are those that derive from chemical equilibrium among all of the phases in the system of interest, and (2) the compositions of minerals in the natural system of application reflect a state of chemical equilibrium among them at the time and conditions of their crystallization. The attainment of the same final result through a variety of reaction paths, in which case the result might be construed as an equilibrium state, is rarely achieved in experimental studies; depending on the design of the experiment and its goals, reversibility of the result from multiple starting states is impossible. In most studies, researchers accept the attainment of a steady-state result (e.g., the compositions of crystal rims and adjacent melt do not change with time) as a close approach to equilibrium. Of the two sources of uncertainty, that of the chemical equilibrium among all phases in the natural assemblage is the least constrained.

For the reasons explained by London (2014a), the most widely-used mineral thermometers – Ti in quartz, Ti in muscovite, Ti in biotite, FeMg exchange between garnet-biotite, FeTi exchange in oxides, and zircon saturation temperatures – are not applicable to the vast majority of pegmatites. Feldspar solvus thermometry is relevant, and it has been calibrated on the basis of multiple experimental data sets (e.g., Fuhrman and Lindsley, 1988; Elkins and Grove, 1990). The method can give erroneous results if the original bulk composition of either feldspar has been modified. In most such cases, the feldspar pairs do not converge to a common temperature of crystallization, and the test for a single solvus temperature fails. In pegmatites, much of the K-feldspar is recrystallized as perthitic maximum microcline. Geochemical tests based on the compatibility and zonation of trace elements in feldspars (e.g., Parsons et al., 2009; London et al., 1999, 2012b) serve to assess whether the bulk composition of the feldspar has been modified. When such tests have ascertained that the composition of the perthitic microcline is likely that of the original K-feldspar, then solvus pairs record temperatures of ~450° ± 50 °C (Morgan and London, 1999; London et al., 2012b; Colombo et al., 2012).

8.2.2. Stable isotopes

Reliable stable isotope data from pegmatites are so sparse as to offer no clear indication of temperature. In one of the most thorough and widely cited studies, Taylor et al. (1979) used oxygen isotope distributions between quartz-garnet and quartz-muscovite to calculate temperatures of crystallization from the margins to the central miarolitic cavities in the Himalaya pegmatite, California, a thin tabular dike of ~50–100 cm width (their Tables 1 and 3 and Fig. 7). Based on that data, they state that the margins reflect crystallization at 750 °C, and the pockets formed in the narrow range of 550°-560 °C. Inspection of their Tables 1 and 3 and Fig. 7 shows the reverse: they have plotted it correctly from the tables, but the outer zones record $\Delta^{18}O$ temperatures of ~550 °C, while the pockets, which contain laumontite, stilbite, carbonates, and clay, fall at ~750 °C.

8.2.3. Fluid inclusions

In one of the first comprehensive studies of fluid inclusions in any rock type, the pioneering geochemist F.G. Smith (1953) surveyed fluid inclusions in several different pegmatites, from which he concluded that most if not all of the inclusions were secondary and hence of no value in understanding the magmatic history of the deposits. Jahns (1955) cited Smith's cautionary note, and perhaps for this reason elected to pursue experimental petrology rather than fluid inclusion analysis to make his case for the importance of an aqueous fluid during the primary crystallization of pegmatites. Nevertheless, fluid inclusion analysis has been the foundation of many studies of pegmatites. As noted above, most of these studies yield estimates of entrapment temperatures, and by implication or explicit statement, the temperatures of magmatic crystallization in pegmatites at the extremes of the temperature ranges listed in Table 3. For example, Thomas and Spooner (1988) report inclusion-based temperatures of magmatic crystallization along the border zone of the Tanco pegmatite, Manitoba, as ~720°–780 °C, which is nearly 100 °C above the *liquidus* temperature of even a chemically simple hydrous haplogranite minimum liquid at ~250–300 MPa. In other studies, Thomas et al. (1988) and Sirbescu and Nabelek (2001) cited fluid-inclusion evidence for the stable existence of silicate liquids down to temperatures of 260°–340 °C, respectively. The lowest solidus temperature reported for a flux-rich analogue to the most evolved Li pegmatites is 450 °C at 200 MPa H_2O (London et al., 1989).

8.2.4. Conductive cooling models

Chakoumakos and Lumpkin (1990) were the first to apply a conductive cooling model to the post-emplacement history of a pegmatite, the Harding mine near Dixon, New Mexico. They observed that the primary crystallization of the pegmatite (20 m thick) at any host-rock temperature below 550 °C would be complete in 100 years or less, assuming that the rate of crystallization kept up with cooling. Using 350 °C as the temperature of the host rocks upon emplacement, their conductive cooling model shows the center of the pegmatite (a half-width of 10 m) cooling to 450 °C, a lowest possible solidus temperature, in ~8 years. This work started a revolution in thinking about the relations of crystal size, temperature, and time in the consolidation of pegmatite dikes.

HEAT3D,[2] a finite-element program that simulates the cooling of plutonic magmas, can be employed to model the cooling of large granite bodies and of dikes that emanate from them. A representative model might begin with mafic host rocks at a depth of 9 km, whose temperature has been elevated to 470 °C (an effective geothermal gradient of 50 °C/km) by the intrusion of a batholithic-scale pluton. A proximal pegmatite dike of 2 m width and consisting of an unfractionated granitic composition intrudes at that depth at a liquidus emplacement temperature of 750 °C (Fig. 23a). Crystallization commences after the pegmatite-forming liquid has cooled to 650 °C, ~100 °C below its liquidus temperature (Swanson, 1977; MacLellan and Trembath, 1991); the dike reaches this temperature in 1050 h (< 44 days) (Fig. 23b). The time to 550 °C (Fig. 23c), a likely lower limit for crystallization before further cooling transforms the melt to glass, is ~6300 h (< 263 days).

Next, consider a more evolved pegmatite-forming dike 1 m wide with an emplacement liquidus temperature of 700 °C that intrudes mafic rocks at 160 °C (along a geothermal gradient of 20 °C/km) at depth of 7 km (Fig. 23d). The margins of the dike cool to 450 °C, the undercooling necessary to initiate sidewall crystallization of strongly oriented pegmatitic fabric and the temperature of crystallization as recorded by feldspars, after < 5 h (Fig. 23e). The dike cools to 450 °C at its center after only 93 h (< 4 days), and 400 °C (Fig. 23f) after 122 h (~5 days), which is the low end of crystallization temperatures as recorded by primary solvus feldspar pairs.

The revolution started by Chakoumakos and Lumpkin (1990) and augmented by others (Morgan and London, 1999; Webber et al., 1999; London et al., 2012b) has reduced the crystallization of pegmatites to timeframes of days, months, or a few tens of years for the really large bodies. If the crystallization of pegmatites begins ~100°–250 °C below their liquidus temperature, and crystallization keeps pace with cooling before the liquids reach their glass-forming temperatures, then crystallization fronts must advance into the bodies at $\sim 10^{-7}$ m/s, a rate that is approximately 10^2 faster than any measured by experiments so far.

9. The compositions of pegmatite-forming melts

Liquidus undercooling by hundreds of degrees appears to precede the crystallization of pegmatites if the bulk compositions of their liquids are those of hydrous granites. Though granitic overall, the explanations of pegmatitic textures and zonation have long been predicated on an abundance of fluxing components including H_2O, B, P, F, and rare alkalis (Li, Rb, and Cs). At weight percent levels, each of these components lowers the solidus temperature of granites by tens of degrees (e.g., Manning, 1981; Pichavant, 1981; London et al., 1993; Maneta et al., 2015). In combination, they lower the solidus of the hydrous granite melt to 450 °C at 200 MPa (London et al., 1989), which is more than 200 °C below the solidus of simple hydrous granitic melt at its thermal minimum or eutectic. These same components reduce the viscosities of granitic melts (e.g., Dingwell et al., 1996), which promotes an increase in the diffusivity of ionic components through the melt (e.g., Mungall, 2002). Components of B and F enhance the isobaric-isothermal solubility of H_2O in melt in the proportion of 1 mol H per mole of B or F, and 2 mol H per mole of P up to at least several weight percent of each fluxing component (London, 2009). That additional H_2O further lowers viscosity, and more importantly, forestalls the exsolution of a separate aqueous solution. By extending the time-temperature interval of crystallization and facilitating the diffusive transfer of ions to and from crystal surfaces, these fluxes enhance the probability of forming large crystals and zoned assemblages.

There are so few actual chemical analyses of pegmatites as composite whole rocks that there is no quantitative or authoritative basis for the abundance of these fluxing components and other trace elements that pegmatites contain. As noted, the trace element contents of the Tanco composite are derived from modal analysis. Composite samples of the Spruce Pine and Harding pegmatites thought to represent their bulk compositions were chemically analyzed (Vaughn, 1963); a few of the normally rare elements (Li, Rb, Cs, P, F) were included, but Be, B, Nb, Ta, Sn and other high field-strength elements (HFSE), such as REE, were not.

Because of the incompatible nature of these components in quartz and feldspar, their abundances in whole rocks might not be representative of the liquids from which the pegmatites formed. That is

[2] Available at http://www.lanl.gov/orgs/ees/geodynamics/Wohletz/KWare/Index.htm (last accessed 05 October 2017).

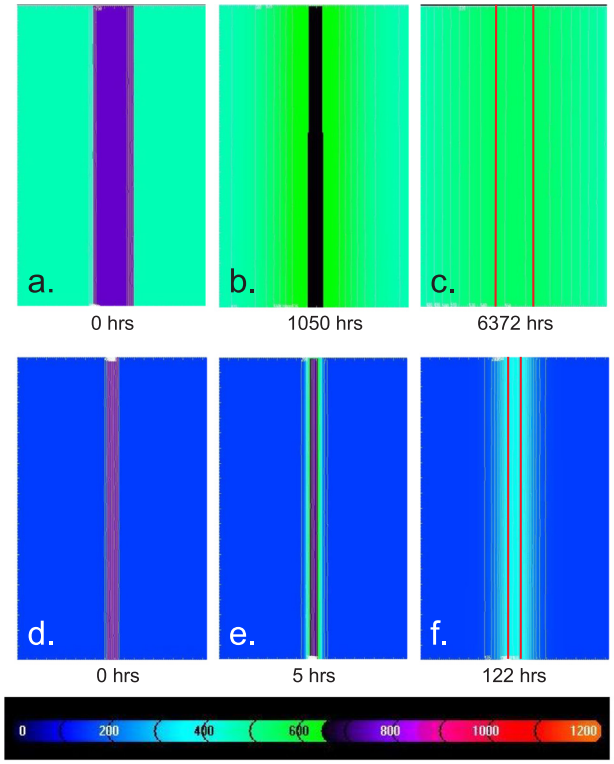

Fig. 23. HEAT3D time-temperature sections for (a–c) a proximal pegmatite dike 2 m in width that has intruded a mafic host rock (thermal conductivity = 3 W/m K: Clauser and Huegnes, 1995; heat capacity = 1100 J/kg K: Robertson, 1988, bulk density = 3000 kg/m^3) at a depth of 9 km after heat liberated from an adjacent granitic pluton has raised the temperature near the contact to 470 °C. The heat capacity of the dike is set to 2300 J/kg K based on data in Neuville et al. (1993). (b) A distal pegmatite dike 1 m in width, emplaced as explained in the text. In the last cell, the margins of each dike are indicated by red lines.

almost certainly true of H_2O. There are, however, data from granites (and obsidians) and their sources, relevant melt fractionation models, and experimental studies of mineral stability that collectively help to constrain the likely starting and ending compositions of pegmatite-forming melts, in particular in relation to their concentrations of fluxing and other incompatible components.

9.1. Lithium

Stewart (1978) and Maneta et al. (2015) ascertained that a hydrous granitic melt becomes saturated in petalite, spodumene, or eucryptite at ~1.5 wt% Li_2O. The average content of Li-rich pegmatites is close to 0.5 wt% Li_2O (Stewart, 1978), and it is this value that would be used to model the crystallization of Li-aluminosilicates in pegmatites. When compared to the value at saturation, it becomes evident that Li-aluminosilicates should not be present from the start of crystallization, only after extended fractional crystallization, unless the melt is substantially undercooled (Maneta et al., 2015).

9.2. Boron

Wolf and London (1997) demonstrated that peraluminous granitic liquids that are saturated in other mafic minerals (biotite, cordierite, or garnet) can precipitate common mafic tourmaline with ~1–2 wt% B_2O_3 at liquidus temperatures depending upon the ASI of the melt (increasing ASI decreases the saturation concentration for boron). Pegmatites are commonly tourmaline-saturated at their margins (Fig. 24). London (2016a) proposed two mechanisms to account for the crystallization of

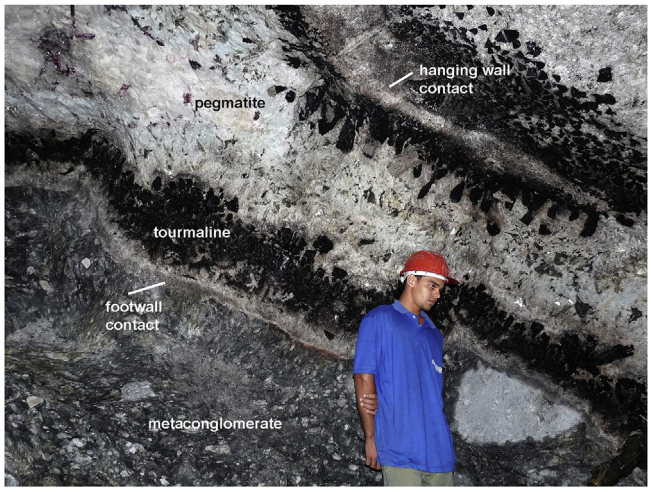

Fig. 24. Tourmaline-rich "fringe" along the margins of a thin pegmatite dike hosted by metaconglomerate, from Capoeira 2, Borborema Pegmatitic Province, Brazil. Photo by Jan Loun, courtesy of Milan Novak.

such large amounts of tourmaline at the margins: (1) diffusive influx of mafic components into the pegmatite from the host rocks, and (2) sharp undercooling of pegmatite-forming melt that comes from a granitic source that is already saturated in tourmaline at the liquidus temperature of the source granite (~1 wt% B_2O_3). Upon sudden cooling to ~450 °C, nearly 95% of the boron in that melt would precipitate as tourmaline at the onset of crystallization of the pegmatite dike.

9.3. Phosphorus

London et al. (1999) presented experimental calibrations of several silicate-phosphate reactions that occur in pegmatites and which buffer the concentrations of P_2O_5 in melt. These concentrations are corroborated by the P content of co-crystallizing alkali feldspars. The initial P contents of melts are those of their whole rocks, ~0.5 wt% P_2O_5 for pegmatites of the LCT family, and that value likely does not exceed 2.5 wt% P_2O_5 at the point that amblygonite-montebrasite precipitate in the latest pegmatite zones.

9.4. Fluorine

London et al. (2001) calibrated the partition coefficient for F between amblygonite-montebrasite solid solutions and hydrous granitic melt. With 5–7 wt% F in the typical primary montebrasite found in association with spodumene or petalite plus quartz, the melt would have contained 1.5–1.8 wt% F. As this is always a late-stage assemblage in pegmatites, the initial pegmatite-forming melts likely contained ~0.5 wt% F.

9.5. Bulk composition, LCT versus NYF

These results above pertain to the most fractionated of the Li-rich, LCT pegmatites that become saturated in a variety of exotic minerals. The NYF pegmatites are depleted in all of these added components except F. Topaz is a common constituent of these pegmatites, and London et al. (2001) suggested that topaz-bearing granites and pegmatites must contain in excess of 3 wt% F. The stability of topaz in granites may increase as H_2O concentrations in melt decrease (London and Morgan, 2017). This observation may explain why topaz is a common constituent of A-type granites and rhyolites, which are considered to possess low H_2O contents because of their derivation from deep crustal gneisses and ponded basaltic sources at the top of the mantle (e.g., Christiansen et al., 2007).

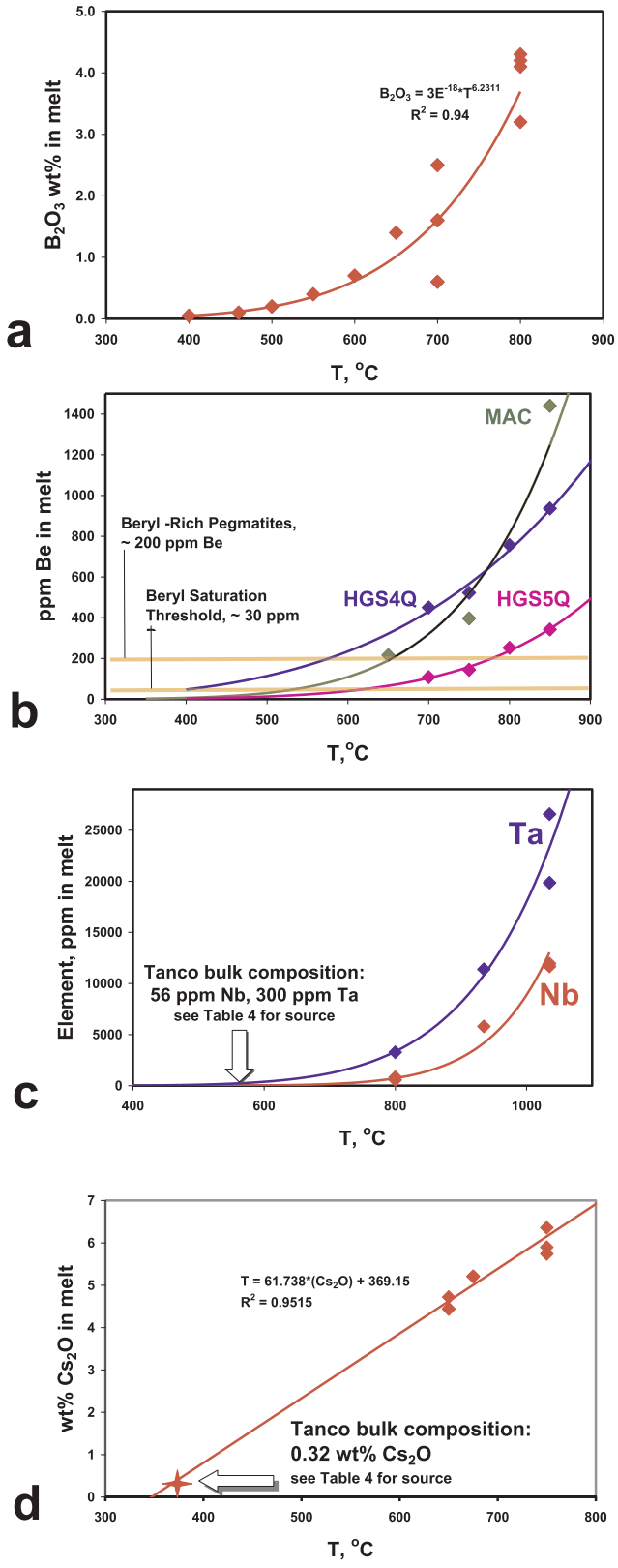

Fig. 25. Temperature-solubility diagrams for B, Be, Nb, and Ta, and Cs. (a) The saturation surface for tourmaline in aqueous solutions (Weisbrod et al., 1986) and hydrous haplogranite melt (Acosta-Vigil et al., 2003) at conditions that are buffered with respect to all components of tourmaline except boron. (b) The saturation surface for beryl in three hydrous melt compositions: HGS4Q is quartz-saturated metaluminous (ASI = 1.0) haplogranite liquid at 200 MPa minimum composition, HGS5Q is the same quartz-saturated composition with an ASI of 1.3, and MAC is the Macusani obsidian (see Evensen et al., 1999). (c) The saturation surfaces for Mn-columbite and Mn-tantalite in hydrous granitic melt at conditions that are at or close to saturation in spessartine, recalculated from Linnen and Cuney (2005). (d) The saturation surface for pollucite, modified from London et al. (1998).

9.6. Mineral saturation-solubility relationships to temperature

Experimental calibrations of mineral saturation and solubility in granitic melt as a function of temperature can be utilized to calculate the compositions of melts if they are saturated in the minerals of interest at a known temperature, or the inverse, to calculate a temperature of crystallization from the known melt composition. Fig. 25 presents saturation surfaces of beryl with respect to Be, tourmaline with respect to B, pollucite in relation to Cs, and Nb-Ta with respect to their oxides. For every case, the concentration of rare element necessary to saturate the melt in that mineral falls by about a factor of 10 for every 100 °C of decreasing temperature.

Table 4 lists several of these rare minerals that are found in the Tanco pegmatite. Most of them, including tourmaline, beryl, columbite, and tantalite, are present in the outer border and wall zones, and hence the pegmatite-forming melt was saturated in these minerals from the start. The table lists the concentrations of the essential elemental components in question as derived from the bulk composition reported by Stilling et al. (2006), and corrected for the losses of certain components to the metasomatic alteration halo around Tanco (Morgan and London, 1989). Also provided are the concentrations needed to crystallize these minerals near the solidus of granitic liquid at 700 °C and elevated H_2O pressure. The temperature dependence of their solubility is known from the experimental sources cited in Table 4. Therefore, the saturation temperature can be derived from the abundance of the essential structural constituent in question. Those values are provided in the last column of Table 4.

Table 4 is modified from a previous version (London, 2015a), which was derived empirically from figures in each of the sources cited. However, a power function best reflects the relations of solubility to temperature, as is evident in the few cases where solubility data extend from high to low temperature experiments (e.g., Weisbrod et al., 1986). Now, the solubility data on which Table 4 is based have been fit to power functions, where applicable, to project saturation values for various rare minerals to temperatures below the range of the calibrations. For beryl, the data for the Macusani obsidian are utilized (Evensen et al., 1999). For tourmaline, the saturation values are derived from the power-function fit of data presented as Fig. 3 in London (2011). The melt saturation temperature for pollucite (London et al., 1998) and the leucite component of pollucite at Tanco as a function of temperature converge to the same value, unchanged from the original table. The data for Mn-columbite and Mn-tantalite are problematic. Linnen and Cuney (2005) did not buffer the concentration of Mn in melt by saturation in spessartine or another Mn phase. For the most part, therefore, their solubility data cannot be used to establish the saturation values for Nb and Ta in the melts. Only two experiments in each of the Nb and Ta data sets contain spessartine, which is the Mn-saturating phase for peraluminous (LCT) melts. Fig. 25c, therefore, is constructed from the data at the highest ASI of melt (initially 1.22) and Mn-content: 5 data points for Nb, and 4 data points for Ta.

Most of the experiments were conducted at high temperatures where the data form nearly linear arrays. These have been extrapolated to much lower temperatures, wherein the curvature of the power function is large and uncertainty becomes especially large. With this caveat, the calculated saturation temperatures for beryl and NbTa oxides are close to the liquidus temperatures of each phase in haplogranitic melt. The calculated saturation temperature for tourmaline in the wall zone of Tanco is ~504 °C. This lower temperature at the

inception of crystallization along the margins is consistent with the porcelaneous texture of the border zone along the footwall of the pegmatite (Fig. 11). The saturation temperature for montebrasite (~535 °C) is likely close to the actual temperature of crystallization of the intermediate zones. The pollucite saturation temperature (384°–401 °C) derives from two independent methods, and it is consistent with the environment of a hydrous zeolite.

9.6.1. The crystallization interval of Tanco

With the initial melt temperature set at 700 °C at a depth to upper contact of 8 km and a geothermal gradient of 20 °C/km, the interval of time for cooling to 400 °C at the center of the thickest portion of Tanco (120 m), where pollucite is prevalent, can be calculated from the HEAT3D conductive cooling model. That interval is 615 years. Many rare-element pegmatites contain subsolidus assemblages including zeolites, carbonates, clays, and opal. The cooling intervals necessary to reach the low-temperature stability fields of these minerals can be many thousands of years after the initial primary crystallization.

9.7. Alternatives to granitic sources of pegmatites

9.7.1. Direct anatexis

It is evident from Figure 25 that the concentrations of Be, B, Cs, Nb, and Ta needed to saturated granitic melts with respect to beryl, tourmaline, pollucite, columbite, and tantalite at anatectic temperatures in excess of 700 °C are orders of magnitude higher than the abundances of these rare elements in likely crustal protoliths to anatexis (e.g., Leeman and Sisson, 1996; Bebout et al., 2007; Coveney, 2000). Bea (1996) has presented a convincing argument that the partition coefficients for trace elements between minerals and anatectic melts are essentially unity, especially when the trace elements in question reside in the principal minerals that contribute to the anatectic melt. Because of fundamental differences between a slow rate of heating, leading to anatexis, and the high degree of liquidus undercooling that is necessary to initiate crystallization in granitic liquids (e.g., Swanson, 1977; Fenn, 1977; Fenn, 1986; Evensen, 2001; London and Morgan, 2017; Sirbescu et al., 2017), the processes of melting and crystallization are not reversible as Stewart (1978) envisioned. The bulk compositions of mica schists and aluminous gneisses are close to the peraluminous granitic liquids they produce; therefore, the fraction of melt at the onset of anatexis is large (London et al., 2012a), which substantially dilutes the trace elements in melt. It is for this reason that rhyolite obsidians, which are substantially more fractionated than their sources, possess concentrations of these elements not far above the averages for their likely protoliths (Macdonald et al., 1992). It is possible that some protoliths of anatectic liquids might be uncommonly enriched in a normally trace element such as Be, for example, which is compatible in cordierite (Evensen and London, 2003). In total, however, these observations indicate that rare-element pegmatites like Tanco, Greenbushes, Bikita, and their ilk cannot originate from the direct anatexis of common metamorphic rocks (cf. Simmons et al., 2016).

Some common pegmatites may arise directly from anatexis if the leucosomes of partially melted rocks possess granitic compositions and develop one of the distinctive pegmatitic textures upon crystallization. The only requisite condition for coarse-grained crystals of igneous origin is a low density of crystal nuclei in the melt from which they grow (e.g., see Chapter 14 of London, 2008). Low densities of crystal nuclei are prevalent at high temperature, close to the liquidus of the melt (Swanson, 1977). The other distinctive textures of pegmatites – sidewall crystallization, unidirectional solidification texture, skeletal and radial habits, graphic mineral intergrowths, and sequential precipitation of feldspars and quartz – arise only from the crystallization of melts at highly undercooled states. Such undercooling is possible only to the extent that melts migrate from their source into cooler host rocks; otherwise, migmatitic leucosomes cool and crystallize at the rate of cooling of their host rocks by tectonic exhumation.

Therefore, homogeneous granitic pegmatites distinguished solely by their coarse crystal size are plausible products of direct anatexis and local, if not *in situ*, crystallization of the melt (melts must cool below their anatectic temperatures to initiate and sustain crystallization). All of the other distinguishing textures of pegmatites arise from liquidus undercooling by more than 100 °C. Along a normal geothermal gradient of 20 °C/km, a granitic melt would have to migrate more than 5 km upward to achieve the necessary undercooling to promote the development of the other prevalent features of pegmatites. For reasons stemming from the work of Rubin (1995; Baker, 1998), this is not feasible for the small volumes of melt that leucosomes represent.

9.7.2. Hydrothermal pegmatites

A hydrothermal origin for pegmatites, especially for those that contain rare-element mineral assemblages, has also had its advocates over the years (e.g., Gresens, 1969; Roedder, 1981). The principal objection to this hypothesis comes from the exceedingly low solubility of aluminum in saline aqueous solutions typical of those found in metamorphic rocks and in hydrothermal ore deposits (Anderson and Burnham, 1983). Chloride-bearing solutions can transport alkalis and silica (e.g., Fournier, 1983), and such solutions deposit abundant quartz as veins in base-metal porphyry deposits (e.g., Burnham, 1979). Pegmatites, however, have granitic compositions consisting of nearly two-thirds feldspar, an Al-rich mineral. The solubility of aluminum is enhanced in aqueous solutions that contain B, P, or F (Manning, 1981; London et al., 1988; London et al., 1993), but only in proportion to the molar abundance of these components in natural hydrothermal fluids.

9.8. Summary of pegmatite-forming liquids

The majority of evidence indicates that pegmatites acquire most of their compositional attributes at source, that there is little open-system flow or exchange of material in or out of a pegmatite body once emplaced, and that the compositions of pegmatites are close to their igneous liquids. Origins for pegmatites primarily by hydrothermal processes, and of rare-element pegmatites by hydrothermal or anatectic means, are untenable based on current evidence. Estimates of pegmatite bulk compositions indicate that they are granitic, and that the abundances of fluxing components (B, P, and F), rare alkalis (Li, Rb, Cs) and HFSE (Sn, Nb, Ta, U), though significantly higher than in common granites, amount to at most a few weight percent of the bulk composition in total. Rare-element pegmatites arrive at their most fractionated stage with weight-percent levels of Li, Rb, Cs, and B for the LCT family, and Cl and F for the NYF affiliation. These incompatible elements are also volatile (London et al., 1989; Webster et al., 1989), which implies that an aqueous fluid that might disperse these elements was not present throughout the entire crystallization process. Miarolitic cavities, the surest evidence that pegmatite-forming melts attained H_2O-saturation prior to consolidation, are exceedingly rare in pegmatites as a whole, and where they occur, they normally occupy just a few volume percent of the pegmatite body.

10. Internal evolution of pegmatitic texture and zonation

The principal problem posed by pegmatites is that they are associated with granites, they possess the compositions of granites, but their sharp internal zonation by mineral assemblage and by textural zones is very unlike that of granites. On the presumption that quartz and feldspars crystallize simultaneously from silicate melt in their eutectic proportions to make granite, Jahns (1982) and Burnham and Nekvasil (1986) believed that pegmatites, too, must crystallize as eutectic systems at equilibrium, and this required some other process or agent to generate the mineralogical and textural segregation of zones, including monominerallic ones.

Experiments with silicate systems form the basis of our understanding of igneous rocks (e.g., Bowen, 1918, 1928). However, a

relatively few experimental programs have attempted to achieve the crystallization of hydrous granitic melts through cooling (see reviews in London, 1992, 2014a, London and Morgan, 2017), which is the process that lies at the heart of the igneous textures described above. Much of that experimental evidence as it applies to pegmatites stems from work in my laboratory (e.g., London et al., 1988, 1989; London, 2009; Acosta-Vigil et al., 2010, 2017; London and Morgan, 2017). The results and their applications to pegmatites are discussed extensively in these and other publications (London, 2014a, 2015a), and what follows is an abbreviated summary.

10.1. Crystallization of hydrous granitic melt at undercooled states

Undercooling below the liquidus temperature, the temperature at which the bulk properties of the first-formed crystals are in chemical equilibrium with the liquid, is the principal process by which silicate liquids become supersaturated with respect to crystals. Therefore, it is the magnitude of liquidus undercooling, measured by the parameter ΔT, that relates the crystallization response of the liquid (or its quenching to glass) to the textures of igneous rocks.

The magnitude of ΔT is proportional to the driving force, ΔG_{rxn}, the Gibbs Free Energy change of the reactions of liquid → crystals. Cast in terms of a mineral-forming component (*i*) of the melt (e.g., Si_4O_8, $NaAlSi_3O_8$, etc.), the partial molar Gibbs Free Energy change for the reaction $G_{i,liquid} \rightarrow G_{i,crystal}$ becomes increasingly negative with increasing liquidus undercooling (e.g., see Fig. 14-3 of London, 2008). Hence, in an undercooled liquid, including those of eutectic composition, values of ΔG_{rxn} for each crystallization reaction will become increasingly negative with increasing ΔT, but not at the same rate (e.g., see Fig. 17–12 of London, 2008).

The relative magnitudes of ΔG_{rxn} for reactions of the type $G_{i,liquid} = G_{i,crystal}$ for quartz, anorthite, albite, K-feldspar, and feldspar solid solutions can be derived from the cryoscopic liquidus relations in Tables 1a and b of Burnham & Nekvasil (1986). At 500 °C, an undercooled state of ΔT ≅ 190 °C for an H_2O-saturated granitic melt of minimum composition at 200 MPa, the cryoscopic equations of Burnham and Nekvasil (1986) yield values of ΔG_{rxn} of −18.6 kJ/m for quartz (Si_4O_8), −28.1 kJ/m for pure K-feldspar, −23.7 kJ/m for pure albite, and −50.1 kJ/m for pure anorthite. Recast as ideal solid solutions,[3] the same cryoscopic equations project a Gibbs Free Energy of formation of −26.8 kJ/m for plagioclase of $Ab_{85}An_{15}$, and −27.2 kJ/m for K-feldspar of $Or_{80}Ab_{20}$, which are compositions similar to those in the outer zones of pegmatites. Close to the solidus, the difference in energy between quartz and feldspars is small, and from an energetic standpoint, both should crystallize. The result of the simultaneous crystallization of quartz and feldspars close to the liquidus, therefore, should be homogeneous granite. At a highly undercooled state, the much larger negative Gibbs Free Energies of crystallization of the feldspars favor their precipitation more than quartz. The result should be that feldspars dominate the first-formed assemblages, followed by increasing quartz.

10.2. Experimental simulations

Some experiments in which granitic liquids were melted completely and then cooled below their liquidus temperatures were meant as simulations of the pegmatite-forming process (e.g., Swanson and Fenn, 1986; London et al., 1989; MacClellan and Trembath, 1991; Evensen, 2001; Maneta et al., 2015; Sirbescu et al., 2017; London and Morgan, 2017). Many of the salient features of pegmatites, including graphic granite, unidirectional solidification texture, spatial zonation of minerals by grain size and assemblage, and even pure quartz cores have been reproduced by these experiments.

Culminating with experiments using the Macusani, Peru, obsidian as a proxy for a Li-rich pegmatite-forming melt (London and Morgan (2017), experimental simulations of pegmatite-forming processes can now account for these features of pegmatites:

(1) feldspathic outer zones and quartz-rich to pure quartz cores;
(2) massive fine-grained border zones, followed by coarsening wall zones with unidirectional solidification texture, culminating in central domains of more isotropic fabric and coarse grain size;
(3) locally, alternating laminations of mineral assemblages as in layered pegmatites and layered aplites;
(4) a steady decrease in the An content of plagioclase from margin to core via subsolidus isothermal fractional crystallization;
(5) spatial segregation of plagioclase and alkali feldspar along opposite margins of the melt body via far-field chemical diffusion;
(6) an inward increase in the size of individual crystals by $\sim 10^2$ due to the accumulation of fluxing components in a boundary layer of melt adjacent to crystal surfaces, and
(7) albite + lepidolite bodies as the latest primary assemblage, and following the crystallization of pure quartz bodies.

All of these experimental results followed from the appreciable undercooling of the melt prior to the onset of crystallization. All of the features cited, except for the formation of miarolitic cavities, are entirely igneous in origin, owing nothing to the simultaneous occurrence of an aqueous solution.

10.3. Graphic granite

Fenn's (1986) model for the origin of graphic granite hinged upon the low diffusivity of Si in viscous melt adjacent to a growing feldspar crystal surface. London (2009) suggested that graphic intergrowths would not likely crystallize from aqueous solutions because the solubilities of the essential structural constituents are low and their diffusivities are high. This condition precludes the high degree of localized supersaturation necessary to precipitate quartz on the minute reentrants of a feldspar crystal surface (Fenn, 1986). The experiments presented as Fig. 26 were conducted to assess whether graphic feldspar-quartz intergrowths could form by crystallization from an aqueous solution that was highly supersaturated with respect to the essential structural constituents (ESCs) of quartz and feldspar. The aqueous solutions in those experiments were first equilibrated with the Macusani obsidian at 800 °C, 200 MPa, in order to dissolve a high mass fraction of solutes in the aqueous phase (Fig. 26a). The temperatures were quickly dropped isobarically to 550 °C (experiment MAC212) and 450 °C (MAC213) and continued for 240 h to crystallize the components of the solution or its quenched glasses. No graphic intergrowths of any minerals were observed in either experiment, and an assemblage of quartz-feldspar at 500 °C gave way to a potassic zeolite at 450 °C. It is unlikely that any aqueous solution formed in nature could be more highly oversaturated in quartzofeldspathic components than those in these two undercooled experiments.

10.4. Far-field chemical diffusion

The long-range, coordinated, and instantaneous nature of chemical diffusion of the alkalis was discovered by Acosta-Vigil et al. (2003, 2006), who identified a systematic redistribution of Na and K in response to chemical gradients caused by other components with which the alkalis associate. London (2009) demonstrated that far-field chemical diffusion of all melt components except Si could erase gradients in the silica concentration of melt at rates $\sim 10^4$ faster than by the diffusion of Si itself. London and Morgan (2017) demonstrated how far-field chemical diffusion leads to the formation of plagioclase- versus K-

[3] The feldspar pairs represent compositions on the strain-free solvus; therefore, an ideal mixing model is a viable approximation for the purposes of this comparison.

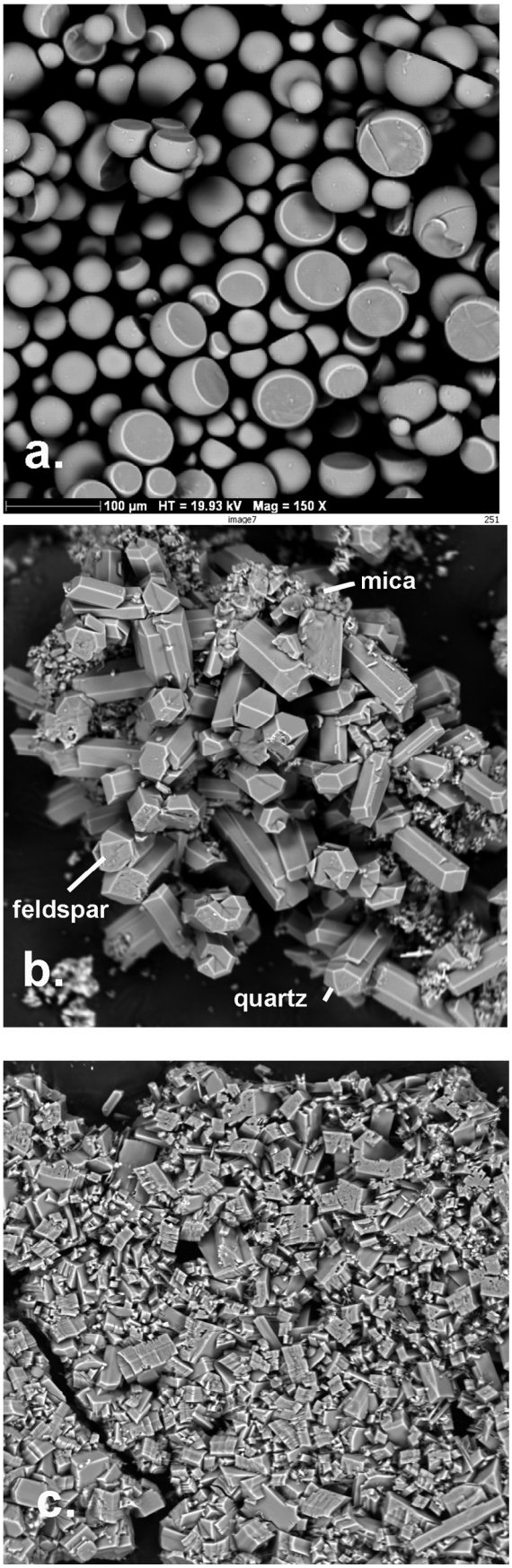

Fig. 26. (a) Backscattered electron image of glass spheres quenched from aqueous solution equilibrated with the Macusani obsidian at 800 °C, 200 MPa. The abundance of spheres attests to a high solubility (~11 wt% dissolved solids: London et al., 1988) in the aqueous solution at T and P. (b) Backscattered electron image of feldspar, quartz, and mica that crystallized from the solute-rich aqueous solution at 550 °C, 200 MPa. (c) A potassic zeolite-like phase dominates the mineral assemblage crystallized from the solution at 450 °C, 200 MPa.

Table 5
Diffusion coefficients for some elements in hydrous granitic liquids at 800 °C, 200 MPa.

Element	Diffusion coefficient, m^2/s	Method[1]	Source
Si	$2.0–2.8 * 10^{-15}$	EBDC	[1]
Al	$0.6–2.4 * 10^{-14}$	EBDC	[1]
Na	$1.52 * 10^{-8}$	FICK	[2]
K	$1.38 * 10^{-10}$	FICK	[2]
H	$2.5 * 10^{-10}$	FICK	[3]
P	$1.9 * 10^{-13}$	FICK	[3]
B	$5.6 * 10^{-12}$	FICK	[3]
F	$1.9 * 10^{-10}$	FICK	[3]

[1] Acosta-Vigil et al. (2006), [2] Morgan et al. (2008), [3] London (2009).
[1] EBDC: effective binary diffusion coefficient, FICK: Fick's Law.

feldspar-rich domains on opposite sides of a melt column, even in melts that may be near their glass-forming temperatures. The diffusion of alkalis, B, and F through melt in response to chemical gradients, for example as resulting from crystallization, is rapid in comparison to the diffusivities of those elements as a function of their own concentration gradients (Table 5). The nearly instantaneous nature of field diffusion in highly undercooled and viscous melt resolves the underlying dilemma that faced Jahns and Burnham (1969) in the zonal segregation of feldspars. They turned to an aqueous fluid to effect the necessary mass transfer because they could not envision that ionic diffusion through melt would be rapid enough on the timescale of pegmatite cooling.

10.5. Summary of crystallization at undercooled states

The temperatures of crystallization in pegmatites as derived from feldspar solvus thermometry and conductive cooling models fall around $T \cong 450^\circ \pm 50\,^\circ C$, which corresponds to $\Delta T = 250^\circ \pm 50\,^\circ C$ with respect to hydrous haplogranite liquid. Based on experiments, this range of undercooling coincides with the maximum growth rates of quartz and feldspar (Swanson, 1977; Fenn, 1977), the maximum percentage of crystallization with respect to time (London and Morgan, 2017), and the shortest delay in the onset of crystal nucleation following undercooling (Evensen, 2001; Sirbescu et al., 2017; London and Morgan, 2017). At those undercooled states, crystallization begins along the margins of melt bodies and proceeds inward, usually with the development of prominently unidirectional crystal growth. As a result, the initial advance of crystals in pegmatites is essentially one-dimensional, as highly elongate crystals of micas, tourmaline, and beryl, and K-feldspar compete to remain in contact with the silicate melt. Simultaneous crystallization of quartz and feldspar in graphic granite is also elongate in the direction of growth (quartz rods) and initially fine-grained (e.g., see Figs. 17-7 and 17-8 in London, 2008). These textures of the outer zones are dominated by the high degree of supersaturation of the melt in crystal-forming components as a result of liquidus undercooling. Inwardly flaring habits of crystals and the coarse isolated crystals of the intermediate zones and cores follow when the crystals expand from 1D lines to 2D surfaces (Fig. 17-10 of London, 2008, and Fig. 7 of London, 2009).

11. Liquid line of descent in pegmatite-forming melts

The chemical evolution of the melt composition within individual pegmatites is manifested by the decreasing An content of plagioclase, increasing concentrations of incompatible elements in major minerals, and the appearance of normally rare minerals in the some of the first-formed and last-formed mineral assemblages of the rare-element pegmatites. Those final exotic mineral assemblages contain an abundance of boron as tourmaline, lithium in spodumene, petalite, and lepidolite, phosphorus in a variety of primary phosphates, and fluorine as amblygonite, topaz, and fluorite, and numerous oxides of Nb, Ta, and Sn. Based on the information that has been marshaled above, the low temperatures and commensurately high viscosity of pegmatite-forming melts should significantly impede the diffusion of ions on the time scales of cooling. For this reason, the fractionation of the melt entails a more complex process than can be modeling through Rayleigh fractional crystallization for most elements. The exceedingly high viscosity of hydrous granitic melt at pegmatite-forming temperatures inhibits the diffusion of some ions to and from crystal surfaces, and laterally along crystallization fronts. At the modest concentrations indicated by pegmatite bulk compositions and mineral equilibria, the viscosity-reducing effects of fluxes of B, P, F, and Li in addition to H_2O are insignificant in highly undercooled liquids of granitic composition (cf. London and Morgan, 2017).

11.1. Boundary layer liquids

An important result of rapid crystal growth into a viscous medium is that ions that are excluded from the growing crystals (incompatible behavior) pile up in the region of melt along the crystallization front. In so doing, those elements create a boundary layer of melt whose composition differs from that of the bulk melt, and increasingly so as crystallization advances. There are two consequences of boundary-layer pile up of excluded components. Increasing concentrations of excluded components can promote the local saturation and precipitation of minerals on adjacent crystal surfaces (see Fig. 17-3 of London, 2008, and Fig. 9 of London, 2009) even if the bulk melt is not saturated in those minerals. This is the foundational process behind the origin of graphic granite (Fenn, 1986), and it is responsible for the homogeneous textures of granites and of massive and layered aplites (London, 2009). Alternatively, the excluded ions along the crystallization front may act as fluxes to lower solidus temperatures, lower the activities of mineral forming components, and increase diffusivity of ions through the boundary layer liquid. In this case, the boundary layer liquid facilitates the dissolution of bulk melt into the boundary layer and the transport of ions to and from the growing crystal surfaces, while suppressing the nucleation of competing phases along the crystallization front. This is the process of constitutional zone refining (e.g., see Chapter 17 of London, 2008). Some of the fluxing components in pegmatite-forming melts, including H_2O, B, P, F, and an excess of alkalis over Al and Si, are utilized in the commercial fabrication of large crystals; hence, a knowledge has been gained that fluxes diminish the numbers of crystals that nucleate while promoting the growth of a few individuals to large size through their viscosity-reducing effects. Though fluxes have always been thought to play an important role in the generation of pegmatitic textures, a mechanism to attain high concentrations of fluxes in melts that are not appreciably enriched in them from the start (a few to tens to hundreds of ppm of B, P, and F) has proven to be a conundrum in the field. Constitutional zone refining (CZR) provides a mechanism to reconcile this apparent disparity.

Experiments with flux-bearing melts at pegmatite-forming temperatures have captured the formation of flux-rich boundary layer liquids adjacent to feldspar-quartz crystallization fronts (London, 1999; Morgan and London, 2005; London and Morgan, 2017). The liquids so formed are mostly more sodic than the bulk melt composition (London, 1999), poor in silica (55 wt% SiO_2) but quartz-saturated, and contain substantially higher H_2O concentrations due to the accumulated effects of B, P, and F (London, 2009).

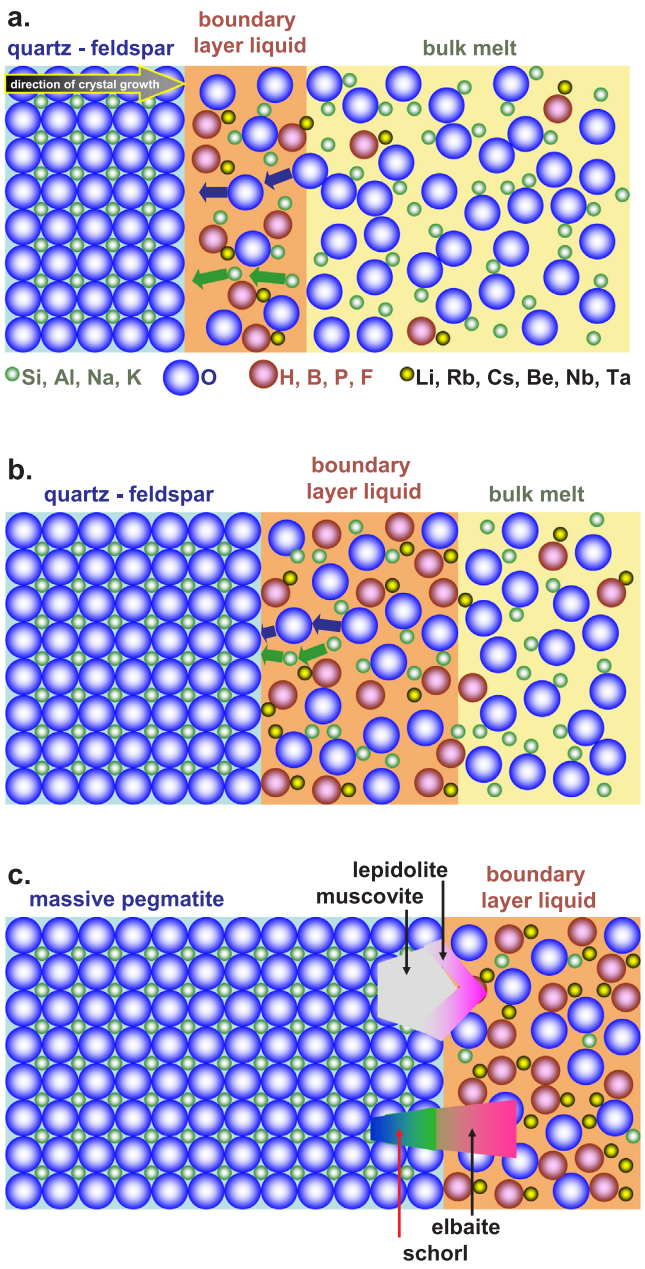

Fig. 27. Schematic rendition of constitutional zone refining (CZR) in the development of a flux- and incompatible element-rich boundary layer in a typical pegmatite-forming liquid. (a) As CZR operates, compatible components dissolve from the bulk melt through the boundary layer to attach to the surfaces of rock-forming minerals. (b) Excluded components become enriched in the boundary layer liquid because fluxes lower the solidus temperature and enhance the miscibility of all components. (c) Once the components of the bulk melt are exhausted, crystallization ensues from the boundary layer liquid, leading to abrupt changes in the compositions of minerals (micas, tourmaline) that grow through that interval.

As a conceptual aid, Fig. 27 illustrates the changes in melt composition in the boundary layer liquid as crystallization proceeds. The components of the bulk melt dissolve into the boundary layer and are transported through it to the growing crystal surfaces. Incompatible elements become enriched in the boundary layer liquid, but they are continuously diluted by the flux of compatible, mineral-forming components so long as the bulk melt remains. As crystallization advances,

the boundary layer of melt sweeps inward with the crystallization front, accumulating much of the melt content of incompatible components due to the fluxing effects of H, B, P, and F. Once the bulk melt is consumed, the remaining melt is that of the boundary layer liquid (e.g.,. see Table 8 of London and Morgan, 2017). It is in this manner that the crystallization of flux-bearing and viscous granitic melt resembles the process behind CZR.

The boundary layer liquid becomes the last silicate liquid in the pegmatite-forming environment once the bulk melt has been exhausted through crystallization. Liquids of that nature have been generated through the crystallization of the Macusani obsidian, wherein the B-rich boundary layer liquid evolves to the last fraction of melt that contains a combined 18.8 wt% of B_2O_3, P_2O_5, and F, and remains quartz-saturated with only 54.95 wt% SiO_2 in the remnant glass pools (compared to 72.32 wt% SiO_2 in the Macusani obsidian) (London and Morgan, 2017).

The consequences of a flux-rich boundary layer liquid on the diffusive transport of ions adjacent to growing crystal surfaces were modeled based on experiments that entailed the dissolution of quartz into an alkaline, flux-rich, silica-poor liquid that was a close approximation to the boundary layer liquids produced in prior experiments involving crystallization (London, 2009). London (2009) showed that in relation to simple hydrous haplogranitic melt and aqueous solution at 800 °C, 200 MPa, the rate at which the melt approached saturation in quartz via diffusive equilibration was $\sim 10^7$ times faster than in simple hydrous haplogranite liquid, and the mass transport with respect to time and distance was $\sim 10^7$ greater than in a comparable volume of aqueous solution. A dense, hydrous, alkaline, and flux-enriched liquid, therefore, fosters the mass transport of ions that is needed to grow giant crystals at low temperatures in time frames of the cooling history of thin pegmatite dikes.

11.2. Summary of liquid lines of descent

At the conditions of pegmatite consolidation, the pegmatite-forming melt can be characterized as a hydrous granitic liquid containing not more than a few percent of other fluxing components (Li, B, P, and F). As such, it possess exceedingly high viscosity in the undercooled regions along the contacts (see London and Morgan, 2017), where crystallization commences. The high viscosity of melt along the margins inhibits the diffusion of excluded components away from the nascent crystallization front, which initiates CZR in a boundary layer that becomes enriched in H_2O, fluxes, and other excluded components. The composition of the bulk melt may change little due to the low diffusivity of the HFSE, and as a result of the high diffusivity of Na and K that rapidly erases gradients in their concentration across the melt volume (Acosta-Vigil et al., 2006). Crystallization consumes the bulk melt via the diffusion of its components through the boundary layer liquid, and the boundary layer liquid grows in width and in the concentrations of excluded components. Local pile-up of excluded components causes sporadic crystallization of some phases along the crystallization front (e.g., tourmaline, garnet, beryl, etc.) even if the bulk melt is not saturated in these minerals. As the bulk melt is consumed by crystallization of quartz and feldspars predominantly, the residual melt approaches the composition of the boundary layer liquid. In thick pegmatite bodies that cool more slowly, the transition from bulk melt to boundary layer melt may be gradual. In thin dikes that experience more abrupt undercooling, the crystallizing assemblage changes sharply once crystallization ensues from the boundary liquid composition (Fig. 28).

12. Pegmatites as sources of industrial minerals, metals, and gems

Some commercial market exists for virtually ever mineral found in pegmatites. The economic viability of pegmatites depends principally on the volumes of the materials involved, their value, and their proximity to ore processing plants.

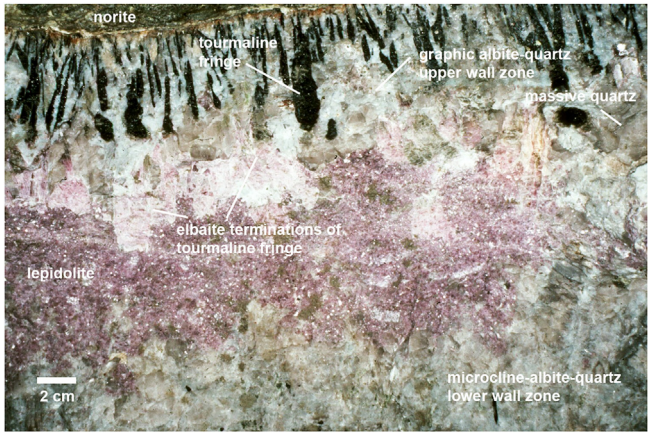

Fig. 28. A section through the Himalaya pegmatite, near Lake Henshaw, San Diego County, California, exposed in 1986. The host norite along the upper contact of the pegmatite is completely fresh; a layer of biotite < 1 mm thick separates the norite from the pegmatite. The hanging wall zone consists of mafic tourmaline in UST with graphic albite-quartz intergrowth, followed by sporadic pods of massive gray quartz. Extensions of the mafic tourmaline in the hanging wall sharply evolve to pink elbaite in the core, where they are intergrown with massive lepidolite. The lower wall zone visible in the photo contains microcline, albite, and quartz with prominent UST upward.

12.1. Industrial minerals: feldspars, quartz, muscovite, and lithium aluminosilicates

A review by Glover et al. (2012) summarizes the utilization of these industrial minerals in non-metallic products. Feldspars and quartz are principal components of glasses and ceramics. Muscovite is no longer widely used in sheet form, as it was when electronic vacuum tubes utilized sheet muscovite to separate the electronic grids, but it is still employed as a milled powder for use in paints, pressed composite construction board, glazes, and cosmetics. Pegmatitic quartz has a special application in the production of vitreous silica for high-temperature glass applications, and as the feed stock for Si in the semiconductor industry. Glover et al. (2012) note that high-purity quartz for vitreous silica contains < 100 ppm total impurities, and that ultra-pure quartz used in the manufacture of semiconductors comes principally from pegmatites and contains < 10 ppm total impurities. Large volumes, low cost of production in open-pit mines, and an abundance of suitable granite-pegmatite sources in most continental terrains mean that the ceramic grades of feldspar, quartz, and mica are sold mostly on local or regional markets rather than international ones. These deposits, referred to as “ceramic” pegmatites (e.g., Glover et al., 2012), encompass the cupolas of granites and their adjacent dense dike swarm of large, common granitic pegmatites.

Specialty glass-ceramics and glazes with low coefficients of thermal expansion still consume the much of the supply of spodumene and petalite minerals on the market, but refined Li chemicals for applications of Li in batteries now exceed special glass-ceramics in overall consumption of Li (USGS Mineral Commodity Summaries, 2018). Most Li is derived from intracontinental brines, salars, and altered rhyolites (e.g., Kesler et al., 2012). The deposit at Greenbushes, Western Australia, is the only significant pegmatitic source of Li minerals on the market at present, but numerous prospects elsewhere, most of which are in Western Australia and in Ontario, Canada, and various locations in China are under evaluation. Most of these deposits are Archean in age, but Jiajika, Sichuan, is a relatively young deposit.

12.2. Rare and specialty metals: lithium, beryllium, cesium, tin, niobium, tantalum, and uranium

All of these elements except cesium are derived principally from

non-pegmatitic sources that include brines, altered rhyolites, placers, and granites that may or may not have some pegmatitic components. Their uses are wide-ranging and diverse, from the mundane (corrosion-resistant tin coatings on metal, and as a component of solder) to the highly specialized (cesium formate, produced from pollucite for use as a high-density liquid in deep oil and gas drilling). Tonnages of pegmatitic ores are mostly held as proprietary information, but the Tanco pegmatite bulk composite composition (Table 1) gives a useful measure of the degree of enrichment for Li, Be, Cs, Sn, and Ta, all of which have had episodes of profitable mining there. Much of what makes a pegmatite like the Tanco mine profitable is the concentration of ores in zones; selective mining of zones then dramatically increases the grade of an ore metal over its whole-rock abundance.

12.3. Gem materials: tourmaline, beryl, topaz, and others from miarolitic cavities

Simmons et al. (2012) reviewed the principal varieties of gem materials found in pegmatites, some of the most important pegmatitic sources, the chemical affiliation of the gem-bearing pegmatites with the LCT or NYF families, and major gem-producing pegmatite provinces. As they affirm, gem production from pegmatites is a hit-or-miss, boom-or-bust endeavor that is mostly pursued as sporadic artisanal mining projects.

The rarity of miarolitic cavities in pegmatites has already been noted, and that rarity is surprising in light of the volume of aqueous fluid that would be exsolved upon the crystallization of initially H_2O-saturated granitic melt at pegmatite-forming depths. In addition, miarolitic cavities in pegmatites are not normally voids that were once water-filled, but rather packed with exceedingly dense clay that represents the last silicate component of the crystal-forming medium (London, 2013). Hence, the volume of the cavities far exceeds the volume of water that they contained.

Gem-bearing pegmatites run the gamut of types from moderately (beryl-bearing) to highly fractionated (pollucite-bearing) pegmatites in the LCT family. Gem materials include colored varieties of beryl (principally aquamarine, heliodor, and morganite), Li-rich tourmaline (mostly elbaite-rossmanite and liddicoatite), blue and sherry topaz, transparent varieties of spodumene (kunzite), low-iron (orange) spessartine, and optical-grade quartz (rock crystal and smoky). In the NYF family, gem minerals are mostly aquamarine and heliodor, topaz, rock crystal or smoky quartz, and optical-grade fluorite. Emerald and alexandrite (chromian chrysoberyl), and hiddenite (chromian spodumene) form in replacement bodies and veins within the exocontact of some Be-rich peraluminous pegmatites that are hosted by mafic or ultramafic rocks. These gem varieties are only rarely found within the pegmatites because of their extreme depletion in Cr and V.

13. Ore-forming processes within granitic pegmatites

13.1. Industrial minerals: feldspars and quartz

The glass-ceramics industries utilize both sodic and potassic feldspars for which the principal requirements are low Ca content (which raises melting temperatures) and low Fe contents (which impart color to glasses that is undesirable in all but brown or green bottle glass). Evolved S-type granites meet those requirements well; alkali feldspars in the more oxidized A-types may host appreciable ferric iron.

Calcium is removed by the fractional crystallization of plagioclase, such that the calcic content of plagioclase in the evolved upper portions of granites and in the first-formed border zones of pegmatites is oligoclase near An_{20} or less and falls sharply with the continued crystallization of plagioclase in pegmatites. K-feldspars are perthitic with bulk compositions of $\sim Or_{80\text{-}90}Ab_{20\text{-}10}$ and an anorthite component near zero.

In the S- and A-type granites and their pegmatites, iron is hosted principally by biotite, lesser amphibole, and minor ilmenite or magnetite. In magnetite-bearing granites, ferric iron can enter the alkali feldspar structure at weight percent levels; the recrystallization of such feldspars can render them brick red due to the exsolution of submicroscopic grains of hematite (Putnis et al., 2007). However, the solubility of mafic components – Fe, Mn, and Mg – in hydrous granitic liquids falls sharply with decreasing temperature. Synthetic liquids saturated in biotite, cordierite, garnet, or tourmaline at near-solidus temperatures contain ~1.5 wt% total mafic oxides (e.g., Wolf and London, 1997). Insofar as the last melts of large granite plutons are largely crystal-free liquids near their cupolas, and their pegmatites are crystal-free upon emplacement, then iron is a negligible contaminant, especially in the more reduced (ilmenite) S-type granites. Therefore, the mafic component of granites decreases by two means: as crystal-free liquid is separated from more mafic restite or cumulate constituents, and as the temperature of crystallization on the liquidus falls.

Aluminum is the principal trace-elemental impurity in quartz from granites and pegmatites. Typical Al contents range from tens to hundreds of parts per million (see pp. 39–40 of London, 2008); Li can exceed 1000 ppm, but values < 100 ppm Li are more typical limits of substitution (e.g., Breiter and Müller, 2008; Müller et al., 2008; Beurlen et al., 2011; Breiter et al., 2014). Lithium, potassium, and hydrogen provide most of the charge balance for Al in tetrahedral coordination. Complete solid solution between quartz and $LiAlSiO_4$ (β-eucryptite) exists in synthetic ceramics (e.g., Hatch, 1943), but such extensive solid solution by LiAl-substituted-quartz derivatives is not observed in pegmatites, where quartz coexists with spodumene, petalite, and eucryptite, all of near end-member composition. In experiments with Li-rich granitic melt, the H and Li contents of quartz vary inversely: quartz that crystallizes from highly supersaturated melt contains low Al with H in a charge-balancing role, while quartz that crystallizes closer to the equilibrium of the liquidus contains higher Al with mostly Li as a charge-balancing cation (London and Morgan, 2017).

The low contaminant levels of natural pegmatitic quartz, and especially the high-purity and ultra-high purity products that are the industry's standards, indicate that the extensive solid solution between quartz and its various Al-stuffed derivatives, such as β-eucryptite, are negligible at the natural conditions of crystallization. The decreasing miscibility between quartz and its stuffed derivatives may arise from the combination of elevated H_2O content of melt and low temperature of crystallization (London and Morgan, 2017). Subsequent hydrothermal recrystallization of primary quartz moves Al and its associated charge-balancing cations to grain boundaries, where minute crystals including micas may precipitate (e.g., Müller et al., 2008)). Comminution and processing can remove the minerals at grain boundaries, leaving the quartz as ultra-high purity. Such quartz possesses saccharoidal texture, or is opaque milky-white “bull” quartz. Therefore, the unique suitability of pegmatitic quartz for the specialized glass and an electronics industries derives from the low temperatures of crystallization in pegmatites, and from the widespread subsolidus hydrothermal recrystallization that ensues in large granite-pegmatite bodies (e.g., Neves and Godinho, 1999).

13.2. Enrichment of rare metals in pegmatites

Summarized from London (2008, 2016b), these are the key precepts for the enrichment of rare metals to ore-forming grades in pegmatites:

(1) The elements must be incompatible in the rock-forming assemblages of their source granites. That is, including quartz, feldspars, micas, garnet or cordierite, and accessory apatite, monazite, tourmaline, and oxides in their proper proportions, the bulk distribution coefficient for the elements in question must be appreciably less than one.
(2) The derivation of pegmatite-forming melts requires multiple stages in the extraction of silicate liquid from partially crystalline mush to

achieve the enrichment necessary to produce pegmatitic ores of rare metals.

(3) The abundances of rare metals in economically viable pegmatites and their melts are mostly lower than their saturation values at the solidus of the hydrous granite system (Table 4). Pegmatite-forming melts attain saturation in rare-element minerals by appreciable liquidus undercooling prior to the beginning of crystallization.

(4) Inward from the margins of the melt body, the growth rates of crystals are at their maxima, and the viscosity of the bulk melt is exceedingly high. That condition leads to the creation of flux-enriched boundary layer liquids through which CZR operates.

(5) The creation of a flux-rich boundary layer liquid fosters the mass transport of ions in the melt solution to growing crystal surfaces. The increased diffusivity and high mass transport capacity of the flux-rich boundary layer liquid eventually lead to the formation of large, monophase crystals in the interior zones.

(6) The pile-up of excluded components along the crystal-melt interface can lead to the precipitation of minerals in which they are essential structural constituents (ESCs), whether that mineral is saturated in the bulk melt or not (e.g., episodic deposition of tourmaline, beryl, garnet, etc). Because crystallization advances inward as a front, such episodic and sometimes cyclic local saturation results in mineralogical banding parallel to the contacts of the melt body, as in the formation of layered aplites, but also with unidirectional solidification texture in some minerals.

(7) The increasing chemical complexity of the boundary layer liquid, and especially the accumulation of components that act as fluxes, reduces the activities of some mineral-forming components in melt, and thereby forestalls saturation in otherwise insoluble minerals (e.g., London, 1987). An association of H with B, P, and F increases the solubility of H_2O in melt, which delays the separation of an aqueous solution from melt. The effects are particularly relevant to HFSE, as their abundances increase in the boundary layer liquid via CZR.

(8) The boundary layer liquid evolves to become the last silicate liquid in the pegmatite-forming environment. All fractionation indices point to the quartz-poor, albite-lepidolite bodies as the products of crystallization of the last such liquid in Li-pegmatites, and these bodies are most enriched in rare alkalis, Be, and HFSE, of which the Fe/Mn and Nb/Ta ratios approach zero.

(9) Rare-metal ores in pegmatites are igneous in origin, subject to some subsequent hydrothermal redistribution that mostly results in the dispersal rather than concentration of rare elements (especially true for Li and Cs).

13.3. The example of beryllium and beryl

The average abundance of Be in the continental crust is ~2.4 ppm Be (Wedepohl, 1995), and only 4.0 ppm Be in black and gray shales (Coveney, 2000), the most Be-enriched parental source material for anatectic granitic liquids. The average abundance of Be in twelve of the most beryl-rich pegmatites for which bulk compositions have been assessed is 205 ppm Be, with a beryl saturation threshold of ~35 ppm Be (Evensen and London, 2002; London, 2015b). With these constraints, greater than 95% crystallization of a granitic liquid that has accumulated from S-type anatectic sources is necessary to bring two-mica granites and pegmatite-forming melts to the beryl saturation threshold of ~35 ppm Be, and more than 99% crystallization is needed to reach the average of the beryl-rich pegmatites.

In the zoning scheme presented by Trueman and Černý (1982), beryl is the first rare-element mineral to crystallize in the proximal, muscovite-rich pegmatites of the LCT family. The beryl-saturation threshold value, ~35 ppm Be (e.g., Benson #2, Mtoko, Zimbabwe, Table 4), is applicable to these pegmatites, which are represented by composition HGS5Q in Fig. 25b.

In a geochemical survey that assessed muscovite as a prospecting tool for beryllium, Smeds (1992) noted that muscovite in "barren" pegmatites contained 120 ppm Be, whereas muscovite from beryl-bearing pegmatites contained just 25 ppm Be. Smeds (1992) observed that high values of Be in muscovite do not correlate with the precipitation of beryl, and he speculated that in these barren pegmatites, Be was entirely contained within rock-forming minerals. That hypothesis was borne out by experimental data from Evensen and London (2002), who showed the Be is compatible in muscovite and in oligoclase (An_{10-30}), a common composition of plagioclase in two-mica granites. Smeds' (1992) surprising observation, however, can be explained by two factors. One is the sharp decrease in the An content of plagioclase from source granite and proximal common pegmatites to the more fractionated distal ones. Beryllium is compatible in plagioclase close to An_{30} in composition, but almost completely incompatible in albite (Evensen and London, 2002). Thus, as the composition of plagioclase shifts from oligoclase in granite to albite in pegmatite, less Be is extracted by plagioclase, and the chemical activity of Be increases in the melt. The second and more important factor is the sharp decrease in temperature attending the emplacement of pegmatite-forming melts outside of and away from their granitic source. Using 25 ppm Be in muscovite and $D_{Be}^{muscovite/melt} = 1.35$ (Evensen and London, 2002), the coexisting beryl-saturated melt might have contained as little as 19 ppm Be, assuming that the pegmatites were saturated in beryl at the onset of crystallization. The solution of the power function (Fig. 25b) for beryl saturation at 19 ppm Be in melt yields a temperature of 332 °C. The very low solubility of beryl in highly undercooled melts accounts for the common appearance of beryl in the border zones of pegmatites (Fig. 10).

13.3.1. Spatial distribution of beryl in pegmatites

Beryl most commonly and abundantly occurs in three different pegmatitic zones. It is a common accessory mineral in the border and early wall zones of pegmatites (Cameron et al., 1949), where it forms conical and skeletal bluish-green crystals filled with quartz and feldspar that expand inward from the border (e.g., Case #1 pegmatite, Portland, Connecticut). At the Tanco mine, abundant beryl forms anhedral white crystals with tourmaline, columbite, and muscovite in coarse albite throughout the lower wall zone.

Beryl is mostly absent in the ensuing coarse-grained feldspathic intermediate zones (zones 4 or 7 of Cameron et al., 1949) and in aplites where these overlie the lower wall zone. Beryl reappears as a nearly monominerallic layer at the contacts between the innermost feldspathic intermediate zone or aplite and an adjacent quartz core. Beryl reappears in abundance in the latest-stage albitic (cleavelandite habit) zones, normally in association with lepidolite, spodumene, apatite, Ta-rich oxides, polychrome Li-tourmaline, and others of the rarer and more chemically exotic minerals of pegmatites. The episodic nature of the deposition of beryl is most consistent with precipitation due undercooling along the outer zones, and boundary-layer pile-up along inward crystallization fronts. An abundance of beryl in this latest-stage assemblage implies that CZR operates to enhance the solubility of Be in the boundary layer melt.

13.4. The example of cesium and pollucite

The average crustal abundance of Cs is 3.4 ppm (Wedpohl, 1995), and Cs attains a mean value of 7.4 ppm in marine shales that are the most enriched crustal sources of the element (Coveney, 2000). Approximately 90% of the initial Cs content of the white micas formed in metamorphosed marine sediments is lost during prograde metamorphism up to anatectic conditions (Bebout et al., 2007). That would mean that anatectic melts might begin with ≤1 ppm Cs (e.g., see samples AM in Table 2 of Bebout et al., 2007).

Unlike beryllium, Cs is highly soluble in silicic melts (London et al., 1998). As a consequence, hydrous granitic melts at their solidus temperature become saturated in beryl at tens of ppm of Be, whereas melts

are saturated in pollucite at weight-percent (10^4 ppm) levels of Cs (London et al., 1998).

At Tanco, pollucite first appears as small masses in association with the spodumene-rich intermediate zone (Černý, 1972), and as gigantic monominerallic masses in association with similarly coarse-grained petalite, quartz, montebrasite, and fine-grained albite-lepidolite bodies, in the latest-stage units. The spodumene-rich intermediate zone lies mostly in the upper portion of the pegmatite and begins ~40–50% of the distance inward from the hanging wall toward center line (Stilling et al., 2006). The Cs content of the Tanco body is estimated as 3036 ppm Cs, which is well below the liquidus saturation value of 51,880 ppm Cs at 700 °C (Table 4). With 3036 ppm Cs, the pollucite saturation temperature is only ~384 °C.

The leucite ($KAlSi_2O_6$) component of pollucite varies linearly with temperature in granitic melt (London et al., 1998). Based on compositions at Tanco reported by Černý and Simpson (1978), primary pollucite with an average of 0.84 mol% leucite crystallized at ~401 °C. At that temperature, a granitic melt could be saturated in pollucite with at little as ~7000 ppm Cs in melt (Fig. 25d). Using a bulk distribution coefficient of 0.06 for Cs (London, 2015a), the pegmatite-forming melt at Tanco would have reached that value, 7000 ppm Cs, with 41% crystallization of the body, which is consistent with the first appearance of pollucite in the spodumene-rich upper intermediate zone.

13.5. Niobium, tantalum, and tin

In most respects, the solubility/saturation surfaces of cassiterite (Sn), columbite (Nb), and tantalite (Ta) are more similar to Cs than to Be: the oxide components of these minerals possess solubilities in granitic melts at liquidus temperatures that are significantly higher than any of their major ore deposits (e.g., Taylor and Wall, 1992; Linnen and Cuney, 2005). That solubility increases with increasing alkalinity of a flux-enriched melt (Taylor and Wall, 1992; Linnen and Cuney, 2005; van Lichtervelde et al., 2010), as might be the case in the formation of a strongly alkaline and sodic boundary layer liquid (e.g., London, 1999; 2009). Textural evidence (Fig. 29) points to a predominantly magmatic, as opposed to hydrothermal origin for these HFSE oxides (e.g., van Lichtervelde et al., 2007).

Despite the complete diadochy between Nb-Ta and Zr-Hf, their principal minerals of columbite-tantalite and zircon-hafnon exhibit an extreme range of compositions. In both pairs, the more abundant of the two elements, Nb and Zr, are enriched in the least fractionated rocks, and their counterparts, Ta and Hf, predominate in the most fractionated pegmatites (see Figs. 13 and 14 of Černý et al., 1985). Linnen and Cuney (2005) suggested that the fractionation trend of decreasing Nb/Ta in oxides derives from the lower solubility of columbite with respect to tantalite in granitic melt. Stepanov et al. (2014) proposed that the fractionation trend of decreasing Nb/Ta from granites to pegmatites stems from the crystallization of biotite and muscovite from granite- and pegmatite-forming melts. Stepanov et al. (2014) make the valid point that the crystallization of oxides, in which Nb and Ta are compatible, would deplete the melt in these components; consequently, the mode of mafic oxides must be and remain exceedingly low in the magmas that give rise to pegmatitic deposits of Nb and Ta.

Among the HFSE that include Nb, Ta, Zr, Hf, and Sn, only tin possesses a variable ionic charge, 2+ or 4+, at oxidation states ranging from FMQ (fayalite-magnetite-quartz) to NNO (Ni-NiO). The fraction of the more soluble Sn^{2+} falls by ~15 mol% at 800 °C, 200 MPa, from FMQ to NNO in hydrous granite (Taylor and Wall, 1992), and that increase in oxidation state of melt could promote the precipitation of cassiterite or Sn as a component of other oxides. The S-type granites with which the LCT pegmatite family is associated originate from graphitic sources that lead to reduced partial melts in which ilmenite rather than magnetite predominates the oxide assemblage (Ishihara, 2005). However, pegmatites are so depleted in mafic components that they possess little if any intrinsic oxidation buffering capacity. Pichavant et al. (2016) postulate that fO_2 in pegmatite-forming melts increases with increasing dissolved H_2O in the melt via its dissociation to $H_2 + ½O_2$, but other workers find little or no influence of the H_2O content of the melt on the redox state of Fe (e.g., Moore et al., 1995; Baker and Rutherford, 1996). Evidence from pegmatites points to an fO_2 in pegmatite-forming melts close to NNO: (1) pegmatites generally contain no minerals in which Fe^{3+} is an essential structural constituent; (2) the fO_2 in H_2O-saturated rhyolitic melt at 800 °C, 200 MPa yields a ratio of Fe^{3+}/Fe_T of ~0.1, which is the ratio close to a NNO buffer (Moore et al., 1995); and (3) that is the same Fe^{3+}/Fe_T ratio as in common black pegmatitic tourmaline at the NNO buffer (Fuchs et al., 1998). Nonetheless, the solubility of Sn in melt at fO_2 between FMQ and NNO buffers is so high (400–2500 ppm Sn: Taylor and Wall, 1992) in relation to Sn contents of ore-bearing granites (e.g., the cassiterite-bearing Cornubian granites, with < 20 ppm Sn: Simons et al., 2017) that melts at or near their liquidus temperatures cannot be saturated in cassiterite. Thus for Sn, as for the other HFSE, attaining magmatic saturation in cassiterite is most likely the result of crystallization at low temperature via liquidus undercooling.

13.6. Gem-bearing pegmatites

Miarolitic cavities in pegmatites have been likened to bubbles of aqueous solution that rise through granitic melt to collect in the roof-ward portions of what become miarolitic pegmatites (Simmons et al., 2012). Jahns (1982), who originally invoked thermal gradients as the driving force for the redistribution of mineral constituents (Jahns and Burnham, 1969), eventually turned to the ascent of bubbles generated by the initial crystallization of pegmatite-forming melt along the footwall portion as the principal agent for pegmatitic textures and zonation. In neither case has a viable mechanical model been presented. As explained above, the viscosity of the pegmatite-forming melt prohibits the ascent of small aqueous bubbles in the short duration of crystallization of thin miarolitic pegmatites.

In recent experimental simulations of crystallization entailing a Li-pegmatite composition, London and Morgan (2017) observed that vesicles formed in melt along the solidification fronts of crystals even when the bulk melt was undersaturated in H_2O. From a succession of increasingly crystallized products, it appears that the bubbles get pushed along by the advance of the crystallization front and finally coalesce in the central region of the synthetic pegmatite body, where they constitute ~25% of the volume of the charge when the melt is initially H_2O-saturated (see Figs. 2a,c and 5 of London and Morgan, 2017). This measured volume of aqueous solution matches the volumetric calculations that apply to the crystallization of a haplogranitic liquid (liquid → crystals + H_2O) that is just saturated in H_2O (6.6 wt% H_2O: e.g., Acosta-Vigil et al., 2003) at 200 MPa at its thermal minimum (685 °C: Tuttle and Bowen, 1958). The volume change of the crystallization is +24%, in which aqueous fluid will occupy 25% of that total volume (London, 2008). Miarolitic cavities, therefore, should be an appreciable volumetric component of all pegmatites if their melts are saturated in H_2O at the inception of crystallization. If not contained within pegmatites as miarolitic cavities, that volume of aqueous solution should make a significant metasomatic alteration halo around pegmatite bodies. London (2008) considered these and other lines of evidence that should constitute evidence of an aqueous phase during the consolidation of pegmatites, and concluded that for the most part, and except for miarolitic cavities, that evidence is lacking or negative.

Though the miarolitic pegmatites have always been regarded as the shallow (100–150 MPa) equivalents of the deeper rare-element pegmatites, the point has already been made that the depths of emplacement are not much different between these two classes of pegmatites. What makes some pegmatites miarolitic, but most not, might hinge upon the initial H_2O content of the melt, or on the physical nature of crystallization in the pegmatite. Miarolitic pegmatites commonly exhibit prominent unidirectional solidification texture, even into their

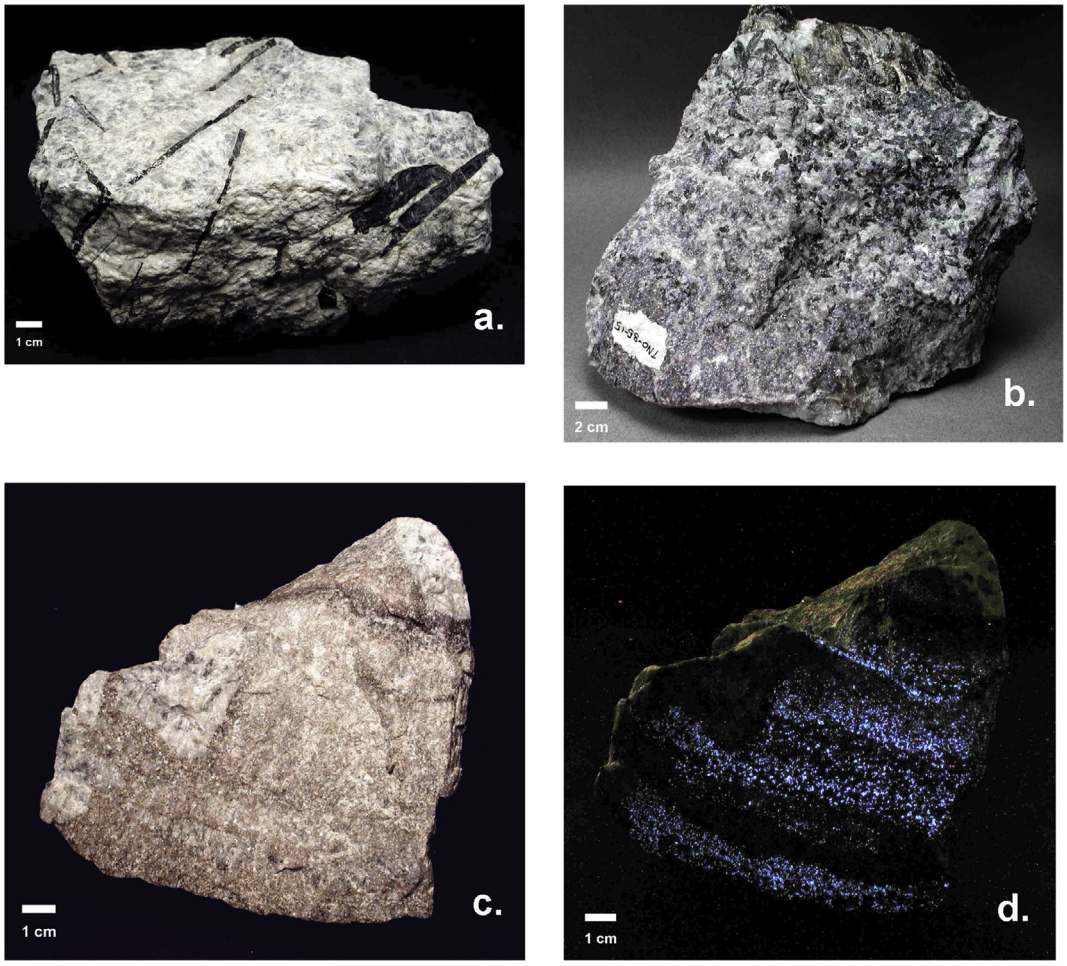

Fig. 29. Representative ore samples of Nb and Ta oxides. (a) columbite (black) in albite, part of a late stage assemblage including lithiophilite, apatite, elbaite, lepidolite, and beryl at the Homestead mine, White Picacho district, Arizona. (b) Wodginite (black) with lepidolite, albite, and quartz, Tanco mine, Bernic Lake, Manitoba. (c) Microlite (brown) and colorless simpsonite (white) in layered albitic aplite, Tanco mine, Bernic Lake, Manitoba. (d) Short-wave ultraviolet blue fluorescence of simpsonite, $Al_4(Ta,Nb)_3O_{13}(OH,F)$, in the same sample as (c).

miarolitic cavities, and this is a consequence of crystallization at highly undercooled states. In turn, undercooling promotes continuous crystallization of the border and wall zones along the margins of the body. London and Morgan (2017) observed miarolitic cavities when the solidification fronts completely surrounded the margins of their experimental melt, but no miarolitic cavities when domains of melt remained in contact with the margin of the body. They inferred that aqueous solution was exsolved in both cases, was trapped by the continuous solidification front, but diffused out of the melt when in contact with a surrounding aqueous film.

13.6.1. The pocket-forming medium

The transition from turbid to clear crystals reflects a change in the environment of crystal growth. Turbidity results from the entrapment of solid and fluid inclusions along growth surfaces, a state that is fostered by high rates of crystal growth and high viscosity of the growth medium (e.g., Fig. 17-3 of London, 2008). The density of such defects can be diminished by two means: a decrease in the rate of advance of the growing crystal, which lowers the supersaturation along the crystal surface, or an increase in ionic diffusivity that results from the depolymerizing, viscosity-reducing effect of fluxes. Of these two mechanisms, the effects of H_2O and other fluxing components in the final boundary layer composition are more likely to promote the transition to inclusion-free crystals. There may be other factors, such as selective wetting of crystal surfaces by aqueous fluid in the final stages of pocket formation (e.g., Roedder, 1984). Solute-poor aqueous solution is the last fluid medium in contact with the surfaces of shiny crystals, though it is not the principal source of solutes that comprise the gem crystals (e.g., Peretyazhko et al., 2004; London, 2013).

Roedder (1984) described inclusions in miarolitic topaz from the Volodarsk occurrence as filled with soluble chlorides and fluorides. There, he suggested that the last fluid in the cavities might have been a hydrous salt melt. If correct, then those pegmatites arrived at a very high degree of crystal-chemical fractionation of melt without the prior loss of soluble halides to an aqueous fluid; that is, the evolution of the granite could not have included the early separation of an aqueous phase, as this would have stripped chlorides from the melt prior to the consolidation of the gem-bearing pockets.

The physical state of the miarolitic stage can be deduced in part from the distribution of crystals within. Miarolitic cavities in pegmatites with mostly LCT affinity tend to be packed with exceedingly dense clay, with and without granulated pocket rubble of quartz and feldspars, or cavities are open space as found. In the former case, doubly terminated euhedral crystals and crystal fragments are suspended in the clay; in the latter case, the euhedral pocket minerals lie in a pile along the pocket floor. London (2013) reasoned that the almost perfectly intact crystals piled at the bottom of open-space cavities settled gradually to the floor as a suspending cushion of clay slowly weathered away. London (2013) suggested that this clay forms when an aqueous solution exsolves from the last, flux-rich hydrosilicate liquid in the body. The result is a compositional quench of the remaining silicate material to clay (e.g., Jahns, 1982; London, 2013).

The thermal state of miarolitic cavities is also partly revealed by mineralogy. Zeolites including stilbite-stellerite and laumontite are common, as is calcite or sometimes rhodochrosite, as overgrowths on feldspars, quartz, tourmaline, etc. Opal is known as well. The deposition of these minerals and opal is successive, and it is not affirmed nor likely that all of the associated minerals in miarolitic cavities form an isothermal assemblage; however, the common association of zeolites and carbonates with the main-stage coarse silicates makes likely that the pocket-forming condition is below 550 °C, and continues down to below 300 °C, the upper stability limit for stilbite (Juan and Lo, 1973).

13.6.2. LCT family

Fluid inclusions in nearly gem-quality crystals from miarolitic pegmatites of Afghanistan and southern California possess salinities (based on freezing-point depression) near zero (e.g., London, 1986b; London et al., 2012b), though these inclusions contain an abundance of daughter minerals that include silicates, borates, phosphates, arsenides, and arsenates.

At Mt. Mica, Maine, pollucite occurs in the wall zone, as massive crystals in the core, and within miarolitic cavities (Simmons et al., 2015). Calculated temperatures of crystallization based on the leucite component are 504°-550 °C for two wall zone samples, 443 °C for massive pollucite in the core, and 391 °C for gemmy pollucite in miarolitic cavities (Table 6). These temperatures are consistent with the results of feldspar thermometry in massive and miarolitic pegmatites in California (Morgan and London, 1999; London et al., 2012b).

13.6.3. NYF family

In the NYF family, pegmatites normally form isolated segregations within their source granite. Miarolitic cavities represent an abundant proportion of the entire pegmatitic volume. Crystals line the open-space cavities and may or may not be detached from their substrates. Clay is not normally present, but as in the LCT family of pegmatites, may have been present. London (2013) suggested that gigantic miarolitic cavities of pegmatitic segregations hosted by A-type granite at Volodarsk, Ukraine, may be a case in point: Lyckberg et al. (2009) described meter-scale crystals of quartz and topaz have come to rest at the bottom of decameter-scale cavities with no damage to themselves or to the delicate gem-quality crystals of beryl below. London (2013) hypothesized that these cavities were originally clay-filled, which allowed the crystals to settle gradually once they detached from the roof of the pockets.

The abundant occurrence of miarolitic pegmatites within A-type granites, and rarely found as dikes beyond the margins, might be explained by their environment of emplacement. The A-type granites occur as shallowly emplaced thin sills (e.g., Hogan and Gilbert, 1995). As such, they lack the heat content in their shallower and colder hosts to propagate late-stage dikes beyond the granite margins (Rubin, 1995). Their shallow levels of emplacement may also contribute to the large volume fraction of void space in their pegmatites, as compared to the layered dikes of the LCT affinity. The granites themselves are also pervasively miarolitic, with cavities on the order of a few millimeters.

Finally, note that the rate of pegmatite cooling decreases exponentially as the body approaches the temperature of the host rock at its regional geothermal gradient. At the temperature of the host rocks, the pegmatite body cools at the rate of uplift. Therefore, the final stage of crystallization in cavities that entails zeolites, clays, and even organic matter (Franz et al., 2017) in the range to 300 °C down to 150 °C may ensue thousands of years after the initial rapid cooling and crystallization of the body.

Table 6
Temperature of Crystallization of Pollucite at Mt. Mica, Maine.[1]

Pollucite Crystallization Temperature from Leucite
[2] algorithm: T = 22.769 * Lct + 381.44

Internal Zone	Leucite mole%	T, °C
Lower wall zone, garnet line	7.4	550
Lower wall zone, garnet line	5.4	504
Pods in the core	2.7	443
Miarolitic cavities	0.4	391

[1] From London (2018).
[2] Lct = mole% leucite component among all M^+ cations.

14. Predictive guides to exploration

Exploration guides for pegmatite-hosted ores are not well documented nor advanced in their methods. Virtually all of the pegmatite bodies that have been prospected or mined have been found as surface outcrops; perhaps only one potential economic target has been located in the subsurface purely by indirect means (Galeschuk and Vanstone, 2005).

Logical steps to exploration, however, can be drawn from the systematic attributes of pegmatite groups and their environment of emplacement. The spatial zonation of a group of pegmatites around their common granitic source is the most fundamentally useful guide to specific types of pegmatite deposits. The sharply bounded internal zonation of rare-element pegmatites may facilitate their selective mining, but that same zoning makes the continuity of ore units difficult to predict. Because of this zonation, finite-element models of resource assessment that are commonly applied to more uniform porphyry-vein deposits do not work well on pegmatites.

14.1. Ceramic deposits

The distribution of pegmatites in the Black Hills District, South Dakota, is a prime example of spatial variations in the abundance and compositions of pegmatites in a zoned group (Fig. 7). A dense aureole of pegmatites surrounds the margins of the Harney Peak granite, and it is these proximal pegmatites that have been exploited mostly for industrial minerals. In the Spruce Pine district, North Carolina, the principal quartz and feldspar deposits are located along the margins of the source granites and in the adjacent pegmatite dikes.

The deposits that provide most of the quartz, feldspars, and muscovite for glass-ceramics industries come from small (generally < 10 km^2 in surface exposure) plutons that are the culmination of more voluminous (batholithic) granitic magmatism. The ore-forming granite-pegmatite plutons possess a very low color index owing to almost complete depletion in mafic minerals, and they are unfoliated except in rare instances of alignment by flow. Pegmatitic and aplitic textures predominate in the cupolas of these small plutons, and progress to a greater degree of spatial organization outward into individual pegmatite dikes.

Distal pegmatites are no less suitable as sources of ceramic minerals than are the pegmatite bodies close to their plutons. They tend to be smaller and more isolated, however, such that ore volume becomes the limiting issue. In the LCT family, however, the distal pegmatites are sources of spodumene and petalite for glass-ceramics.

14.2. Rare-element deposits

The regional zonation model presented by Trueman and Černý (1982), which emphasizes the rare-element enrichment trends in the LCT family of pegmatites, is evident in the regional zonation of the Black Hills, in the Hindu Kush of Afghanistan (e.g., Černý et al., 2005), and in the Bernic Lake and Yellowknife pegmatite districts in Canada where the systematic nature of the zonation was first described (e.g., Černý, 1991b). The largest and most fractionated of the Li-rich pegmatites occur at the margins of the pegmatite group (Fig. 7). Their host rocks, typically reflecting the peak metamorphic conditions of the upper greenschist-lower amphibolite facies of metamorphism (~ 550 °C: Moody et al., 1983), lie beyond the thermal aureole of the source pluton.

Beryl is the first rare-element mineral to appear beyond the ceramic pegmatites because Be is incompatible in melt and in most rock-forming minerals except cordierite and in plagioclase of An_{30} (Evensen and London, 2002). Beryl-rich pegmatites – those that possess ~200 ppm Be in their bulk liquids – might be saturated in beryl at their liquidus temperatures, in which case beryl should precipitate in the border and wall zones and at least sporadically with the progress of crystallization. For the proximal pegmatites, which presumably contain lower Be concentrations, appreciable liquidus undercooling might bring them saturation in beryl in the border and wall zones, even if the bulk melt is undersaturated. For this reason, the occurrence of beryl in the border and wall zones is not a good predictor of internal ores.

The same relationship holds for Nb as columbite, the next rare-element mineral to join beryl in the progression of increasing enrichment outward from source (Trueman and Černý, 1982). As an example, the unweighted average of the highest Nb values in ten outcrop areas of the Harney Peak granite, South Dakota, is 23 ppm Nb (Shearer et al., 1987). However, a melt with this Nb content should become saturated in columbite at ~597 °C (Fig. 25c). This explains why the border and wall zones, the most undercooled portions of the pegmatite, commonly contain columbite in relatively unfractionated pegmatites (Cameron et al., 1949).

Jolliff et al. (1992) examined the major and some trace-element abundances of muscovite in wall zones of unfractionated (e.g., Dan Patch) and highly fractionated Li-rich (e.g., Etta) pegmatites of the Black Hills, South Dakota. They found significant overlap in the abundances of indicator elements. For example, muscovite from the Dan Patch body contained 105–540 ppm Rb and 22–95 ppm Cs, whereas the Etta muscovite contained 320–620 ppm Rb, and 56–260 ppm Cs. Gallium, which increases in proportion to Al in mica with increasing chemical differentiation of pegmatites (Černý et al., 1985), was 19–48 ppm Ga in the Dan Patch muscovite, but only 20–23 ppm Ga in muscovite from Etta. At least for the Black Hills district, the mineralogy and compositions of the border zones do not correlate well with the overall extent of chemical fractionation of the pegmatite bodies.

14.2.1. Wallrock alteration haloes

Pegmatite-induced alteration of host rocks is nil to absent around the vast majority of the common and moderately fractionated rare-element pegmatites. When present, the alteration is confined to a few cm from the contacts, and it is most typically manifested as tourmaline or biotite that has replaced some mafic mineral of the host rock. Wallrock alteration becomes more conspicuous, with increasing imprint of more chemically evolved aqueous solutions, within meters around the most fractionated and largest of the LCT family of pegmatites.

Holmquistite, an Li-amphibole that is virtually indistinguishable from glaucophane in hand specimen and thin section, is found around particularly Li-rich pegmatites that are hosted by amphibolite (Heinrich, 1965). London (1986c) demonstrated how the misidentification of holmquistite as glaucophane could reveal Li-rich aureoles around highly fractionated pegmatites.

Tourmaline is particularly abundant the around pegmatites that are hosted by amphibolites or aluminous gneisses or schists. Tourmalinization is pervasive around some bodies or fracture-controlled to distances of tens of meters away along blow-outs that may be traced back to tourmaline-cemented breccias emanating from the cores of the pegmatites (see Figs. 12-5 and 12-6 of London, 2008). Most silicate host rocks contain sufficient mafic components in hornblende, biotite, cordierite, etc. that these rocks are extensively if not completely replaced by tourmaline plus quartz with little else. Rock fabrics of the hosts are commonly preserved by the replacement texture. Tourmalinization may be extensive even around pegmatites that contain no tourmaline themselves (e.g., the Harding pegmatite, New Mexico: Chapter 7 of London, 2008). London and Manning (1995) also found this to be generally the case in association with granites of Cornwall, UK. The latest and most fractionated "topaz granites" contain no tourmaline or other mafic minerals except for small and rare pegmatitic segregations along the contacts, but outward from those contacts, any and all host rocks were extensively replaced by tourmaline. Exceedingly low mafic content accounts for the lack of tourmaline within B-rich granites and pegmatites: Wolf and London (1997) found that when the activities of boron and aluminum in melt are high, and Fe or Mg is the limiting component in the activity product of the tourmaline component of melt, then the crystallization of tourmaline reduces the mafic content of melt to just 0.02 wt% mafic oxides. The low activity of Fe as buffered by crystallization of tourmaline led to in the exceedingly high purity of kaolinite in the china-clay granites of Cornwall.

Metasomatic tourmaline may be a useful guide to miarolitic cavities (discussed below), but tourmalinization is so prevalent around even modestly fractionated pegmatites that it is of little use as an indicator of rare-metal mineralization. The composition of the metasomatic tourmaline more closely matches that of the host rock than of the chemistry of the pegmatite from which boron-bearing fluid was derived (e.g., Morgon and London, 1987; Roda et al., 1995; Selway and Černý, 1998).

Metasomatic biotite, however, can accommodate Rb and Cs in its interlayer site, and Li in its octahedral site, leading to rare-alkali enriched zinnwaldite solid solutions (e.g., Morgon and London, 1987; Hawthorne et al., 1999). In the alteration zone around the Tanco pegmatite, anomalies for Cs and for Rb that are accommodated in metasomatic zinnwaldite correlate closely with the proximity of large masses of pollucite in the western, upper central, and eastern portions of the dike. The rare alkalis reach concentrations of nearly 2 wt% oxides in metasomatic micas, which is easily detectable by electron beam methods.

Shearer et al. (1984a, b) concluded that the metasomatic aureoles around pegmatites in the Black Hills district were the result of interaction between reactive host rocks and a very small volume of solute-rich solution derived from pegmatite. The uniquely large drill core repository through the Tanco pegmatite, Manitoba, facilitated the only complete spatial map of the distributions of Rb, Cs, B, and F around any Li-rich pegmatite (Morgan and London, 1987). As in the Black Hills study, Morgan and London (1987) found the metasomatic aureole around Tanco to be narrowly confined to the first few meters away from the pegmatite body, with extensive to complete replacement of the host amphibolite. The Tanco study also revealed that the wallrock alteration halo surrounded the pegmatite more or less completely, and that the chemistry of the metasomatic aureole correlated with the most evolved internal pegmatitic units in the closest proximity to the alteration halo. This distribution requires that the innermost units were crystallized before aqueous solution left the pegmatite. It further indicates that the egress of aqueous solution occurred through both top and bottom contacts in a direction normal to the pegmatite contacts, i.e., not along the central axis of the pegmatite.

14.2.2. Soil geochemical surveys

Though soil geochemical surveys are gaining wide use in exploration efforts for rare-element pegmatites, very little of that work is published. Only Galeschuk and Vanstone (2005) have presented details of the methods and their results for pegmatites in the Bernic Lake group of Manitoba. They describe soil anomalies as apical (positive elemental anomaly directly above the pegmatite) and combined (positive anomaly over the pegmatite, depletion to the sides). For the unexposed Dibbs pegmatite, which was validated by drilling, they flag combination anomalies for Rb and Cs as highly significant, and a weak to moderate apical signal for Li is flagged as well. They assert that the soil geochemical survey has merit over lithogeochemical anomalies because the latter may be located along fractures that have transported key elements away from their point of origin. However, the regional soil anomaly map for Li (their Fig. 18) shows nearly no apical anomaly over the Tanco pegmatite, but a string of significant highs trending northeast from it. Subsequent drilling over and around these anomalies found

little to no pegmatite at all.

For the most part, the HFSE lack apical anomalies in the soil survey because they are highly insoluble in aqueous solutions. It is the same reason that enrichments of Be, Nb, Ta, and P are internal to pegmatites, and these elements are not significantly enriched in the hard-rock metasomatic halo around rare-element pegmatites, which is hydrothermal in origin.

A key difference between the hard-rock anomaly and the soil anomaly is that in the former, otherwise soluble elements (alkalis) are incorporated into minerals; in soils, they are principally absorbed on surfaces, unless the soil is itself a saprolite formed from weathered remains of a hard-rock aureole. Therefore, the soil anomaly can migrate via groundwater flow, the hard-rock anomaly cannot.

14.3. Gem-bearing miaroles

The development of a gem mining district follows from some initial surface discoveries including hard-rock, eluvium, and alluvium. Gem-bearing pegmatites are not restricted to a particular geologic era, though a consensus remains that miarolitic pegmatites form at shallower depths than their massive counterparts, and hence would not be expected in the deeply eroded portions of collisional mountain belts. Miarolitic pegmatites tend to occur as thin, subhorizontal, layered bodies that form tabular dikes in competent host rocks; discontinuous lenticular pegmatites rarely are miarolitic, perhaps because their lenticular shape reflects a ductile state of the host at deeper levels of emplacement. The stress environment of their emplacement is marked with a large component of vertical dilation. As a result, segments of dikes form an *en chelon* pattern, with the horizontal segments the thickest. Miners know that miarolitic cavities are most likely to occur where a “roll” (the steeply dipping segment of an *en chelon* dike) flattens out into a thick horizontal dike segment. Within subhorizontal dikes or dike segments, miarolitic cavities are also distributed with a systematic spacing along the dike center (Fig. 19). That spacing results from K-feldspar pillars that grow in from one or both sides of the wall zone to pinch off the dike into segments (e.g., right-hand side of Fig. 5). Within each segment, the ensuing intermediate zones isolate small batches of residual melt in cells. The cells contain the most fractionated mineral assemblages, and miarolitic cavities, if present. This cellular structure is evident in the thin miarolitic dikes (e.g., Figs. 5, 19) of San Diego County, California and in the giant Tanco pegmatite (London, 2014c). The vertical sequence of zones and their proportions also are the same. The consistent scaling of zones and their proportionate thickness to the size of the body indicates that the zoning sequence is determined not by the rate of cooling, but the magnitude of undercooling.

Considering that miarolitic pegmatites constitute incontrovertible evidence for the exsolution of an aqueous fluid prior to their complete solidification, it is surprising that there is practically no metasomatic aureole developed around them. In San Diego County, dikes that can be traced and sampled for a kilometer have no more than a thin, mm-scale layer of biotite or tourmaline along their contacts with highly reactive gabbros and norites (Fig. 28). Near miarolitic cavities, however, tourmalinization of those same hosts can be extensive, as observed by the author at the San Diego mine, Mesa Grande district, and the Little Three mine, Ramona district, Calilfornia.

15. Concluding remarks

Pegmatites remain as primary sources of industrial minerals for the glass-ceramics and electronics industries, as primary to secondary resources of rare metals, and as principal sources of several important colored gemstones. There is a market for practically every mineral that occurs in pegmatites, and increasing demand for Li has rejuvenated exploration for rare-element pegmatites. What makes some pegmatites economic and others not has more to do with their small size and, sometimes, complex dike patterns that complicate mining. What miners and explorationists largely do not understand about pegmatitic ores of rare metals and gems, however, is that there are very systematic clues to finding them within: the internal structure of pegmatites is highly organized and readable, if not completely predictable.

Whereas pegmatites used to be thought of as magmas that crystallized slowly over millions of years, their cooling histories as thin dikes in host rocks at the temperature of their geothermal gradient are now known, beyond any reasonable doubt, to be in the range of days to years before the granitic liquids would solidify as glass. This conclusion renders an already enigmatic process – the growth of giant single crystals – even more problematic in a closed system of low and rapidly dwindling thermal energy.

The single most important cause of pegmatitic textures and zonation is appreciable liquidus undercooling, by ~200 °C, before the onset of crystallization (London, 2014b). Undercooling follows from the high viscosity of pegmatite-forming melts, and not necessarily a rapid rate of cooling. All else – mineral habits, rock fabric, and spatial zonation of textures and assemblages – ensues from that state. Variations in the zoning sequence (Cameron et al., 1949) or the spatial location of certain zones (e.g., the vertical distribution of albite and K-feldspar in layered pegmatites) may arise from the particular vagaries of environment: the first phase to crystallize, and where it nucleates, largely determines the spatial distribution of all that follows. In this way, the crystallization of pegmatites can be modeled as fractal systems (Baker and Freda, 1999).

Specialized applications for Li and for Cs have rekindled interest in pegmatites as sources of these commodities. Mineralogically ordinary outer zones and very localized wallrock alteration make pegmatites difficult blind targets for exploration. The occurrence of metasomatic alteration haloes in the host rocks immediately adjacent to pegmatites currently represents the best indirect indicator of internal rare-element mineralization, and of miarolitic cavities in pegmatites that have otherwise not induced a pervasive metasomatic aureole.

References

Ackerman, L., Zacharias, J., Pudilova, M., 1999. P-T and fluid evolution of barren and lithium pegmatites from Vlastějovice, Bohemian Massif, Czech Republic. Geol. Rundsch. 96, 623–638.

Acosta-Vigil, A., Buck, I., Hermann, J., Cesare, B., Rubatto, D., London, D., Morgan, G.B.V.I., 2010. Mechanisms of crustal anatexis: a geochemical study of partially melted metapelitic enclaves and host dacite, SE Spain. J. Petrol. 51, 785–821.

Acosta-Vigil, A., London, D., Morgan, G.B.V.I., Dewers, T.A., 2003. Solubility of excess aluminum in hydrous granitic melts in equilibrium with peraluminous minerals at 700–800 °C and 200 MPa: significance and applications of the aluminum saturation index. Contrib. Miner. Petrol. 146, 100–119.

Acosta-Vigil, A., London, D., Morgan VI, G.B., Dewers, T.A., 2006. Dissolution of quartz, albite, and orthoclase in H_2O-saturated haplogranitic melt at 800°C and 200 MPa: diffusive transport properties of granitic melts at crustal anatectic conditions. J. Petrol. 47, 231–254.

Acosta-Vigil, A., London, D., Morgan VI, G.B., Cesare, B., Buick, I., Hermann, J., Bartoli, O., 2017. Primary crustal melt compositions: Insights into the controls, mechanisms and timing of generation from kinetics experiments and melt inclusions. Lithos 286, 454–479.

Anderson, G.M., Burnham, C.W., 1983. Feldspar solubility and the transport of aluminum under metamorphic conditions. Am. J. Sci. 283-A, 283–297.

Audétat, A., Günther, D., Heinrich, C.A., 2000. Magmatic-hydrothermal evolution in a fractionating granite; a microchemical study of the Sn-W-F-mineralized Mole Granite (Australia). Geochim. Cosmochim. Acta 64, 3373–3393.

Bachmann, O., Bergantz, G.W., 2004. On the origin of crystal-poor rhyolites extracted from batholithic crystal mushes. J. Petrol. 45, 1565–1582.

Baker, D.R., 1996. Granitic melt viscosities: empirical and configurational entropy models for their calculation. Am. Mineral. 81, 126–134.

Baker, D.R., 1998. The escape of pegmatite dikes from granitic plutons: constraints from new models of viscosity and dike propagation. Can. Mineral. 36, 255–263.

Baker, D.R., Freda, C., 1999. Ising models of undercooled binary system crystallization: comparison with experimental and pegmatite textures. Am. Mineral. 84, 725–732.

Baker, L.L., Rutherford, M.J., 1996. The effect of dissolved water on the oxidation state of silicic melts. Geochim. Cosmochim. Acta 60, 2179–2187.

Barker, D.S., 1970. Compositions of granophyre, myrmekite, and graphic granite. Geol. Soc. Am. Bull. 81, 3339–3350.

Bea, F., 1996. Controls on the trace element composition of crustal melts. In: Brown, M., Candela, P.A., Peck, D.L., Stephens, W.E., Walker, R.J., Zen, E.-A. (Eds.), The third Hutton symposium on the origin of granites and related rocks. Geological Society of America Special Paper, 315, pp. 33–41.

Bea, F., 2012. The sources of energy for crustal melting and the geochemistry of heat-producing elements. Lithos 153, 278–291.
Bea, F., Pereira, M.D., Corretge, L.G., Fershtater, G.B., 1994. Differentiation of strongly peraluminous, perphosphorus granites: the Pedrobernardo pluton, central Spain. Geochim. Cosmochim. Acta 58, 2609–2627.
Bebout, G.E., Bebout, A.E., Graham, C.M., 2007. Cycling of B, Li, and LILE (K, Cs, Rb, Ba, Sr) into subduction zones: SIMS evidence from micas in high-P/T metasedimentary rocks. Chem. Geol. 239, 284–304.
Beurlen, H., da Silva, M.R.R., Castro, C., 2001. Fluid inclusion microthermometry in Be-Ta-(Li-Sn)-bearing pegmatites from the Borborema Province, Northeast Brazil. Chem. Geol. 173, 107–123.
Beurlen, H., Müller, A., Silva, D., da Silva, M.R.R., 2011. Petrogenetic significance of LA-ICP-MS trace-element data on quartz from the Borborema Pegmatite Province, northeast Brazil. Mineral. Mag. 75, 2703–2719.
Bowen, N.L., 1918. The significance of glass-making processes to the petrologist. J. Wash. Acad. Sci. 8, 88–93.
Bowen, N.L., 1928. The Evolution of the Igneous Rocks. Princeton University Press.
Boyd, B., Sirbescu, M.L., Matty, D.J., 2003. Crystallization temperatures of the Tin Mountain Pegmatite, Black Hills, South Dakota: insights from compositions of co-existing feldspars. Abstracts Programs-Geol. Soc. Am. 35, 192.
Breiter, K., Ackerman, L., Urisova, J.D., Svojtka, M., Novak, M., 2014. Trace element composition of quartz from different types of pegmatites: a case study from the Moldanubian Zone of the Bohemian Massif (Czech Republic). Mineral. Mag. 78, 703–722.
Brisbin, W.C., 1986. Mechanics of pegmatite emplacement. Am. Mineral. 71, 644–651.
Brookins, D.G., 1986. Rubidium-strontium geochronologic studies of large granitic pegmatites. Neues Jahrbuch für Mineralogie Abhandlungen 156, 81–97.
Brookins, D.G., Chakoumakos, B.C., Cook, C.W., Ewing, R.C., Landis, G.P., Register, M.E., 1979. The Harding Pegmatite, summary of recent research. In: Ingersoll, R.V., Woodward, L.A., James, H.L. (Eds.), Guidebook of Santa Fe Country. New Mexico Geological Society Guidebook, 30, pp. 127–133.
Breiter, K., Müller, A., 2008. Evolution of rare-metal granitic magmas documented by quartz chemistry. Eur. J. Mineral. 21, 335–346.
Burke, K., Kidd, W.S.F., 1978. Were Archean continental geothermal gradients much steeper than those of today? Nature 272, 240–241.
Burnham, C.W., 1979. Magmas and hydrothermal fluids. In: Barnes, H.L. (Ed.), Geochemistry of Hydrothermal Ore Deposits, second ed. John Wiley and Sons, New York, pp. 71–136.
Burnham, C.W., Holloway, J.R., Davis, N.F., 1969. Thermodynamic properties of water to 1,000 °C and 10,000 bars. Geological Society of America Special Paper, 132, pp. 96.
Burnham, C.W., Nekvasil, H., 1986. Equilibrium properties of granite pegmatite magmas. Am. Mineral. 71, 239–263.
Camacho, A., Baadsgaard, H., Davis, D.W., Černý, P., 2012. Radiogenic isotope systematics of the Tanco and Silverleaf granitic pegmatites, Winnipeg River pegmatite district, Manitoba. Can. Mineral. 50, 1775–1792.
Cameron, E.N., Jahns, R.H., McNair, A.H., Page, L.R., 1949. Internal structure of granitic pegmatites. Econ. Geol. Mono. 2, 115.
Cameron, E.N., Larrabee, D.M., McNair, A.H., Page, J.J., Stewart, G.W., Shainin, V.E., 1954. Pegmatite investigations, 1942-45, New England. U.S. Geological Survey Professional Paper, 255, pp. 352.
Catlos, E.J., Harrison, T.M., Kohn, M.J., Grove, M., Ryerson, F.J., et al., 2001. Geochronologic and thermobarometric constraints on the evolution of the Main Central Thrust, central Nepal Himalaya. J. Geophys. Res. 106B8, 16177–16204.
Černý, P., 1972. The Tanco pegmatite at Bernic Lake, Manitoba. VIII. Secondary minerals from the spodumene-rich zones. Can. Mineral. 11, 714–726.
Černý, P., 1991a. Rare-element granite pegmatites. Part I: anatomy and internal evolution of pegmatite deposits. Geosci. Can. 18, 49–67.
Černý, P., 1991b. Rare-element granite pegmatites. Part II: regional to global environments and petrogenesis. Geosci. Can. 18, 68–81.
Černý, P., 2005 The Tanco rare-element pegmatite deposit, Manitoba: regional context, internal anatomy, and global comparisons. In: Linnen, R.L., Sampson, I.A. (Eds.), Rare-element Geochemistry of Ore Deposits. Geological Association of Canada Short Course Notes, 17, pp. 127–158.
Černý, P., Blevin, P.L., Cuney, M., London, D., 2005. Granite-related ore deposits. Economic Geology, 100th Anniversary Volume, 337–370.
Černý, P., Ercit, T.S., 2005. The classification of granitic pegmatites revisited. Can. Mineral. 43, 2005–2026.
Černý, P., Lenton, P.G., 1995. The Buck and Pegli lithium deposits, southeastern Manitoba; the problem of updip fractionation in subhorizontal pegmatite sheets. Econ. Geol. Bull. Soc. Econ. Geol. 90, 658–675.
Černý, P., London, D., Novak, M., 2012. Granitic pegmatites as reflections of their sources. Elements 8, 257–261.
Černý, P., Meintzer, R.E., Anderson, A.J., 1985. Extreme fractionation in rare-element granitic pegmatites: selected examples of data and mechanisms. Can. Mineral. 23, 381–421.
Černý, P., Simpson, F.M., 1978. The Tanco Pegmatite at Bernic Lake, Manitoba: X. Pollucite. Can. Mineral. 16, 325–333.
Chakoumakos, B.C., Lumpkin, G.R., 1990. Pressure-temperature constraints on the crystallization of the Harding pegmatite, Taos County, New Mexico. Can. Mineral. 28, 287–298.
Chappell, B.W., 1999. Aluminum saturation in I- and S-type granites and the characteristics of fractionated haplogranites. Lithos 46, 535–551.
Chappell, B.W., White, A.J.R., 2001. Two contrasting granite types: 25 years later. Aust. J. Earth Sci. 48, 489–499.
Chou, I.-M., Li, J., 2014. Studies of silicate melt inclusions in quartz and crystal-rich inclusions in spodumene from Jiajika granitic pegmatite rare-metal deposit in China. Geol. Soc. Am. Abstracts Programs 46, 696.
Christiansen, R.L., Haapala, I., Hart, G.L., 2007. Are Cenozoic topaz rhyolites the erupted equivalents of Proterozoic rapakivi granites? Examples from the Western United States and Finland. Lithos 97, 219–246.
Christiansen, E.H., McCurry, M., 2008. Contrasting origins of Cenozoic silicic volcanic rocks from the western Cordillera of the United States. Bull. Volcanol. 70, 251–267.
Clauser, C., Huegnes, E., 1995. Thermal conductivity of rocks and minerals. Am. Geophys. Union Ref. Shelf 3, 105–126.
Colombo, F., Sfragulla, J., Gonzáles del Tánago, J., 2012. The garnet–phosphate buffer in peraluminous granitic magmas: a case study from pegmatites of the Pocho District, Córdoba, Argentina. Can. Mineral. 50, 1555–1571.
Coveney, R.M., Jr., 2000. Metalliferous shales and the role of organic matter with examples from China, Poland, and the United States. In: Giordano, T.H., Kettler, R.M., Wood, S.A. (Eds.), Ore Genesis and Exploration: The Roles of Organic Matter. Society of Economic Geologists, Reviews in Economic Geology, 9, pp. 251–280.
Dingwell, D.B., Hess, K.-U., Knoche, R., 1996. Granite and granitic pegmatite melts: volumes and viscosities. Trans. R. Soc. Edinburgh, Earth Sci. 87, 65–72.
Dolejš, D., Baker, D.R., 2007. Liquidus equilibria in the system K_2O-Na_2O-Al_2O_3-SiO_2-F_2O_{-1}-H_2O to100 MPa: II. Differentiation paths of fluorosilicic magmas in hydrous systems. J. Petrol. 48, 807–828.
Dostal, J., 2016 Rare-metal deposits associated with alkaline/peralkaline igneous rocks. In: Verplank, P.L., Hizman, M.W. (Eds.), Rare Earth and Critical Elements in Ore Deposits. Society of Economic Geologists, Reviews in Economic Geology, 18, 33-54.
Dekov, V.M., Damyanov, Z.K., Mandova, E.D., 1996. Native tin and tin alloys from axial metalliferous sediments of an ultra-fast spreading centre: East Pacific Rise, 21S survey. Neues Jahrbüch für Mineralogie Monatshefte 1996, 385–405.
Duc-Tin, Q., Keppler, H., 2015. Monazite and xenotime solubility in granitic melts and the origin of the lanthanide tetrad effect. Contrib. Miner. Petrol. 169. https://doi.org/10.1007/s00410-014-1100-9.
Duke, E.F., Papike, J.J., Laul, J.C., 1992. Geochemistry of a boron-rich peraluminous granite pluton; the Calamity Peak layered granite-pegmatite complex, Black Hills, South Dakota. Can. Mineral. 30, 811–833.
Duke, E.F., Redden, J.A., Papike, J.J., 1988. Calamity Peak layered granite-pegmatite complex, Black Hills, South Dakota. 1. Structure and emplacement. Geol. Soc. Am. Bull. 100, 825–840.
Dutrow, B.L., Henry, D.J., 2011. Tourmaline: a geologic DVD. Elements 7, 301–306.
Eadington, P.J., Nashar, B., 1978. Evidence for the magmatic origin of quartz-topaz rocks from the New England Batholith, Australia. Contrib. Miner. Petrol. 67, 433–438.
Eby, G.N., 1990. The A-type granitoids. A review of their occurrence and chemical characteristics and speculations on their petrogenesis. Lithos 26, 115–134.
Elkins, L.T., Grove, T.L., 1990. Ternary feldspar experiments and thermodynamic models. Am. Mineral. 75, 544–559.
Ercit, T.S., 2005. REE-enriched granitic pegmatites. In: Linnen, R.L., Sampson, I.M. (Eds.), Rare-element Geochemistry and Mineral Deposits. Geological Association of Canada Short Course Notes, 17, pp. 175–199.
Evensen, J.M., 2001. The geochemical Budget of Beryllium in Silicic Melts & Superliquidus, Subliquidus, and Starting State Effects on the Kinetics of Crystallization in Hydrous Haplogranite Melts (Unpublished Ph.D. dissertation). University of Oklahoma, Norman, Oklahoma, pp. 293.
Evensen, J.M., London, D., 2002. Experimental silicate mineral/melt partition coefficients for beryllium, and the beryllium cycle from migmatite to pegmatite. Geochimica Cosmochimica Acta 66, 2239–2265.
Evensen, J.M., London, D., 2003. Experimental partitioning of Be and other trace elements between cordierite and silicic melt, and the chemical signature of S-type granite. Contrib. Miner. Petrol. 144, 739–757.
Evensen, J.M., London, D., Wendlandt, R.F., 1999. Solubility and stability of beryl in granitic melts. Am. Mineral. 84, 733–745.
Fenn, P.M., 1977. The nucleation and growth of alkali feldspars from hydrous melts. Can. Mineral. 15, 135–161.
Fenn, P.M., 1986. On the origin of graphic granite. Am. Mineral. 71, 325–330.
Fournier, R.O., 1983. A method of calculating quartz solubilities in aqueous sodium chloride solutions. Geochim. Cosmochim. Acta 47, 579–586.
Franz, G., Khomenko, V., Vishnyevskyy, A., Wirth, R., Struck, U., Nissen, J., Gernert, U., Rocholl, A., 2017. Biologically mediated crystallization of buddingtonite in the Paleoproterozoic: organic-igneous interactions from the Volyn pegmatite, Ukraine. Am. Mineral. 102, 2119–2135.
Fuchs, Y., Lagache, M., Linares, J., 1998. Fe-tourmaline synthesis under different T and fO_2 conditions. Am. Mineral. 83, 525–534.
Fuertes-Fuente, M., Martin-Izard, A., Boiron, M.C., Vinuela, J.M., 2000. P-T Path and Evolution in the Franquiera Granitic Pegmatite, Central Galicia, Northwestern Spain. Can. Mineral. 38, 1163–1175.
Fuhrman, M.L., Lindsley, D.H., 1988. Ternary-feldspar modeling and thermometry. Am. Mineral. 73, 201–215.
Galeschuk, C.R., Vanstone, P.J., 2005. Exploration for buried rare-element pegmatites in the Bernic Lake area of southeastern Manitoba. In: Linnen, R.L., Sampson, I.M. (Eds.), Rare-element Geochemistry and Mineral Deposits. Geological Association of Canada Short Course Notes, 17, pp. 159–173.
Gammel, E.M., Nabelek, P.I., 2016. Fluid inclusion examination of the transition from magmatic to hydrothermal conditions in pegmatites from San Diego County, California. Am. Mineral. 101, 1906–1915.
Glover, A.S., Rogers, W.Z., Barton, J.E., 2012. Granitic pegmatites: storehouses of industrial minerals. Elements 8, 269–273.
Goad, B.E., Černý, P., 1981. Peraluminous pegmatitic granites and their pegmatite aureoles in the Winnipeg River District, southeastern Manitoba. Can. Mineral. 19, 177–194.
Gresens, R.H., 1969. Tectonic-hydrothermal pegmatites. I. The model. Contrib. Miner.

Petrol. 15, 345–355.
Gysi, A.P., Williams-Jones, A.E., 2013. Hydrothermal mobilization of pegmatite-hosted REE and Zr at Strange Lake, Canada: a reaction path model. Geochim. Cosmochim. Acta 122, 324–352.
Hatch, R.A., 1943. Phase equilibrium in the system Li_2O-$A1_2O_3$-SiO_2. Am. Mineral. 28, 471–496.
Hawthorne, F.C., Teertstra, D.K., Černý, P., 1999. Crystal-structure refinement of a rubidian cesian phlogopite. Am. Mineral. 84, 778–781.
Heinrich, E.W., 1965. Holmquistite and pegmatitic lithium exomorphism. Indian Minerals 6, 1–13.
Hildreth, W., 1981. Gradients in silicic magma chambers: implications for lithospheric magmatism. J. Geophys. Res. 86, 10153–10192.
Hildreth, W., Wilson, C.J.N., 2007. Compositional zoning of the Bishop tuff. J. Petrol. 48, 951–999.
Hogan, J.P., Gilbert, M.C., 1995. The A-type Mount Scott Granite sheet: importance of crustal magma traps. J. Geophys. Res. 100, 15779–15792.
Holtz, F., Behrens, H., Dingwell, D.B., Taylor, R.P., 1992. Water solubility in aluminosilicate melts of haplogranite composition at 2 kbar. Chem. Geol. 96, 289–302.
Holtz, F., Roux, J., Ohlhorst, S., Behrens, H., Schulze, F., 1999. The effects of silica and water on the viscosity of hydrous quartrzofeldspathic melts. Am. Mineral. 84, 27–36.
Hulsbosch, N., Hertogen, J., Dewaele, S., André, L., Muchez, P., 2014. Alkali metal and rare earth element evolution of rock-forming minerals from the Gatumba area pegmatites (Rwanda): quantitative assessment ofcrystal-melt fractionation in the regional zonation of pegmatite groups. Geochim. Cosmochim. Acta 132, 349–374.
Hunt, T.S., 1871. Notes on granitic rocks. Am. J. Sci. 1, 82–89 and 182–191.
Icenhower, J.P., London, D., 1996. Experimental partitioning of Rb, Cs, Sr, and Ba between alkali feldspars and peraluminous melt. Am. Mineral. 81, 719–734.
Ishihara, S., 2005. The redox state of granitoids relative to tectonic setting and earth history: the magnetite-ilmenite series 30 years later. Geol. Soc. Am. Spec. Pap. 389, 23–33.
Jahns, R.H., 1952. Pegmatite deposits of the White Picacho district, Maricopa and Yavapai Counties, Arizona. Arizona Bureau of Mines Bulletin 162, 105.
Jahns, R.H., 1953. The genesis of pegmatites. I. Occurrence and origin of giant crystals. Am. Mineral. 38, 563–598.
Jahns, R.H., 1954. Pegmatites of southern California. In: Jahns, R.H. (Ed.), Geology of Southern California. California Division of Mines Bulletin, 170, pp. 37–50.
Jahns, R.H., 1955. The study of pegmatites. Economic Geology, 50th Anniversary Volume: 1025–1130.
Jahns, R.H., 1979. Gem-bearing Pegmatites in San Diego County. In: Abbott, P.L., Todd, V.R. (Eds.), Mesozoic Crystalline Rocks, Peninsular Ranges Batholith and Pegmatites, Point Sal Ophiolite. Department of Geological Sciences, San Diego State University, San Diego, California, pp. 1–38.
Jahns, R.H. 1982. Internal evolution of pegmatite bodies. In: Černý, P. (Ed.), Granitic Pegmatites in Science and Industry. Mineralogical Association of Canada Short Course Handbook 8, pp. 293–327.
Jahns, R.H., Burnham, C.W., 1969. Experimental studies of pegmatite genesis: I. A model for the derivation and crystallization of granitic pegmatites. Econ. Geol. 64, 843–864.
Jahns, R.H., Ewing, R.C., 1977. The Harding Mine, Taos County, New Mexico. Mineral. Rec. 8, 115–126.
Jahns, R.H., Tuttle, O.F., 1963. Layered pegmatite-aplite intrusives. Mineral. Soc. Am. Special Paper 1, 78–92.
James, R.H., Palmer, M.R., 2000. Marine geochemical cycles of the alkali elements and boron: the role of sediments. Geochim. Cosmochim. Acta 64, 3111–3122.
Jolliff, B.L., Papike, J.J., Laul, J.C., 1987. Mineral recorders of pegmatite internal evolution: REE contents of tourmaline from the Bob Ingersoll Pegmatite, South Dakota. Geochim. Cosmochim. Acta 51, 2225–2232.
Jolliff, B.L., Papike, J.J., Shearer, C.K., 1992. Petrogenetic relationships between pegmatite and granite based on geochemistry of muscovite in pegmatite wall zones, Black Hills, South Dakota, USA. Geochim. Cosmochim. Acta 56, 1915–1939.
Juan, V.C., Lo, H.-J., 1973. Stability field of stilbite. Proc. Geol. Soc. China 16, 37–49.
Kesler, S.E., Gruber, P.W., Medina, P.A., Keoleian, G.A., Everson, M.P., 2012. Global lithium resources: relative importance of pegmatite, brine and other deposits. Ore Geol. Rev. 48, 55–69.
Kleck, W.D., Foord, E.E., 1999. The chemistry, mineralogy, and petrology of the George Ashley Block pegmatite body. Am. Mineral. 84, 695–707.
Kontak, D.J., 2006. Nature and origin of an LCT-suite pegmatite with late-stage sodium enrichment, Brazil Lake, Yarmouth County, Nova Scotia. I. Geological setting and petrology. Can. Mineral. 44, 563–598.
Kontak, D.J., Ansdell, K., Dostal, J., Halter, W., Martin, R.F., 2001. The nature and origin of pegmatites in a fluorine-rich leucogranite, East Kemptville tin deposit, Nova Scotia, Canada. T. Roy. Soc. Edin: Earth 92, 173–200.
Kontak, D.J., Dostal, J., Kyser, T.K., Archibald, D.A., 2002. A petrological, geochemical, isotopic and fluid inclusion study of 370 Ma pegmatite-aplite sheets, Peggys Cove, Nova Scotia, Canada. Can. Mineral. 40, 1249–1286.
Kontak, D.J., Martin, R.F., 1997. Alkali feldspar in the peraluminous South Mountain Batholith, Nova Scotia: trace-element data. Can. Mineral. 35, 959–977.
Kortemeier, W.T., Burt, D.M., 1988. Ongonite and topazite dikes in the Flying W Ranch area, Tonto Basin, Arizona. Am. Mineral. 73, 507–523.
Landes, K.K., 1933. Origin and classification of pegmatites. Am. Mineral. 18, 33–56.
Lee, C.-T., Morton, D.M., 2015. High silica granites: terminal porosity and crystal settling in shallow magma chambers. Earth Planet. Sci. Lett. 409, 23–31.
Leeman, W.P., Sisson,V.B., 1996. Geochemistry of boron and its implications for crsustal and mantle processes. In: Grew, E.S., Anovitz, L.M. (Eds.), Boron: Mineralogy, Petrology, and Geochemistry. Mineralogical Society of America Reviews in Mineralogy and Geochemistry, 33, pp. 645–708.
Linnen, R.L., Cuney, M., 2005. Granite-related Rare Element Deposits and Experimental Constraints on Ta-Nb-W-Sn-Zr-Hf Mineralization. In: Linnen, R.L., Sampson, I.M. (Eds.), Rare-element Geochemistry of Ore Deposits. Geological Association of Canada Short Course Notes, 17, pp. 45–68.
Lira, R., Galliski, M.A., Bernard, F., Roquet, M.B., 2012. The intragranitic Potrerillos NYF pegmatites and their A-type host granites of the Las Chacras-Potrerillos Batholith, Sierra de San Luis, Argentina. Can. Mineral. 50, 1729–1750.
Liu, C.-Q., Zhang, H., 2005. The lanthanide tetrad effect in apatite from the Altay No. 3 pegmatite, Xingjiang, China: an intrinsic feature of the pegmatite magma. Chem. Geol. 214, 61–77.
London, D., 1984. Experimental phase equilibria in the system $LiAlSiO_4$-SiO_2-H_2O: a petrogenetic grid for lithium-rich pegmatites. Am. Mineral. 69, 995–1004.
London, D., 1985. Pegmatites of the Middletown district, Connecticut. 77th Annual Meeting, New England Intercollegiate Geological Conference, Yale University. Connecticut Geological and Natural History Survey Guidebook 6, 509–533.
London, D., 1987. Internal differentiation of rare-element pegmatites: effects of boron, phosphorus, and fluorine. Geochim. Cosmochim. Acta 51, 403–420.
London, D., 1986a. The magmatic-hydrothermal transition in the Tanco rare-element pegmatite: evidence from fluid inclusions and phase equilibrium experiments. Am. Mineral. 71, 376–395.
London, D., 1986b. Formation of tourmaline-rich gem pockets in miarolitic pegmatites. Am. Mineral. 71, 396–405.
London, D., 1986c. Holmquistite as a guide to pegmatitic rare metal deposits. Econ. Geol. 81, 704–712.
London, D., 1989. Lithophile rare element concentration in silicic rocks: the alkaline trend in granitic systems. Geol. Mineral. Assoc. Canada, Program with Abstracts 14, A21.
London, D., 1992. The application of experimental petrology to the genesis and crystallization of granitic pegmatites. Can. Mineral. 30, 499–540.
London, D., 1999. Melt boundary layers and the growth of pegmatitic textures. (abstr.). Can. Mineral. 37, 826–827.
London, D., 2008. Pegmatites. Canadian Mineralogist Special Publication, 10, pp. 368.
London, D., 2009. The origin of primary textures in granitic pegmatites. Can. Mineral. 47, 697–724.
London, D., 2011. Experimental synthesis and stability of tourmaline: a historical overview. Can. Mineral. 49, 117–136.
London, D., 2013. Crystal-filled cavities in granitic pegmatites: bursting the bubble. Rocks Miner. 88, 527–534.
London, D., 2014a. A petrologic assessment of internal zonation in granitic pegmatites. Lithos 184–187, 74–104.
London, D., 2014b. Subsolidus isothermal fractional crystallization. Am. Mineral. 99, 543–546.
London, D., 2014c. Zonal structure of layered pegmatites: thin versus thick dikes. (abstr) Geol. Soc. Am. Programs Abstracts 46, 751.
London, D., 2015a. Reply to Thomas and Davidson on “A petrologic assessment of internal zonation in granitic pegmatites” (London, 2014a). Lithos 212–215, 469–484.
London, D., 2015b. Reading pegmatites: what beryl says. Rocks Miner. 90, 138–149.
London, D., 2016a. Reading pegmatites: what tourmaline says. Rocks Miner. 91, 132–149.
London, D., 2016b. Rare-element Granitic Pegmatites. In: Verplanck, P.L., Hitzman, M.W. (Eds.), Rare Earth and Critical Elements in Major Deposit Types, Reviews in Economic Geology. Society of Economic Geologists, Inc, Littleton, CO, 18, pp. 165–193.
London, D., 2018. Reading pegmatites: what pollucite says. Rocks Miner., accepted.
London, D., Hervig, R.L., Morgan VI, G.B., 1988. Melt-vapor solubilities and element partitioning in peraluminous granite-pegmatite systems: Experimental results with Macusani glass at 200 MPa. Contrib. Mineral. Petrol. 99, 360–373.
London, D., Manning, D.A.C., 1995. Compositional variation and significance of tourmaline from southwest England. Econ. Geol. 90, 495–519.
London, D., Morgan, G.B.V.I., 2017. Experimental crystallization of the Macusani obsidian, with applications to lithium-rich granitic pegmatites. J. Petrol (in press).
London, D., Morgan, G.B.V.I., Acosta-Vigil, A., 2012a. Experimental simulations of anatexis and assimilation involving metapelite and granitic melt. Lithos 153, 292–307.
London, D., Morgan VI, G.B., Babb, H.A., Loomis, J.L., 1993. Behavior and effects of phosphorus in the system Na_2O-K_2O-Al_2O_3-SiO_2-P_2O_5-H_2O at 200 MPa (H_2O). Contrib. Mineral. Petrol. 113, 450–465.
London, D., Morgan VI, G.B., Hervig, R.L., 1989. Vapor-undersaturated experiments in the system macusanite-H_2O at 200 MPa, and the internal differentiation of granitic pegmatites. Contrib. Mineral. Petrol. 102, 1–17.
London, D., Morgan, G.B.V.I., Icenhower, J., 1998. Stability and solubility of pollucite in granitic systems at 200 MPa H_2O. Can. Mineral. 36, 497–510.
London, D., Morgan IV, G.B., Paul, K.A., Guttery, B.M., 2012b. Internal evolution of a miarolitic granitic pegmatite: the Little Three Mine, Ramona, California (USA). Can. Mineral. 50, 1025–1054.
London, D., Morgan IV, G.B., Wolf, M.B., 2001. Amblygonite-montebrasite solid solutions as monitors of fluorine in evolved granitic and pegmatitic melts. Am. Mineral. 86, 225–233.
London, D., Wolf, M.B., Morgan, G.B.V.I., Gallego Garrido, M., 1999. Experimental silicate-phosphate equilibria in peraluminous granitic magmas, with a case study of the Alburquerque batholith at Tres Arroyos, Badajoz, Spain. J. Petrol. 40, 215–240.
Lyckberg, P., Chournousenko, V.A., Wilson, W.E., 2009. Volodarsk-Volhynsk, Zhitomirskaja Oblast, Ukraine. Mineral. Rec. 40, 473–506.
Macdonald, R., Smith, R.L., Thomas, J.E., 1992. Chemistry of the subalkalic silicic obsidians. U.S. Geological Survey Professional Paper 1523, 214.
MacLellan, H.E., Trembath, L.L., 1991. The role of quartz crystallization in the development and preservation of igneous texture in granitic rocks: experimental evidence at 1 kbar. Am. Mineral. 76, 1291–1305.
Mallik, A., Dasgupta, R., Tsuno, K., Nelson, J., 2016. Effects of water, depth and

temperature on partial melting of mantle wedge fluxed by hydrous sediment-melt in subduction zones. Geochim. Cosmochim. Acta 195, 226–243.
Maneta, V., Baker, D.R., Minarik, W., 2015. Evidence for lithium-aluminosilicate supersaturation of pegmatite-forming melts. Contrib. Mineral. Petrol. 170. https://doi.org/10.1007/s00410-015-1158-z.
Manning, D.A.C., 1981. The effect of fluorine on liquidus phase relationships in the system Qz-Ab-Or with excess water at 1 kb. Contrib. Miner. Petrol. 76, 206–215.
Marsh, B.D., Gunnarsson, B., Cogdon, R., Carmody, R., 1991. Hawaiian basalt and Icelandic rhyolite, indicators of differentiation and partial melting. Geol. Rundsch. 80, 481–510.
Masuda, A., Ikeuchi, Y., 1979. Lanthanide tetrad effect observed in marine environment. Geochem. J. 13, 19–22.
McCauley, A., Bradley, D.C., 2014. The global age distribution of granitic pegmatites. Can. Mineral. 52, 183–190.
Merritt, C.A., 1924. The function of colloids in pegmatitic growths. Trans. R. Soc. Can. 17, 61–68.
Methot, R.L., 1973. Internal Geochronologic Study of Two Large Granitic Pegmatites, Connecticut (Unpublished Ph.D. dissertation). Kansas State University, Manhattan, Kansas, pp. 123.
Michael, P., 1983. Chemical differentiation of the Bishop Tuff and other high-silica magmas through crystallization processes. Geology (Boulder) 11, 31–34.
Miller, W.J., 1919. Pegmatite, silexite, and aplite of northern New York. J. Geol. 27, 28–54.
Mohammad, Y., Kareem, H., Anma, R., 2016. The Kuradawe granitic pegmatite from the Mawat Ophiolite, northeastern Iraq; anatomy, mineralogy, geochemistry, and petrogenesis. Can. Mineral. 54, 989–1019.
Moody, J.B., Meyer, D., Jenkins, J.E., 1983. Experimental characterization of the greenschist/amphibolite boundary in mafic systems. Am. J. Sci. 283, 48–92.
Moore, G., Righter, K., Carmichael, I.S.E., 1995. The effect of dissolved water on the oxidation state of iron in natural silicate liquids. Contrib. Mineral. Petrol. 120.
Morgan, G.B.V.I., Acosta-Vigil, A., London, D., 2008. Diffusive equilibration between hydrous metaluminous-peraluminous liquid couples at 200 MPa (H_2O), and alkali transport in granitic liquids. Contrib. Miner. Petrol. 155, 257–269.
Morgan VI, G.B., London, D., 1987. Alteration of amphibolitic wallrocks around the Tanco rare-element pegmatite, Bernic Lake, Manitoba. Am. Mineral. 72, 1097–1121.
Morgan VI, G.B., London, D., 1989. Experimental reactions of amphibolite with boron-bearing aqueous fluids at 200 MPa: implications for tourmaline stability and partial melting in mafic rocks. Contrib. Mineral. Petrol. 102, 281–297.
Morgan VI, G.B., London, D., 1999. Crystallization of the Little Three layered pegmatite-aplite dike, Ramona District, California. Contrib. Miner. Petrol. 136, 310–330.
Morgan VI, G.B., London, D., 2005. Phosphorus distribution between potassic alkali feldspar and metaluminous haplogranite liquid at 200 MPa (H_2O): the effect of undercooling on crystal-liquid systematics. Contrib. Miner. Petrol. 150, 456–471.
Morgan VI, G.B., London, D., 2012. Process of granophyre crystallization in the Long Mountain Granite, southern Oklahoma. Geol. Soc. Am. Bull. 124, 1251–1261.
Müller, A., Ihleni, P.M., Kronz, A., 2008. Quartz chemistry in polygeneration Sveconorwegian pegmatites, Froland, Norway. Eur. J. Mineral. 20, 447–463.
Mungall, J.E., 2002. Empirical models relating viscosity and tracer diffusion in magmatic silicate melts. Geochim. Cosmochim. Acta 66, 125–143.
Neuville, D.R., Courtial, P., Dingwell, D.B., Richet, P., 1993. Thermodynamic and rheological properties of rhyolite and andesite melts. Contrib. Miner. Petrol. 113, 572–581.
Neves, L.J.P.F., Godinho, M.M., 1999. Structural state of K-feldspar in some Hercynian granites from Iberia; a review of data and controlling factors. Can. Mineral. 37, 691–700.
Norton, J.J., 1964.Geology and mineral deposits of some pegmatites in the southern Black Hills, South Dakota. U. S. Geological Survey Professional Paper 297-E, 293–341.
Norton, J.J., 1966. Ternary diagrams of the quartz-feldspar content of pegmatites in Colorado. U.S. Geol. Survey Bull. 1241, D1–D16.
Norton, J.J., 1983. Sequence of mineral assemblages in differentiated granitic pegmatites. Econ. Geol. 78, 854–874.
Ottolini, L., Le Fever, B., Vannucci, R., 2004. Direct assessment of mantle boron and lithium contents and distribution by SIMS analyses of peridotite minerals. Earth Planet. Sci. Lett. 228, 19–36.
Pabst, S., Thomas, Z., Savov, I.P., Ludwig, T., Rost, D., Vicenzi, E.P., 2011. Evidence for boron incorporation into the serpentine crystal structure. Am. Mineral. 96, 1112–1119.
Page, L.R., Norton, J.J., Stoll, W.C., Hanley, J.B., Adams, J.W., Pray, L.C., Steven, T.A., Erickson, M.P., Joralemon, P., Stopper, R.F., Hall, W.E., 1953. Pegmatite investigations, 1942–1945, Black Hills, South Dakota. U.S. Geological Survey Professional Paper 247, 228.
Palinkaš, S.S., Wegner, R., Čobić, A., Palinkaš, L.A., De Brito Barreto, S., Váczi, T., Bermanec, V., 2014. The role of magmatic and hydrothermal processes in the evolution of Be-bearing pegmatites: Evidence from beryl and its breakdown products. Am. Mineral. 99, 424–432.
Palmer, M.R., Swihart, G.H., 1996. Boron Isotope Geochemistry: An Overview. In: Grew, E.S., Anovitz, L.A. (Eds.), Boron; Mineralogy, Petrology and Geochemistry. Mineralogical Society of America Reviews in Mineralogy, 33, pp. 709–744.
Parsons, I., Magee, C.W., Allen, C.M., Shelley, J.M.G., Lee, M.R., 2009. Mutual replacement reactions in alkali feldspars II: trace element partitioning and geothermometry. Contrib. Miner. Petrol. 157, 663–687.
Peretyazhko, I.S., Zagorsky, V. Ye., Smirnov, S.Z., Michailov, M.Y., 2004. Conditions of pocket formation in the Oktyabrskaya tourmaline-rich gem pegmatite (the Malkhan field, Central Transbaikalia, Russia). Chem. Geol. 210, 91–111.
Pichavant, M., 1981. An experimental study of the effect of boron on a water saturated haplogranite at 1 kbar vapour pressure, geological applications. Contrib. Miner. Petrol. 76, 430–439.
Pichavant, M., Villaros, A., Deveaud, S., Scaillet, B., Lahlafi, M., 2016. The influence of redox state on mica crystallization in leucogranitic and pegmatitic liquids. Can. Mineral. 54, 559–581.
Pirajno, F., 2015. Intracontinental anorogenic alkaline magmatism and carbonatites, associated mineral systems and the mantle plume connection. Gondwana Res. 27, 1181–1216.
Pistone, M., Blundy, J., Brooker, R.A., EIMF, 2017. Water transfer during magma mixing events: insights into crystal mush rejuvenation and melt extraction processes. Am. Mineral. 102, 766–776.
Putnis, A., Hinrichs, R., Putnis, C.V., Golla-Schindler, U., Collins, L.G., 2007. Hematite in porous red-clouded feldspars: evidence of large-scale crustal fluid-rock interaction. Lithos 95, 10–18.
Ramberg, H., 1952. The Origin of Metamorphic and Metasomatic Rocks. The University of Chicago Press, Chicago, Illinois, pp. 317.
Redden, J.A., Norton, J.J., MacLaughlin, R.J., 1982. Geology of the Harney Peak Granite, Black Hills, South Dakota. U.S. Geological Survey Open File Report 82-481, pp. 18.
Roberts, M.D., Reid, D.L., Miller, J.A., Basson, I.J., Roberts, M., Roberts, M., Smith, D., 2007. The Merensky cyclic unit and its impact on footwall cumulates below normal and regional pothole reef types in the western Bushveld Complex. Miner. Deposita 42, 271–292.
Robertson, E.C., 1988. Thermal Properties of Rocks. U.S. Geological Survey Open-File report 88-441, pp. 106.
Rockhold, J.R., Nabelek, P.I., Glascock, M.D., 1987. Origin of rhythmic layering in the Calamity Peak satellite pluton of the Harney Peak Granite, South Dakota: the role of boron. Geochim. Cosmochim. Acta 51, 487–496.
Roda, E., Pesquera, A., Velasco, F., 1995. Tourmaline in granitic pegmatites and their country rocks, Fregeneda area, Salamanca, Spain. Can. Mineral. 33, 835–848.
Roda Robles, E., Pesquera, A., Gil, P., Torres-Ruiz, J., 2012. From granites to highly evolved pegmatites: a case study of the Pinilla de Fermoselle granite-pegmatite system (Zamora, Spain). Lithos 153, 192–207.
Roedder, E., 1981. Natural occurrence and significance of fluids indicating high pressure and temperature. Phys. Chem. Earth. 13, 9–39.
Roedder, E., 1984. Fluid inclusions. Mineral. Soc. Am. Rev. Mineral. 12, 644.
Rossovskiy, L.N., Konovalenko, S.I., 1979. Features of the formation of the rare-metal pegmatites under conditions of compression and tension (as exemplified by the Hindu Kush region). Int. Geol. Rev. 21, 755–764.
Rubin, A.M., 1995. Getting granite dikes out of the source region. J. Geophys. Res. 100B, 5911–5929.
Salvi, S., Williams-Jones, A.E., 2005. Alkaline Granite-syenite Deposits. In: Linnen, R.L., Sampson, I.M. (Eds.), Rare-element Geochemistry of Ore Deposits. Geological Association of Canada Short Course Notes, 17, pp. 315–341.
Schmidt, C., Leeder, O., 1992. Temperature and pressure conditions during the formation of pegmatites and pneumatolytic tin-tungsten mineralizations in Mongolia. Neues Jahrbuch fuer Mineralogie. Abhandlungen 165, 29–52.
Schmidt, K., Bau, M., Hein, J.R., Koschinsky, A., 2014. Fractionation of the geochemical twins Zr/Hf and Nb/Ta during scavenging from sea water by hydrogenetic ferromanganese crusts. Geochim. Cosmochim. Acta 140, 468–487.
Selway, J.B., Černý, P., 1998. Feruvite from lepidolite pegmatites at Red Cross Lake, Manitoba. Can. Mineral. 36, 433–439.
Shaw, R.A., Goodenough, K.M., Roberts, N.M.W., Horstwood, M.S.A., Chenery, S.R., Gunn, A.G., 2016. Petrogenesis of rare-metal pegmatites in high-grade metamorphic terranes: a case study from the Lewisian Gneiss Complex of north-westScotland. Precambr. Res. 281, 338–362.
Shearer, C.K., Papike, J.J., Jolliff, B.L., 1992. Petrogenetic links among granites and pegmatites in the Harney Peak rare-element granite-pegmatite system, Black Hills, South Dakota. Can. Mineral. 30, 785–809.
Shearer, C.K., Papike, J.J., Laul, J.C., 1987. Mineralogical and chemical evolution of a rare-element granite-pegmatite system: Harney Peak granite, Black Hills, South Dakota. Geochemica et Cosmochimica Acta 51, 473–487.
Shearer, C.K., Papike, J.J., Simon, S.B., Laul, J.C., 1984a. Pegmatite-wallrock interactions, Black Hills, South Dakota: interaction between pegmatite-derived fluids and quartz-mica schist wallrock. Am. Mineral. 71, 518–539.
Shearer, C.K., Papike, J.J., Simon, S.B., Laul, J.C., Christian, R.P., 1984b. Pegmatite/wallrock interactions, Black Hills, South Dakota: progressive boron metasomatism adjacent to the Tip Top pegmatite. Geochim. Cosmochim. Acta 48, 2563–2579.
Siegel, K., Wagner, T., Trumbull, R.B., Jonssond, E., Matalin, G., Wälle, M., Heinrich, C.A., 2016. Stable isotope (B, H, O) and mineral-chemistry constraints on the magmatic to hydrothermal evolution of the Varuträsk rare-element pegmatite (Northern Sweden). Chem. Geol. 421, 1–16.
Simmons, W. B., Falster, A.U., Felch, M., 2015. Pollucite from three distinct assemblages in the Mount Mica pegmatite, Paris, Oxford County, Maine, USA. (abstr). In: 7th International Symposium on Granitic Pegmatites, PEG 2015 Książ, Poland, pp. 96.
Simmons, W., Falster, A., Webber, K., Roda-Robles, E., Boudreaux, A.P., Grassi, L.R., Freeman, G., 2016. Bulk composition of the Mt. Mica pegmatite, Maine, USA: implications for the origin of an LCT type pegmatite by anatexis. Can. Mineral. 54, 1053–1070.
Simmons, W.B., Pezzotta, F., Shigley, J.E., Beurlen, H., 2012. Granitic pegmatites as sources of colored gemstones. Elements 8, 281–287.
Simons, B., Andersen, J.C.O., Shail, R.K., Jenner, F.E., 2017. Fractionation of Li, Be, Ga, Nb, Ta, In, Sn, Sb, W and Bi in the peraluminous Early Permian Variscan granites of the Cornubian Batholith: precursor processes to magmatic-hydrothermal mineralisation. Lithos 278–281, 491–512.
Sirbescu, M.C., Nabelek, P.I., 2001. Pegmatite melts at 340 °C? Abstracts Programs-Geol. Soc. Am. 33, 333.
Sirbescu, M.L., Nabelek, P.I., 2003. Crystallization conditions and evolution of magmatic

fluids in the Harney Peak Granites and associated pegmatites, Black Hills, South Dakota – evidence from fluid inclusions. Geochim. Cosmochim. Acta 67, 2443–2465.
Sirbescu, M.L., Schmidt, C., Veksler, I.V., Wittington, A.G., Wilke, M., 2017. Experimental crystallization of undercooled felsic liquids: generation of pegmatitic texture. J. Petrol. 2017, 1–30. https://doi.org/10.1093/petrology/egx027.
Smeds, S.A., 1992. Trace elements in potassium-feldspar and muscovite as a guide in the prospecting for lithium- and tin-bearing pegmatites in Sweden. J. Geochem. Explor. 42, 351–469.
Smirnov, S.Z., Konovalenko, S.I., Danyushevsky, L., Thomas, V.G., Vladimirov, A.G., 2009. The Leskhozovskaya Pegmatite (SW Pamir, Tajikistan); a case of forming fluids at the magmatic-hydrothermal transition.). (abstr.). In: Proceedings of the European Current Research on Fluid Inclusions (ECROFI), 20, pp. 219–220.
Smith, F.G., 1953. Complex inclusions in pegmatitic minerals. Am. Mineral. 38, 559–560.
Smorkanicz, J.R., Dusas, F.O., 1999. Reconaissance fluid inclusion study of the Morefield pegmatite, Amelia County, VA. Am. Mineral. 84, 746–753.
Stepanov, A., Mavrogenes, J.A., Meffre, S., Davidson, P., 2014. The key role of mica during igneous concentration of tantalum. Contrib. Mineral. Petrol. 167, 1009. https://doi.org/10.1007/s00410-014-1009-3.
Stewart, D.B., 1978. Petrogenesis of lithium-rich pegmatites. Am. Mineral. 63, 970–980.
Stilling, A., Černý, P., Vanstone, P.J., 2006. The Tanco pegmatite at Bernic Lake, Manitoba. XVI. Zonal and bulk compositions and their petrogenetic significance. Can. Mineral. 44, 599–623.
Streckheisen, A.F., 1976. To each plutonic rock its proper name. Earth-Sci. Rev. 12, 1–33.
Swanson, S.E., 1977. Relation of nucleation and crystal-growth to the development of granitic textures. Am. Mineral. 62, 966–978.
Swanson, S.E., 2012. Mineralogy of spodumene pegmatites and related rocks in the tin-spodumene belt of North and South Carolina, USA. Can. Mineral. 50, 1589–1608.
Swanson, S.E., Fenn, P.M., 1986. Quartz crystallization in igneous rocks. Am. Mineral. 71, 331–342.
Sweetapple, M.T., Collins, P.L.F., 2002. Genetic framework for the classification and distribution of Archean rare metal pegmatites in the North Pilbara Craton, Western Australia. Econ. Geol. 97, 873–895.
Tang, Y., Zhang, H., 2015. Lanthanide tetrads in normalized rare element patterns of zircon from the Koktokay No. 3 granitic pegmatite, Altay,NW China. Am. Mineral. 100, 2630–2636.
Taylor, B.E., Foord, E.E., Friedrichsen, H., 1979. Stable isotope and fluid inclusion studies of gem-bearing granitic pegmatite-aplite dikes, San Diego Co., California. Contrib. Mineral. Petrol. 68, 187–205.
Taylor, J.R., Wall, V.J., 1992. The behavior of tin in granitoid magmas. Econ. Geol. Bull. Soc. Econ. Geol. 87, 403–420.
Thomas, A.V., Bray, C.J., Spooner, E.T.C., 1988. A discussion of the Jahns-Burnham proposal for the formation of zoned granitic pegmatites using solid-liquid-vapour inclusions from the Tanco pegmatite, SE Manitoba, Canada. Trans. R. Soc. Edinburgh, Earth Sci. Sect. 79, 299–315.
Thomas, R., Davidson, P., 2010. Hambergite-rich melt inclusions in morganite crystals from the Muiane pegmatite, Mozambique and some remarks on the paragenesis of hambergite. Mineral. Petrol. 100, 227–239.
Thomas, A.V., Spooner, E.T.C., 1988. Fluid inclusions in the system H_2O-CH_4-NaCl-CO_2 from metasomatic tourmaline within the border unit of the Tanco zoned granitic pegmatite, S.E. Manitoba. Geochim. Cosmochim. Acta 52, 1065–1075.
Thomas, A.V., Spooner, E.T.C., 1992. The volatile chemisty of magmatic H_2O-CO_2 inclusions from the Tanco zoned granitic pegmatite, southeastern Manitoba, Canada. Geochim. Cosmochim. Acta 56, 49–65.
Thomas, W.M., Ernst, W.G., 1990. The aluminum content of hornblende in calc-alkaline granitic rocks: a mineralogic barometer calibrated experimentally to 12 kbars. Geochem. Soc. Special Publ. 2, 59–63.
Trueman, D.L., Černý, P., 1982. Exploration for rare-element granitic pegmatites. In Granitic pegmatites in science and industry (Černý, P., ed.). Mineral. Assoc. Canada Short Course Handbook 8, 463–494.
Trumbull, R.B., 1995. Tin mineralization in the Archean Sinceni rare element pegmatite field, Kaapvaal Craton, Swaziland. Econ. Geol. Bull. Soc. Econ. Geol. 90, 648–657.
Tuttle, O.F., Bowen, N.L., 1958. Origin of granite in the light of experimental studies in the system $NaAlSi_3O_8$-$KAlSi_3O_8$-SiO_2-H_2O. Geol. Soc. Am. Memoir 74, 153.
Üebel, P.-J., 1977. Internal structure of pegmatites, its origin and nomenclature. Neues Jarbuch für Mineralogie Abhandlungen 131, 83–113.
U.S. Geological Survey, 2018. Mineral commodity summaries 2018: U.S. Geological Survey. p. 200. https://doi.org/10.3133/70194932.
van Lichtervelde, M., Salvi, S., Baziat, D., Linnen, R.L., 2007. Textural features and chemical evolution in tantalum oxides; magmatic versus hydrothermal origins for Ta mineralization in the Tanco lower pegmatite, Manitoba, Canada. Econ. Geol. Bull. Soc. Econ. Geol. 102, 257–276.
van Lichtervelde, M., Holtz, F., Hanchar, J.M., 2010. Solubility of manganotantalite, zircon and hafnon in highly fluxed peralkaline to peraluminous pegmatitic melts. Contrib. Miner. Petrol. 160, 17–32.
Vaughn, D.E.W., 1963. The Crystallization Ranges of the Spruce Pine and Harding Pegmatites (Unpublished Ph.D. dissertation). Pennsylvania State University at University Park, University Park, PA, United States (USA), pp. 61.
Vlasov, K.A., 1961. Principles of classifying granite pegmatites and their textural-paragenetic types. Transactions of the Academy of Sciences, U.S.S.R. Geol. Ser. 1, 5–20.
Wahlberg, J.S., Fishman, M.J., 1962. Adsorption of cesium on clay minerals. U. S. Geol. Survey Bull. 1140-A, A1–A30.
Webber, K.L., Falster, A.U., Simmons, W.B., Foord, E.E., 1997. The role of diffusion-controlled oscillatory nucleation in the formation of line rock in pegmatite-aplite dikes. J. Petrol. 38, 1777–1791.
Webber, K.L., Simmons, W.B., Falster, A.U., Foord, E.E., 1999. Cooling rates and crystallization dynamics of shallow level pegmatite-aplite dikes, San Diego County, California. Am. Mineral. 84, 708–717.
Wedepohl, K.H., 1995. The composition of the continental crust. Geochim. Cosmochim. Acta 59, 1217–1232.
Webster, J.D., Holloway, J.R., Hervig, R.L., 1989. Partitioning of lithophile trace elements between H_2O and H_2O + CO_2 fluids and topaz rhyolite melt. Econ. Geol. 84, 116–134.
Weisbrod, A, Polak, C., Roy, D., 1986. Experimental study of tourmaline solubility in the system Na-Mg-Al-Si-B-O-H, applications to the boron content of natural hydrothermal fluids and tourmalinization processes. (abstr.). In: International Symposium on Experimental Mineralogy and Geochemistry, Nancy, France (symposium abstracts volume), pp. 140–141.
Wolf, M.B., London, D., 1997. Boron in granitic magmas: stability of tourmaline in equilibrium with biotite and cordierite. Contrib. Miner. Petrol. 130, 12–30.
Yin, W.W.-S., 2000. Tin Placer Deposits on Continental Shelves. In: Cronan, D.S. (Ed.), Handbook of Marine Mineral Deposits. CRC Press, Boca Raton, FL, United States (USA), pp. 27–42.